

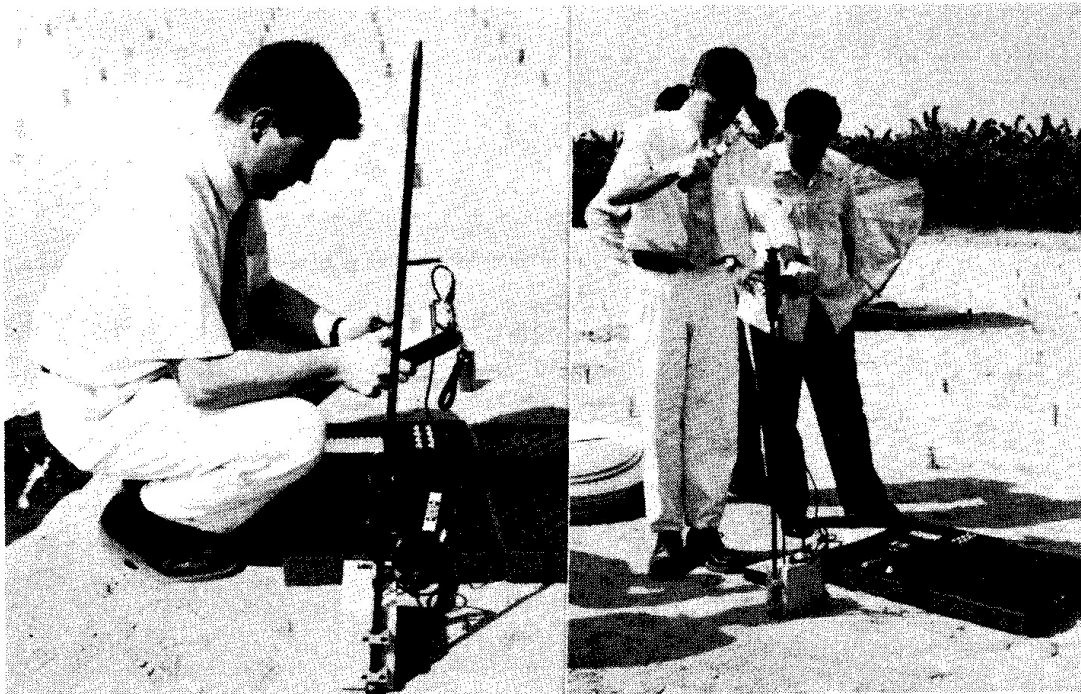
Volume 27 Number 1 June 1996

ISSN 0046-5828

GEOTECHNICAL ENGINEERING

Journal of
SOUTHEAST ASIAN GEOTECHNICAL SOCIETY

Sponsored by
ASIAN INSTITUTE OF TECHNOLOGY



CONTENTS

Photographic Feature:

Modernization of Laboratory Testing Equipments to Measure Strength and Deformation of Geomaterials

by *S. Shibuya*

Main Papers:

Compressibility and Flow Parameters from PVD Improved Soft Bangkok Clay
by *D.T. Bergado, P.V. Long and A.S. Balasubramaniam* 1

Interactive Behavior of Cylindrical Anchors in Dense Sand
by *H.J. Liao, J.K. Chen and S.C. Shu* 21

Analysis and Design of a Tied Back-To-Back Geosynthetic Reinforced Soil Wall
by *S.C.R. Lo, S.Q. Li, M. Gopalan and Z.Gao* 37

Case Studies of Rock-Socketed Piles
by *C.F. Leung* 51

Effects of Slip Between a Pile and Surrounding Soil on Negative Skin Friction
by *P. Karasudhi, A.C. Wijeyewickrema and S. Katawaethwarag* 69

Book Review:

Soft Ground Improvement in Lowlands and Other Environment
by *D.T. Bergado, L.R. Anderson, N. Miura, and A.S. Balasubramaniam* 83

Errata:

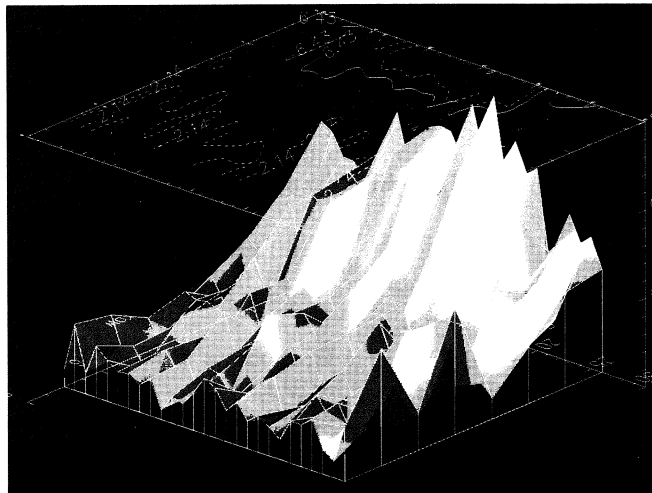
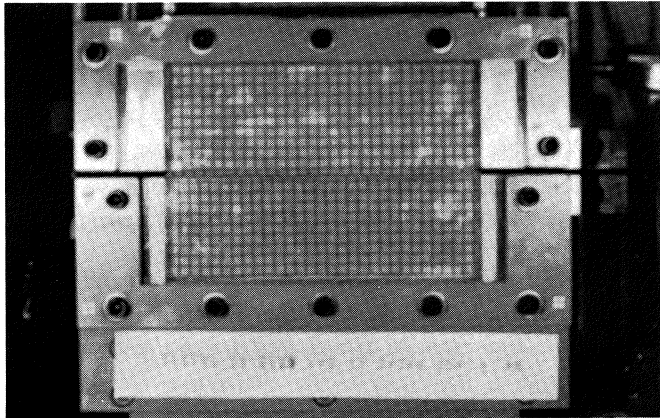
Cation Exchange Studies on a Lime Treated Marine Clay
by *G. Rajasekaran and S. Narasimha Rao*, Geotechnical Engineering,
Vol. 26, No. 2, December 1995 85

PHOTOGRAPHIC FEATURE

Modernization of Laboratory Testing Equipments to Measure Strength and Deformation of Geomaterials *by S. Shibuya*

Soil testing plays an important rule in geotechnical engineering design since the soil properties at one site can never be identical to those at the other. Moreover, soils exhibit the strength and stiffness which depend very much on the conditions of kinematic deformation and the stress path experienced in the laboratory. Therefore, in laboratory testing, it is crucial to achieve a complete simulation of boundary conditions for in-situ subsoil to be experienced during construction work.

Much efforts have been made in order to improve the accuracy of stress and deformation measurements of soil specimens by introducing updated techniques. The pictures show below an example of optimization of the conventional direct shear box (DSB) test. The photo-analysis into the boundary strain of the DSB specimen suggested that the DSB test may be interpreted as quasi-simple shear if the specimen is tested under the optimized boundary conditions.



COMPRESSIBILITY AND FLOW PARAMETERS FROM PVD IMPROVED SOFT BANGKOK CLAY

D.T. Bergado¹, P.V. Long², and A.S. Balasubramaniam³

ABSTRACT: The utilization of prefabricated vertical drain (PVD) has been increasingly popular in the improvement of soft Bangkok clay. Recently, three full scale test embankments were constructed on PVD improved very soft to soft Bangkok clay at Nong Ngu Hao site. Both vertical and lateral deformations as well as the excess pore pressures were monitored. Different PVD spacings at 1.0 m, 1.2 m and 1.5 m were used corresponding to each test embankment. Based on Asaoka's method, the relationships between the coefficient of horizontal consolidation, c_h , and the discharge capacity, q_w , can be established assuming the ratios of k_h/k_s and d_s/d_w . Thus, the flow and compressibility parameters can be derived. The back-calculated c_h values compared very well with the results of piezocone tests. The q_w values were also confirmed from the results of other investigators.

INTRODUCTION

The consolidation settlement of soft clay subsoil creates numerous problems in foundation engineering. To shorten the consolidation time, prefabricated vertical drains (PVD) are installed together with preloading by surcharge loads. Vertical drains are artificially-created drainage paths which can be installed by one of several methods and which can have a variety of physical characteristics. In this method, pore water squeezed out during consolidation of the clay due to the hydraulic gradients created by preloading, can flow a lot faster in the horizontal direction towards the drain and then flow freely along the drains vertically into the permeable drainage layers. Thus, the installation of the vertical drains in the clay reduces the length of drainage paths and, thereby, reduce the time required to complete the consolidation process.

CONSOLIDATION WITH PVD

Barron (1948) presented the first exhaustive solution to the problem of consolidation of a soil cylinder containing a central sand drain. Barron's theory enable one to solve the problem of consolidation under two conditions, namely: (i) free vertical strain assuming that the vertical surface stress remains constant and the surface displacements are non-uniform during the consolidation process; ii) equal vertical strain assuming that

¹ Associate Professor, School of Civil Engineering, Asian Institute of Technology (AIT), P.O.Box 2754, Bangkok, Thailand

² Doctoral Student, School of Civil Engineering, AIT, P.O. Box 2754, Bangkok, Thailand

³ Chair Professor, School of Civil Engineering, AIT, P.O. Box 2754, Bangkok, Thailand

FULL SCALE TEST EMBANKMENT AND PVD IMPROVEMENT

Three full scale test embankments were constructed in stages on PVD improved soft Bangkok clay at Nong Ngu Hao site up to maximum height of 4.2 m with 3:1 side slope. Later on berms were added. The test embankments were square in plan with base dimensions of 40 m by 40 m. The site is located in Samutprakan Province, about 30 km east of Bangkok, Metropolis in Thailand. The site plan of the three test embankments designated as TS1, TS2, and TS3 is shown in Fig. 1. The generalized soil profile and soil properties are shown in Fig. 2. The soil profile is relatively uniform consisting of a thin weathered crust (2 m thick) overlying very soft to soft Bangkok clay approximately 10 m thick. Underlying this soft clay layer is a medium clay layer of about 4 m thickness. A stiff clay layer underlies the medium clay and extends to a depth of 22 m below the ground surface. The profiles of strength and compressibility parameters are shown in Fig.3. Measurements of piezometric drawdown at the site were made and the values are presented in Fig. 4.

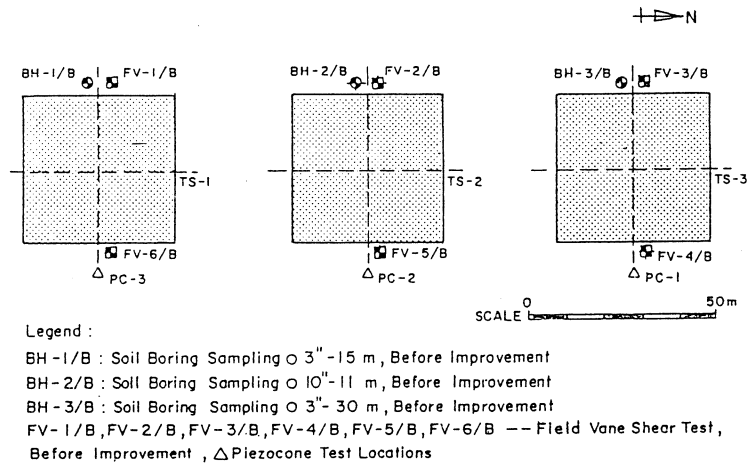


Fig. 1 Locations of Boreholes and Test Embankments.

The PVD's were installed to a depth of 12 m and were cut off so that each PVD protruded 0.25 m above the sand blanket located on top of the ground surface. The sand blanket has thickness of 1.0 m. The PVD spacing were 1.0 m, 1.2 m, and 1.5 m at TS-3, TS-2, and TS-1, respectively. The respective drains were Mebra 7007, Castle Board CS-1, and Flodrain FD4-EX. The mandrel was rectangular in cross-section with thickness of 6 mm and with outside dimensions of 120 mm by 45 mm. The rectangular shaped anchoring shoe has dimensions of 150 mm by 45 mm. The section view of PVD installed at TS-3 is shown in Fig. 5.

COMPRESSIBILITY AND FLOW PARAMETERS

the vertical surface stress is non-uniform. For the case of equal vertical strain, the differential equation governing the consolidation process is given as:

$$\frac{\partial u}{\partial t} = c_h \left[\left(\frac{\partial^2 u}{\partial r^2} \right) + \frac{1}{r} \left(\frac{\partial u}{\partial r} \right) \right] \quad (1)$$

where u is the average pore pressure at any point and any given time; r is the radial distance of the considered point from the center of the drained soil cylinder; t is the time after instantaneous increase in the total vertical stress, and c_h is the horizontal coefficient of consolidation. For the case of radial drainage only, the solution of Eq. 1 assuming ideal conditions (no smear and no well-resistance) was given by Barron (1948).

Hansbo (1979) modified the solution developed by Barron (1948) for PVD applications. The modifications dealt mainly with simplifying assumptions due to the physical dimensions, characteristics of prefabricated vertical drains, and the effects of PVD installation. The modified general expression for average degree of horizontal consolidation, U_h , is given as:

$$U_h = 1 - \exp \left(\frac{-8T_h}{F} \right) \quad (2)$$

$$T_h = \frac{c_h t}{D_e^2} \quad (3)$$

and

$$F = F_n + F_s + F_r \quad (4)$$

where F is the factor which expresses the additive effect due to the PVD spacing, F_n ; smear effects, F_s ; and well-resistance, F_r . The components of F are defined as follows:

$$F_n = \log_e (D_e/d_w) - 0.75 \quad (5)$$

$$F_s = (k_h/k_s - 1) \log_e (d_s/d_w) \quad (6)$$

$$F_r = \pi z (2L - z) k_h/q_w \quad (7)$$

where D_e is the equivalent diameter of a unit PVD influence zone, d_w is the equivalent diameter of PVD, k_h is the horizontal permeability in the undisturbed soil, k_s is the horizontal permeability of the smeared zone, z is the distance from the drainage end of the drain, L is the length of PVD for one-way drainage and is half of drain length for drainage boundary at both ends of PVD, and q_w is the discharge capacity of the PVD at hydraulic gradient of 1. Neglecting the vertical consolidation, the settlement due to radial consolidation at time t , S_t is given as:

$$S_t = S_{fc} \cdot U_t \quad (8)$$

where S_{fc} is the final consolidation settlement.

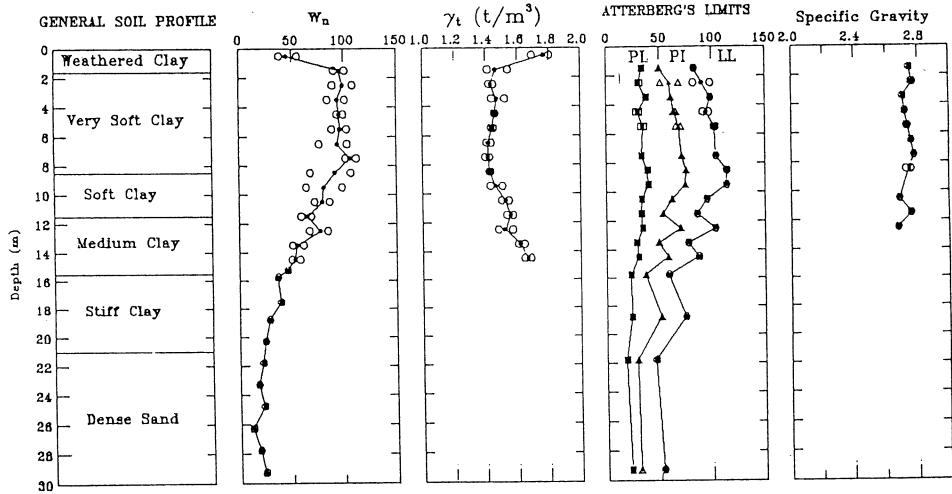


Fig. 2 Generalised Soil Profile and Properties.

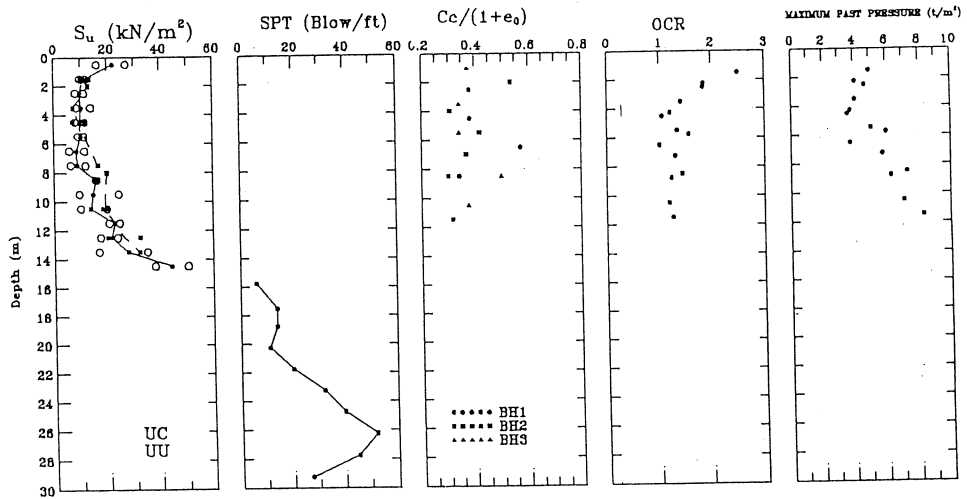


Fig. 3 Strength and Compressibility Parameters with Depth.

FIELD PERFORMANCES OF TEST EMBANKMENTS

Measurements were made on the surface and subsurface settlements, lateral movements, and excess pore pressures in the three test embankments by settlement plates, inclinometers, and piezometers, respectively. A clear trend of settlement magnitudes emerged in Fig. 6 taken from test embankment TS-3, at depth intervals 0-2 m, 0-8 m, 0-12 m and 0-16 m. A comparison of surface settlements of the three test embankments is given in Fig. 7. It is shown that the test embankment TS-3, with the

COMPRESSIBILITY AND FLOW PARAMETERS

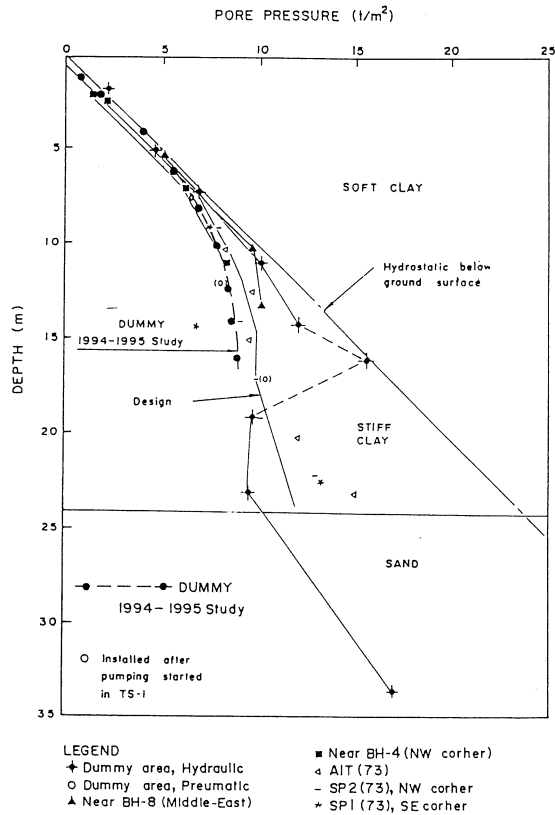


Fig. 4 Variation of Piezometric Pressures with Depth.

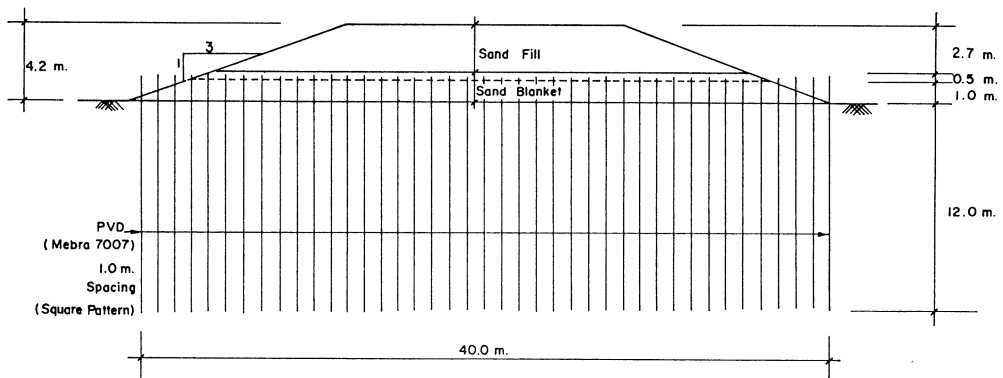


Fig. 5 Test Embankment TS3 (4.2 m. Height).

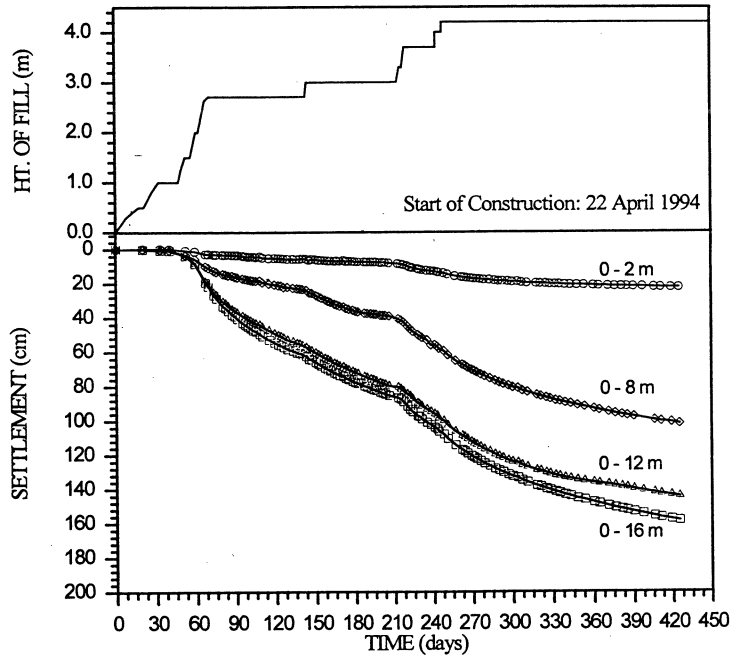


Fig. 6 Settlement of Layers of Increasing Thickness from the Ground Surface.

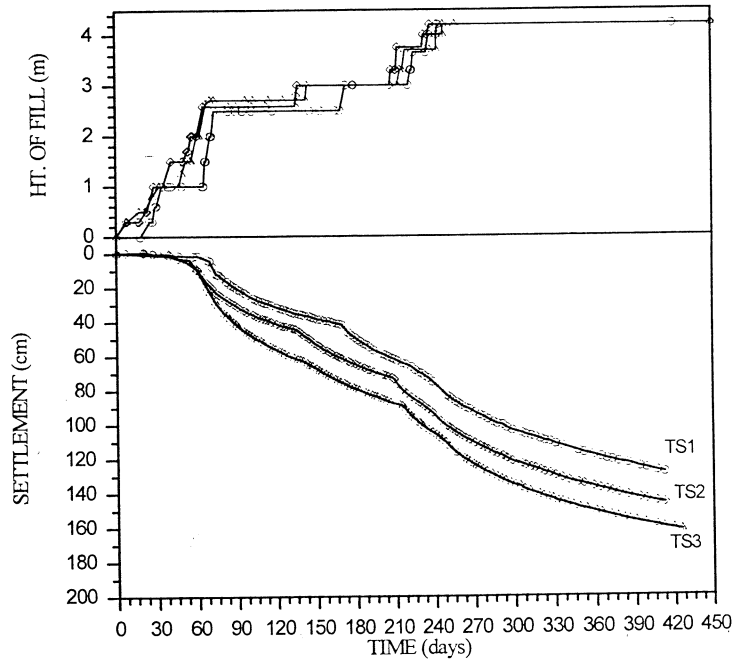


Fig. 7 Comparison of Surface Settlement in TS1, TS2 and TS3.

COMPRESSIBILITY AND FLOW PARAMETERS

closest spacing of PVD, indicates the largest settlements. The next larger settlements occurred at test embankment TS-2 with 1.2 m spacing while TS-1 with 1.5 m spacing have the lowest settlement.

Two slope indicators labelled I1 and I2 were installed in each of the three test embankments. The inclinometer I1 was located at the outermost edge of the embankment at a distance of 20 m from the center, while inclinometer I2 was installed at the shoulders of maximum fill height where the side slope of the test fill begins. The results of measurement for inclinometer I2 at TS-2 is shown in Fig. 8.

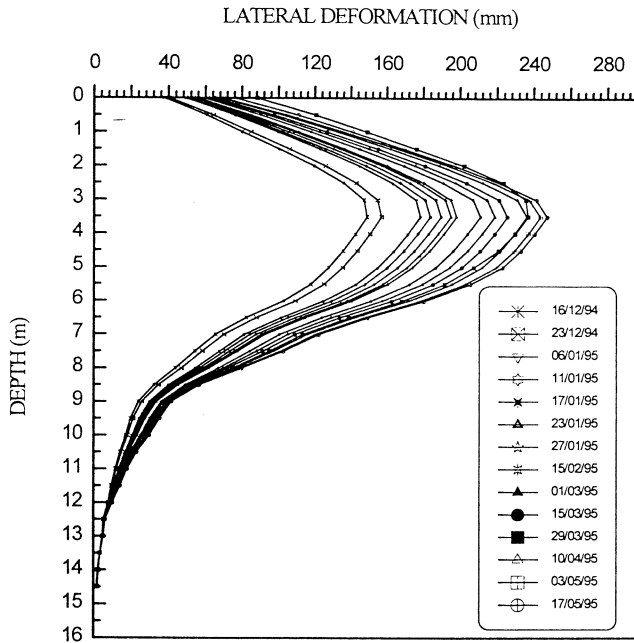


Fig. 8 Profile of Lateral Deformation with Depth for Section TS2-I2.

The total pore pressures were measured redundantly by pneumatic, hydraulic and open standpipe piezometers. All three piezometers indicate similar pattern of responses. The readings were corrected for the respective settlements of the piezometer tips. Figure 9 shows the measurements from hydraulic piezometers at test embankment TS-2.

CALCULATIONS OF COMPRESSIBILITY AND FLOW PARAMETERS

Final Settlement and Coefficient of Compressibility

Asaoka (1978) proposed a graphical method to determine the final settlements based on observational procedures. The observed time-settlement curves plotted to an

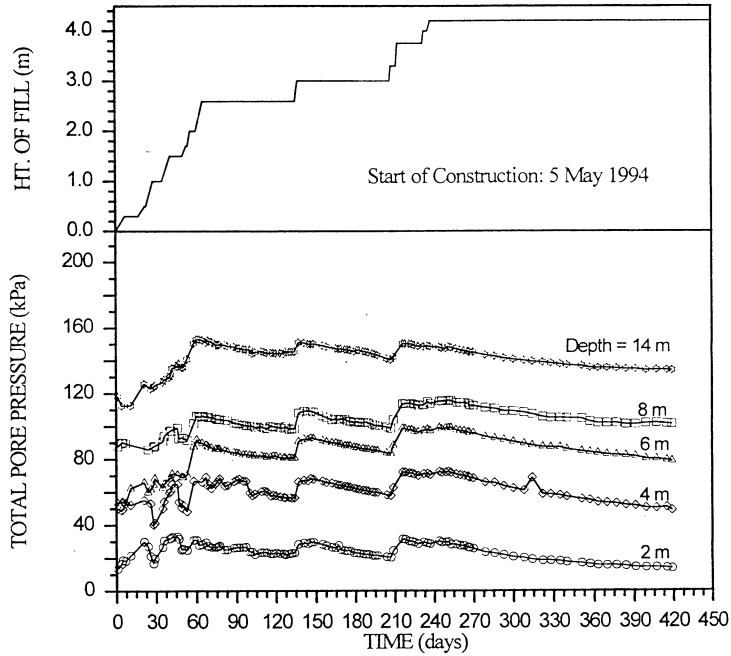


Fig. 9 Pore Pressures from Hydraulic Piezometers Corrected for Settlements (TS2).

arithmetic scale were divided into equal time intervals, Δt . The settlements S_i corresponding to t_i are read off and then the relation of $(S_i \sim S_{i-1})$ is plotted in the coordinate system as shown in Fig. 10 for test embankment TS-3 where Δt is taken as 30 days. A straight line is fitted through the points. The slope of this line is β , and its intercept with the ordinate axis is β_0 . The 45° line with $S_i = S_{i-1}$ is also plotted. The

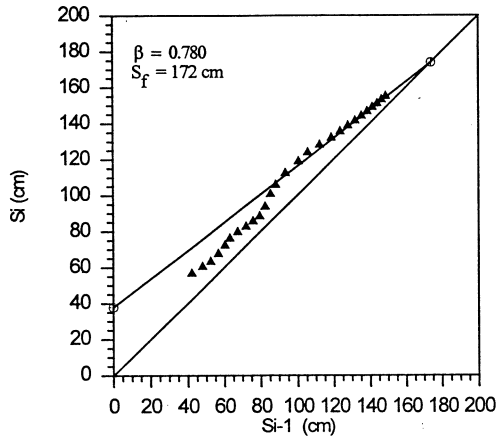


Fig. 10 Settlement Plot for Test Embankment TS3.

COMPRESSIBILITY AND FLOW PARAMETERS

point where the plotted line intersect the 45° line yields the final settlement, S_f . Subsequently, the final settlements for test embankments TS-1, TS-2, and TS-3 were obtained as 1.70 m, 1.70 m, and 1.72 m, respectively. The same magnitude of final settlements of three test embankments indicated the uniform soil profile at the test site. Similar conclusions on the uniformity of soft soils in Nong Ngu Hao site were made by NGI (1992)

The compression coefficient, m_v , can be back-calculated from the final settlement as follows:

$$m_v = \frac{\Delta H}{H (\Delta\sigma)} \quad (9)$$

where ΔH is the final settlement of the considered soil layer having thickness of H and $\Delta\sigma'$ is the increase of final effective stress. The values of ΔH can be calculated from Asaoka's method and then the corresponding values of m_v for the subsoils under test embankment TS-2 are computed and tabulated in Table 1.

The $c_h \sim q_w$ Relationship

Using Asaoka's approach for radial consolidation with the use of PVD, the horizontal coefficient of consolidation, c_h can be derived as follows:

$$c_h = \frac{(1 - \beta) D_c^2 F}{8\beta\Delta t} \quad (10)$$

where the terms have been defined previously. The value of c_h cannot be obtained directly from Eq. 10 because of the unknown value of k_h existing in the factor F as seen in Eqs. 4 and 7.

Assuming the compression coefficient in vertical direction, m_v as equal to that in horizontal direction, c_h , the following expression can be written:

Table 1 Calculated Values of Final Settlement and Coefficient of Compressibility

Soil layers	Weather crust	Soft clay	Very soft to soft clay	Soft to medium clay
Depth (m)	0-2	2-4	4-8	8-12
ΔH (m)	0.22	0.24	0.72	0.30
m_v ($10^{-3}m^2/kN$)	1.47	1.60	2.40	1.00

$$k_s = m_v c_h \gamma_w \quad (11)$$

Substituting for k_h from Eq. 11, for F using Eqs. 5, 6, and 7 into Eq. 10, the following equation can be derived:

$$c_h = \frac{F_n + F_s}{C_1 - \frac{C_2}{q_w}} \quad (12)$$

where :

$$C_1 = \frac{8\beta\Delta t}{(1-\beta)D_e^2} \quad (13)$$

$$C_2 = \pi z (2L - z) m_v \gamma_w \quad (14)$$

Equation 12 consists of four unknowns: k_h/k_s , d_s/d_w , q_w , and c_h . Hence, the back-calculated values of c_h will be dependent on the assumed values of the other three unknowns. Furthermore, by assuming the diameter of the smeared zone, d_s , as twice as equivalent diameter of the mandrel as suggested by Hansbo (1987) and confirmed for soft Bangkok clay by Bergado et al (1991), the relationship between c_h and q_w can be obtained for different values of the smear ratio, k_h/k_s .

From the measured settlements, the β values together with final settlements for the soft clay layer at depth interval from 4 m to 8 m under test embankments TS-1, TS-2, and TS-3 were obtained as illustrated in Figs. 11 to 13, respectively, in which the time interval, Δt , of 30 days was used. Using the aforementioned assumptions of d_s and k_h/k_s and the other parameters as tabulated in Table 2, the ($c_h \sim q_w$) relationships for different ratios of k_h/k_s are plotted in Figs. 14 to 16 for the corresponding embankments

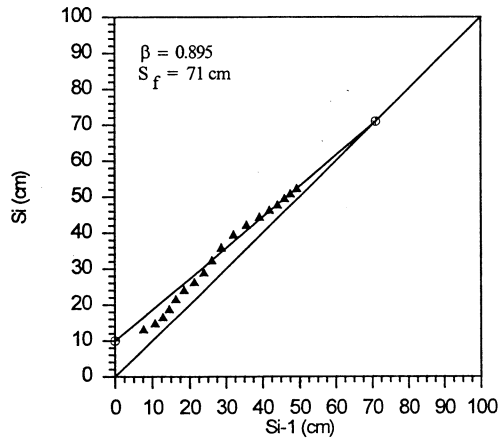


Fig. 11 Settlement Plot for 4-8 m Depth Interval of TS1.

COMPRESSIBILITY AND FLOW PARAMETERS

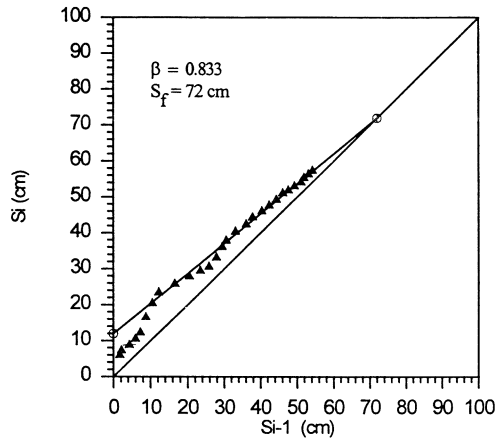


Fig. 12 Settlement Plot for 4-8 m Depth Interval of TS2.

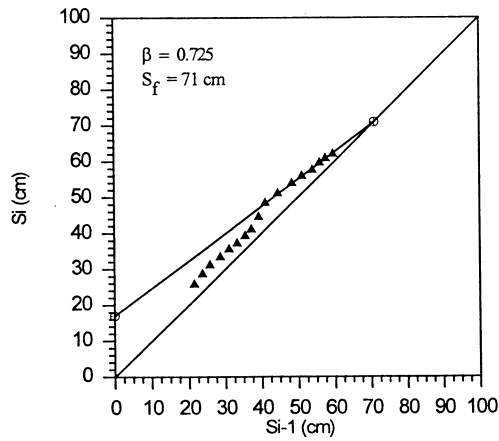


Fig. 13 Settlement Plot for 4-8 m Depth Interval of TS2.

Table 2 Data for PVD Used in Three Test Embankments

1. Dimensions of PVD	a = 0.004 m
	b = 0.100 m
	$d_w = 0.052$ m
2. Dimensions of Mandrel	$a_m = 0.045$ m
	$b_m = 0.150$ m
	$d_m = 0.046$ m
3. Assumed Diameter of Smear Zone	$d_s = 2d_m = 0.093$ m

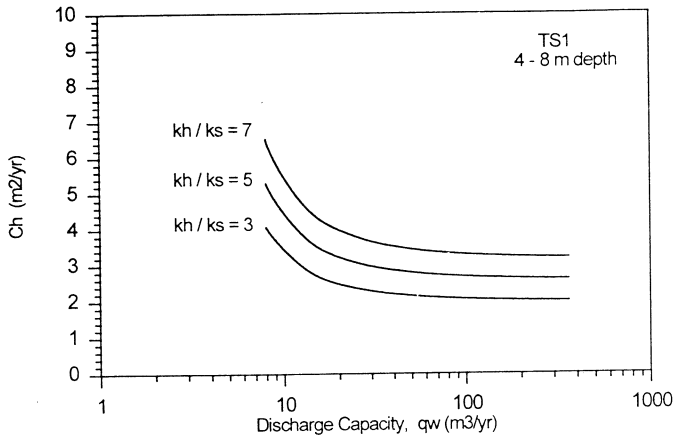


Fig. 14 Back-Calculated c_h - q_w Relations for TS1 Test Embankment.

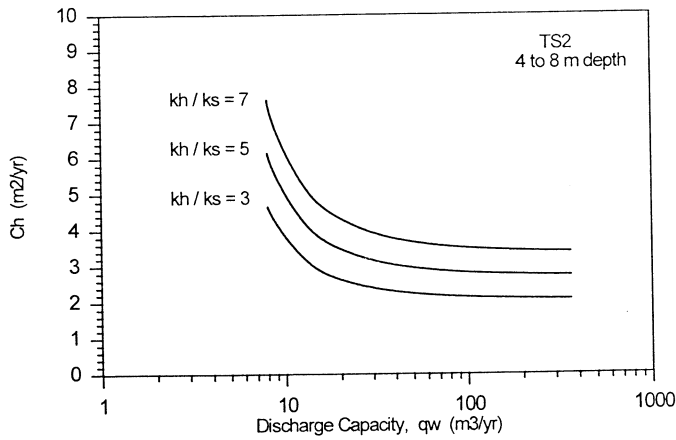


Fig. 15 Back-Calculated c_h - q_w Relations for TS2 Test Embankment.

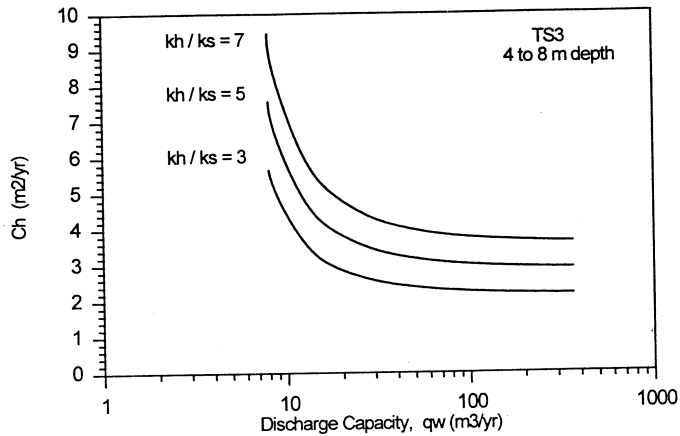


Fig. 16 Back-Calculated c_h - q_w Relation for TS3 Test Embankment.

COMPRESSIBILITY AND FLOW PARAMETERS

Table 3 Back-Calculated Results of $c_h \sim q_w$ Relationship

q_w (m^2/yr)	Embankment TS1			Embankment TS2			Embankment TS3		
	c_h (m^2/yr)			c_h (m^2/yr)			c_h (m^2/yr)		
	$k_h/k_s = 3$	$k_h/k_s = 5$	$k_h/k_s = 7$	$k_h/k_s = 3$	$k_h/k_s = 5$	$k_h/k_s = 7$	$k_h/k_s = 3$	$k_h/k_s = 5$	$k_h/k_s = 7$
4	-66.9	-87.0	-107.1	-16.3	-21.5	-26.7	-8.8	-11.8	-14.7
5	11.2	14.6	18.0	20.4	26.9	33.4	394.4	526.7	659.0
6	6.3	8.2	10.1	8.2	10.8	13.4	12.5	16.7	20.9
7	4.8	6.3	7.7	5.7	7.5	9.4	7.4	9.9	12.4
8	4.1	5.3	6.5	4.7	6.1	7.6	5.7	7.6	9.5
15	2.7	3.5	4.4	2.9	3.8	4.8	3.2	4.3	5.4
30	2.3	3.0	3.7	2.4	3.2	3.9	2.6	3.4	4.3
45	2.2	2.8	3.5	2.3	3.0	3.7	2.4	3.2	4.0
60	2.1	2.8	3.4	2.2	2.9	3.6	2.3	3.1	3.9
90	2.1	2.7	3.3	2.1	2.8	3.5	2.3	3.0	3.8
180	2.0	2.6	3.2	2.1	2.8	3.4	2.2	2.9	3.7
360	2.0	2.6	3.2	2.1	2.7	3.4	2.2	2.9	3.6

TS-1, TS-2, and TS-3, respectively. The calculated results are also tabulated in Table 3.

Based on the physical condition that the coefficient of consolidation, c_h , cannot be negative, the minimum field values of the discharge capacity, q_w , must be greater than $4 m^3/year$ as seen in Table 3. Moreover, Figures 14 to 16 indicated that the calculated c_h values become little affected by the value of discharge capacity when q_w is greater than $30 m^3/year$. Also seen in these figures is the minimum value of c_h cannot be smaller than $2 m^2/year$ if the ratio k_h/k_s is greater or equal to 3.

The back-calculated value of c_h are dependent significantly on the effects of smear. Assuming $k_h/k_s = 5$ and $d_s/d_m = 2$, the β , F , and the average c_h values for a depth interval of 0 -12 m, have been calculated and tabulated in Table 4 for a certain assumed value of q_w of $30 m^3/year$. The corresponding c_h values for the soil profile are given in Table 5. These calculated values can be compared directly with the field values measured by piezocone and piezoprobe tests as presented in Table 6 and Fig. 17. There is an excellent agreement between back-calculated and field values of c_h .

Table 4 Calculated Values of β , F , and c_h for Depth Interval of 0-12 m

Embankment	β	F	c_h ($m^2/year$)
TS1	0.865	6.24	4.2
TS2	0.800	5.98	4.1
TS3	0.725	5.77	4.2

Table 5 Back-Calculated Values of c_h for Subsoils Under TS2 Embankment

Subsoil Layer	Weathered crust	Soft clay	Very soft to soft clay	Soft to medium clay
Depth (m)	0-2	2-4	4-8	8-12
c_h ($m^2/year$)	4.0	3.1	3.0	7.8

Table 6 Values of c_h from Piezocone Tests ($m^2/year$)

Depth (m)	PC-1	PC-2	PC-3
4	3.3	4.4	3.8
8	4.3	4.7	4.2
12	8.8	7.9	7.1

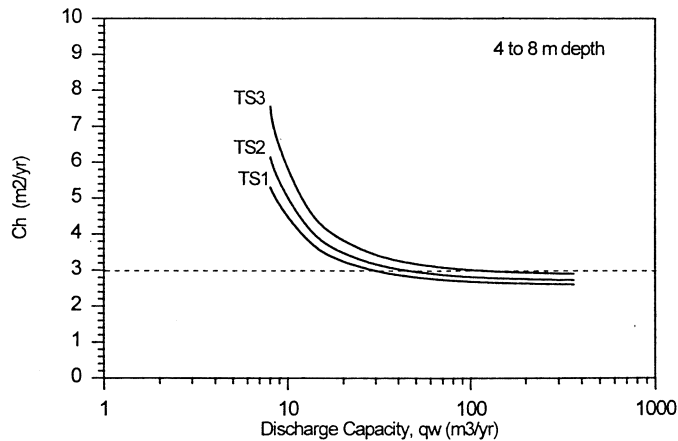


Fig. 17 Comparison of c_h - q_w Relations of Three Test Embankments TS1, TS2 and TS3 Using the Same Value of Smear Ratio, $k_h/k_s = 5$.

The final settlements for the very soft clay layer from 4 to 8 m depth were obtained to be 0.71 m, 0.72 m, and 0.71 m for TS-1, TS-2 and TS-3, respectively, as demonstrated in Figs. 11, 12, and 13. These values again confirmed the uniformity of the soil profiles under these test embankment. Thus, the same values of c_h can be assumed for all three sites. If the $k_h/k_s = 5$ is assumed, and if taking $c_h = 3 m^2/yr$ as obtained from the piezoprobe tests by Moh and Woo (1987) for the subsoil at the depth interval of 4 m to 8 m, then the discharge capacities of 30, 45, and 90 m^3/yr can be obtained by Fig. 18 for PVDs at TS-1, TS-2, and TS-3, respectively.

COMPRESSIBILITY AND FLOW PARAMETERS

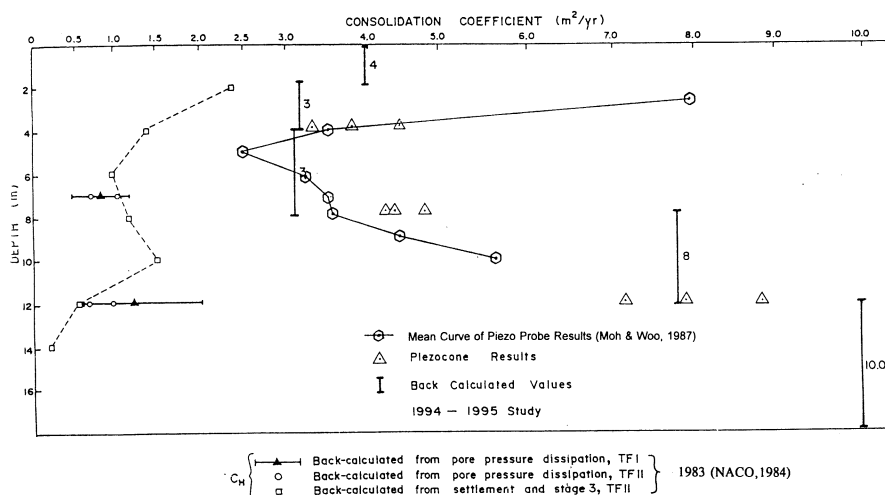


Fig. 18 Comparison of c_h Values Computed from TS2 with the values obtained from 1983 Test Embankment with Sand Drains and the 1994 Piezocone Tests.

COMPARISON OF PVD PERFORMANCE WITH SAND DRAINS IN 1983

In 1983, a field test program was carried out at Nong Ngu Hao site (NACO, 1984). The purpose of the trial test was to determine the effect of using non-displacement type of sand drains for accelerated consolidation of soft clay. The test program included three test areas, one with surcharge fill, and the others with vacuum loading as well as ground water lowering. Difficulties were encountered in maintaining vacuum loading. Thus, only the embankment with surcharge loading was reliable. The pore pressure dissipation in 1983 test fill was lower than the dissipation noted in the present study. As shown in Fig. 18, the c_h values obtained from the current study are much higher than the back-calculated c_h values in 1983 study. As demonstrated in Figs. 14 to 16, it can be seen that the underestimation of smear effects and/or overestimation of the discharge capacity will lead to the underestimation of c_h value. It is thought that the smear effects were ignored in the back-calculated values of the 1983 study.

CURRENT RECOMMENDED VALUES OF DISCHARGE CAPACITY

A wide range of discharge capacity, q_w , values have been specified for proper functioning of vertical drains. Kremer et al (1982) stated that the minimum vertical discharge capacity must be $160 \text{ m}^3/\text{yr}$ under a hydraulic gradient of 0.625 applied across a 400 mm drain length and subjected to a confining pressure of 100 kPa. Jamiolkowski et al (1983) concluded that based on the laboratory data and actual experiences, for an acceptable quality of drain, q_w , should be at least 10 to $15 \text{ m}^3/\text{yr}$

at a lateral stress range of 300 to 500 kPa for drains of 20 m long. Holtz et al (1989) recommended the discharge capacity to be 100 to 150 m³/yr for 15 to 25 m long drains with horizontal permeability, k_h , of 10^{-7} cm/sec. Hansbo (1987) suggested that the proper values of q_w must be 50 to 100 m³/yr. A summary of the recommended discharge capacities are tabulated in Table 7. In this regard, the back-calculated values of discharge capacity obtained from test embankments TS-1, TS-2 and TS-3 are at the lower bound of values in Table 6. Values of maximum flow rates estimated from field measurements vary from 7.88 m³/yr (De Jager and Oostveen, 1990) to 52.56 m³/yr (Lawrence and Koener, 1988). Thus, the discharge capacity values calculated in this study have been confirmed to agree within the range of other investigators. This result is confirmed by the laboratory results shown in Fig. 19 a,b wherein the PVD type

Table 7 Current Recommended Values for Specification of Discharge Capacity

Sources	Values	Lateral stress (kPa)
JAMIOLKOWSKI <i>et al.</i> (1983)	10-15	500-300
DEN HOEDT (1981)	95	50-300
KREMER <i>et al.</i> (1982)	256	100
KREMER (1983)	790	15
HANSBO (1979)	50-100	Not given
RIXNER <i>et al.</i> (1986)	100	Not given
VAN ZANTEN (1986)	790-1580	150-300
HOLTZ <i>et al.</i> (1989)	100-150	500-300
LAWRENCE & KOERNER (1988)	150	Not given
KODA <i>et al.</i> (1984)	100	50
DE JAGER <i>et al.</i> (1990)	315-1580	150-300

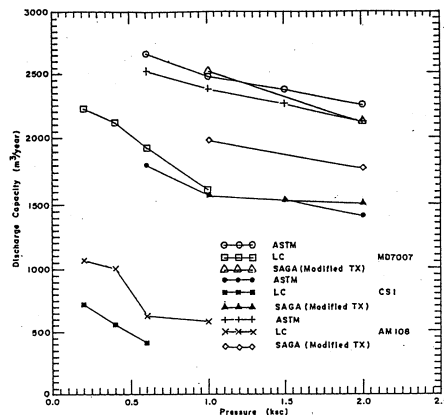


Fig. 19 (a) Discharge Capacity (with Varying Lateral Pressures).

COMPRESSIBILITY AND FLOW PARAMETERS

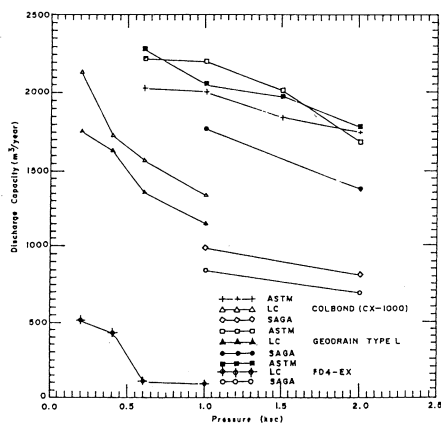


Fig. 19 (b) Discharge Capacity (with Varying Lateral Pressures).

COMPRESSIBILITY AND FLOW PARAMETERS

installed at TS-1 registered the lowest discharge capacity using large consolidometer (LC) in which clay slurry surrounded the PVD specimen. The other results shown in this figure were obtained following the procedures by ASTM and modified triaxial.

Manivannan (1995) has calculated the values of the required discharge capacity, q_{req} , using the approach recommended by Kamon et al (1984) and Pradhan et al (1991). The required discharged capacity values are plotted against the length of PVD with varying c_h values with n values equal to 20, 25, and 30 in Figs. 20 to 22, respectively, where n is the ratio of D_e and d_w . It can be observed that q_{req} decreases as drain spacing (and n) increases. This is attributed to the increase in consolidation time as drain spacing increases. The time (t_{90}) required for 90% degree of consolidation of the soft clay ground have been calculated and plotted against n in Fig. 22. Based from these figures, the specification criterion of discharge capacity can be established. For c_h value of $4 \text{ m}^2/\text{yr}$ and PVD length of 12 m, the required discharge capacity to be used should be $35 \text{ m}^3/\text{yr}$ and $22 \text{ m}^3/\text{yr}$ for n equals 20 and 30, respectively.

CONCLUSIONS

The successful predictions on the behavior of PVD improved soft ground depend very much on the design parameter used. Reliable compressibility and flow parameters can be obtained from back-analyses of full scale load tests. Three full scale test embankments were constructed for preloading on PVD improved soft Bangkok clay. The PVD spacings in each embankment were 1.0, 1.2, and 1.5 m on square pattern. The PVDs were installed down to 12 m below the ground surface. The test embankments were 40 m by 40 m dimensions at the base and were constructed to 4.2 m high. There

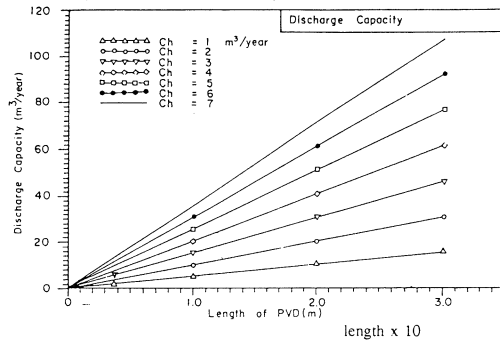


Fig. 20 Discharge Capacity, q_{req} (with Smear Effect for $n = 20$).

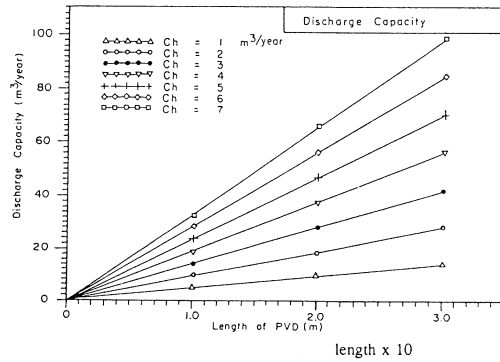


Fig. 21 Discharge Capacity, q_{req} (with Smear Effect for $n = 25$).

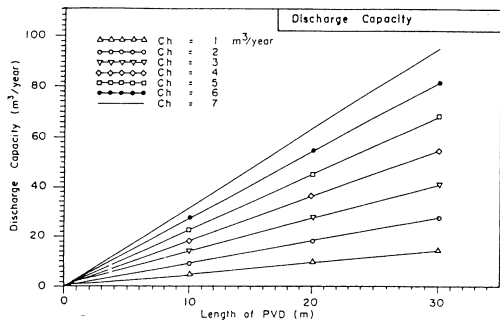


Fig. 22 Discharge Capacity, q_{req} (with Smear Effect for $n = 30$).

is clear trend of settlement with depth and with spacing of PVD. The observational method by Asaoka was applied for calculating the flow and compressibility parameters. The c_h values as calculated using Asaoka's method considering smear effects were found to agree well with those obtained from field piezocone tests. An average c_h value

COMPRESSIBILITY AND FLOW PARAMETERS

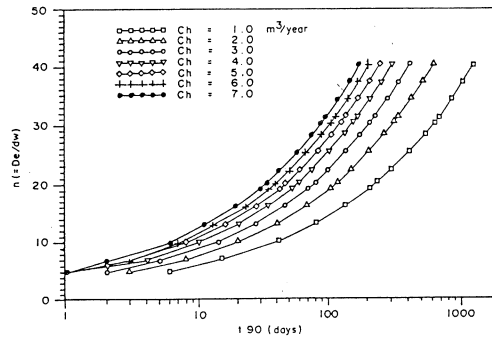


Fig. 23 Values of t_{90} versus n (different c_h Values).

of 4 m²/year was obtained. The values of discharge capacity, q_w , were calculated corresponding to each test embankment. The required discharge capacity decreased with PVD spacing due to corresponding increase of consolidation time. For a given c_h value, length of PVD and PVD spacing, the discharge capacity was computed. This value agreed within the range obtained by the other investigators.

REFERENCES

- ASAOKA, A.(1978). "Observational procedure for settlement prediction". *Soils & Found.* 18, No. 4, pp. 87-101.
- BARRON, R.A. (1948). "Consolidation of fine-grained soils by drain well"., *Trans. ASCE*, 124, pp. 709-739.
- BERGADO, D.T., ASAKAMI, H., ALFARO M. C. and BALASUBRAMANIAM A.S.(1991). "Smear effects of vertical drains on soft Bangkok Clay". *J. Geotech. Eng. Div.*, ASCE, Vol 117, No. 10, pp. 1509-29.
- DE JAGER, W.F.J. and OOSTVEEN, J. P. (1990). "Systematic quality control of vertical drainage". *Proc. 4th Int. Conf. on Geotextiles, Geomembranes and Related Products*, The Hague, pp. 321-26.
- DEN HOEDT, G. (1981). "Laboratory testing of vertical drains". *Proc. 10th Int. Conf. on Soil Mech. and Found. Eng.*, Stockholm, Vol.1, pp. 627-30.
- HANSBO, S. (1979). "Consolidation of clay by band-shaped prefabricated drains". *Ground Eng'g.*, Vol. 12, No. 5, pp. 16-25.
- HANSBO, S. (1987). "Design aspects of vertical drains and lime column installations". *Proc. 9th Southeast Asian Geotech. Conf.*, Bangkok, Thailand, pp. 8-1 to 8-12.
- HOLTZ, R. D., JAMIOLKOWSKI, M., LANCELLOTA, R. and PEDRONI, S. (1989). "Behavior of bent prefabricated vertical drains". *Proc. 12th Intl. Conf. Soil Mech. and Found. Eng.*, Rio de Janeiro, Brazil, Vol. 3, pp. 1657-60.

- JAMIOLKOWSKI, M., LANCELLOTA, R. and WOLSKI, W.(1983). "Summary of discussion to specialty session 6". *Proc. 8th European Conf. on Soil Mech. and Found. Eng.*, Volume 3, Helsinki, Finland.
- KAMON, M., PRADHAN, B.S. and SUWA, S. (1984). "Laboratory evaluation of the prefabricated band shaped drains soil improvement". *Current Japanese Materials Research*, Volume 9, University Press, Cambridge, Mass., U.S.A.
- KODA, E., SZYMANSKI, A. and WOLSKI, W.(1984). "Laboratory tests on Geodrains durability in organic soils". *Seminar on Laboratory Testing of Prefabricated Band-Shaped Drains*, Milano, Italy.
- KREMER, R. (1983). "Discussion to specialty session 6". *Proc. 8th European Conf. on Soil Mech. and Found. Eng.*, Volume 3, Helsinki, Finland, pp. 1235-37.
- KREMER, R., DE JAGER, W., MAAGDENBERG, A., MEXVOGEL, I. and OOSTVEEN, J. (1982). "Quality standards for vertical drains". *Proc. 2nd Int. Conf. on Geotextiles*, Las Vegas, USA, Vol. 2, pp. 319-24.
- LAWRENCE, C. A. and KOERNER, R. M.(1988). "Flow behavior of kinked strip drains geosynthetics for soil improvement". *ASCE Geotechnical Special Publication*, No.18, pp. 22-35.
- MANIVANNAN, (1995). "Systematic review and proposal for specifications criteria for prefabricated vertical drain (PVD) on soft Bangkok clay." *M. Eng. Thesis*, Asian Institute of Technology, Bangkok, Thailand.
- MOH, Z.C. and WOO, S.M. (1987). "Preconsolidation of Bangkok clay by non-displacement sand drains and surcharge." *Proc. 9th Southeast Asian Geotech. Conf.*, Bangkok, Thailand, pp. 8-171 to 8-184.
- NGI (1992), "Independent soil engineering study for Second Bangkok Intl. Airport implementation program". *Final Report Submitted to the Airport Authority of Thailand*.
- PRADHAN, T.B.S., KAMON, M. AND SUWA, S. (1991). "A design method for the evaluation of discharge capacity of prefabricated band shaped drains." *Proc. 9th Asian Regional Conf.*, Bangkok, Thailand, pp. 523-526.
- RIXNER, J.J., KRAEMER, S.R. and SMITH, A. D. (1986). "Prefabricated vertical drains". Vol 1, *Engineering Guidelines*, FHWA/RD-86/168, Federal Highway Administration, Virginia, 107 pp.
- VAN ZANTEN, R. V. (1986). "The guarantee of the quality of vertical drainage systems". *Proc. 3rd Int. Conf. on Geotextile*, Volume 2, Vienna, Austria, pp. 651-55.

INTERACTIVE BEHAVIOR OF CYLINDRICAL ANCHORS IN DENSE SAND

H. J. Liao¹, J. K. Chen², and S. C. Shu³

SYNOPSIS

Aluminum model anchors were used to study the independent and interactive uplift behavior of cylindrical anchor in dense sand. A critical depth of 6D-8D was found to distinguish a shallow anchor from a deep anchor. The behavior of the former is mainly controlled by the shaft resistance while the latter is controlled by the end resistance. But the peak values of the shaft resistance and the end resistance do not occur simultaneously for shallow and deep anchors. During loading, a void is formed beneath the uplifting anchor. This void has a great effect on the residual shaft resistance but it has little effect on the end resistance if the void can be kept some distance (4D) away from the top of the cylindrical anchor. A horizontal spacing of 9D is needed to keep be anchor from influencing other anchors. Based on the model test results, the boundary of anchor interference around the anchor is established for deep cylindrical anchors.

INTRODUCTION

The anchorage resistance of a ground anchor comes from the shaft resistance and the end resistance of the fixed anchor length (Fig. 1). However, due to the possibility of progressive failure that may occur along the shaft of the fixed anchor length, it is not recommended by most of the major anchor specifications (BSI 1989, FIP 1982, DIN 1988, and AASHTO 1992) to increase the fixed length beyond a certain limit. Instead, it is advised to increase the anchorage capacity by underreaming some portions of the fixed anchor length, especially if there is a limitation on the anchor length. However, when the anchors are used as the tieback system for a basement excavation in alluvial soil, they are normally closely spaced due to the relatively low anchorage capacity of each soil anchor. Although a minimum spacing between anchors of 4 times the anchor diameter is commonly recommended for shaft anchors, no guidelines are available to determine the minimum anchor spacing for underreamed anchors. Since the anchorage mechanism of the underreamed anchor is not the same as that of the shaft anchor, the minimum anchor spacings suitable for the shaft anchor is not expected to be applicable to the underreamed anchor.

¹ Professor, Department of Construction Engineering, National Taiwan Institute of Technology, P.O. Box 90-130, Taipei, Taiwan, R.O.C.

² Former Graduate Student, Department of Construction Engineering, National Taiwan Institute of Technology, P.O. Box 90-130, Taipei, Taiwan, R.O.C.

³ Associate Professor, Department of Construction Engineering, National Taiwan Institute of Technology, P.O. Box 90-130, Taipei, Taiwan, R.O.C.

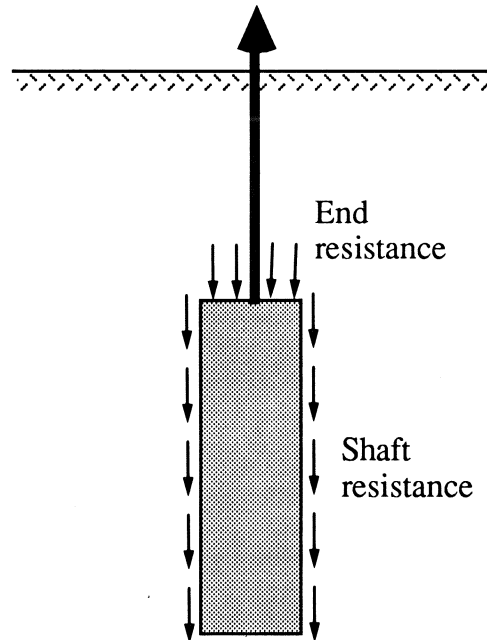


Fig. 1 Resistances Acting on the Uplifting Cylindrical Anchor

Most of the research efforts on the interactive behavior between the underreamed anchors have concentrated on plate anchors (Hanna et al. 1972, and Larnach & MacMullan 1975). However, since the plate anchor can only provide the end resistance, it is not an ideal shape for the anchor from a practical point of view. As a matter of fact, it is better to install a cylindrical shape anchor which can not only generate end resistance but also provide some shaft resistance along the fixed length of anchor. To further understand the behavior of the cylindrical anchor, a series of laboratory model tests in dense sand has been performed and the individual as well as the interactive behavior of the cylindrical anchors has been evaluated. Finally, the minimum spacing which allows the neighboring anchors to be free of the group interaction effect is proposed for the cylindrical anchor.

LABORATORY TEST PROGRAM

In theory, the length-to-diameter (L/D) ratio of the mechanically underreamed cylindrical anchor can be varied as much as needed (Liao & Ou, 1990). However, it was found during the pilot study that L/D ratios ranging between 2 to 4.5 were the optimum anchor dimensions to generate an adequate ratio between the end resistance and the shaft resistance of the anchorage body. Field experience has shown that it is not cost-effective to construct an underreamed body which has a L/D ratio more than

INTERACTIVE BEHAVIOR OF CYLINDRICAL ANCHORS

4.5 given the additional construction time needed and the limited gain in the anchorage capacity. So, the underreamed anchor body with an L/D ratio equal to 4.5 was chosen for the laboratory tests.

The model anchor for the laboratory test was made of aluminum tube which had a diameter of 7.6 cm and a length of 34.2 cm. To make sure that failure did not initiate along the soil-shaft interface, the surface of the shaft was corrugated to better represent the surface condition of the mechanically underreamed anchor in the field. Load cells were mounted on top of the anchor and inside of the anchor to measure the end resistance and the pull out resistance of the anchor during uplift loading. The model anchor was placed in a sand filled tank which had the dimensions of 170 cm : 100 cm : 120 cm (length : width : height) (Fig. 2). To minimize the boundary effect on the anchorage behavior, the minimum distance between the model anchor and the side

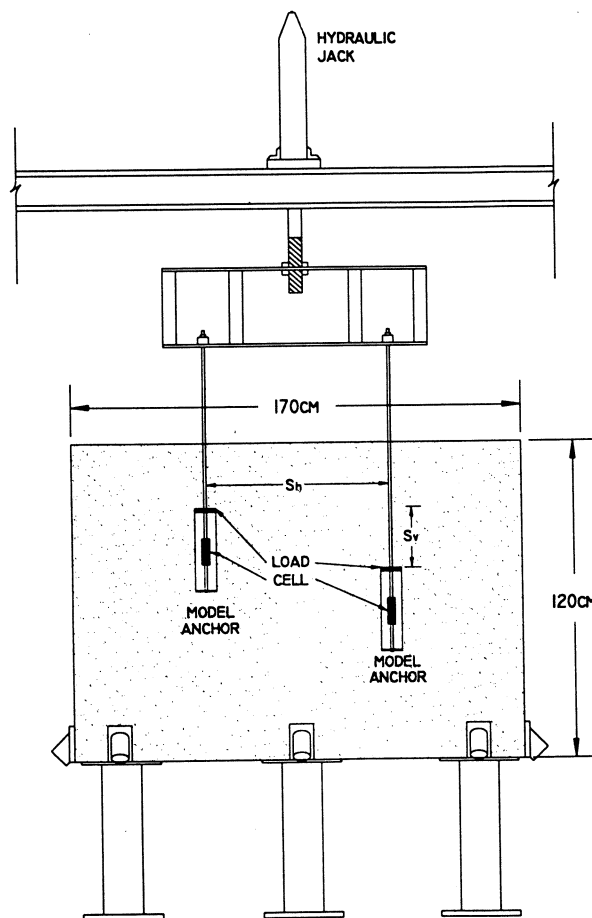
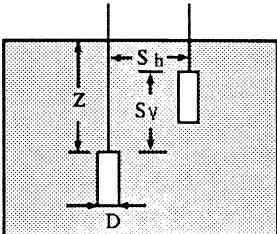


Fig. 2 Schematic Diagram of Testing Apparatus

Table 1 Depth and Spacing of Test Anchors

		Z/D		S_h/D	S_v/D			
Single anchor		0.5						
		2.5						
		4						
		4.5						
		5.0						
		6.0						
		10.0						
Paired anchor	Horizontally spaced	4		2	-			
				4				
				7				
				10				
	Vertically spaced	10		2	-			
				4				
				8				
				10				
		Upper	Lower					
				4.5		10	1	5.5
2.5	10			1	7.5			
0.5	10			1	9.5			
4.5	10			3	5.5			
2.5	10	3	7.5					

wall of the tank was kept at least 6 times the anchor diameter. Depending on the embedded depth and the anchor spacing required, the anchor was placed at different locations of the tank (Table 1). Anchors tested as the independent anchor, were placed at depths varying from 0.5 to 10 times the anchor diameter. Anchors tested as a pair, they were placed at different vertical spacings ($5.5 D \sim 9.5 D$, top-to-top) and horizontal spacings ($1 D \sim 10 D$, center-to-center) (Table 1). The behavior of anchors tested as a pair was then compared with that of the independent anchor and the interaction effect on the anchor behavior was evaluated.

INTERACTIVE BEHAVIOR OF CYLINDRICAL ANCHORS

The sand used in this study has the effective size (D_{10}) of 0.13 mm, D_{30} of 0.2 mm, D_{60} of 0.31 mm, the coefficient of uniformity (C_u) of 2.38, and the coefficient of curvature (C_c) of 1.094. The maximum and minimum dry densities are equal to 17.7 kN/m³ and 13.9 kN/m³, respectively. Since it is essential to maintain the same soil properties for each test, a raining method was adopted to prepare the test sand. During specimen preparation, sand particles were allowed to free fall into the test tank from a perforated plate which was mounted 0.9 m above of the sand surface. Sand was filled into the tank layer by layer at 50 mm lifts. The raining process was terminated when the predetermined depth of model anchor was reached. The model anchor was carefully placed on the sand surface. After the model anchor was located in position, the sand raining process was resumed. The properties of the sand specimen prepared with this raining method had very high reproducibility. A dry density of 16.4 kN/m³ and a relative density of 71 % was obtained. The peak and residual friction angles determined from the direct shear test are equal to 40 degrees and 33.5 degrees, respectively.

There was some concern that the model anchor embedded in the raining prepared sand may not be representative of the anchor installed in the field. To address this, the effect of the field placement techniques on the subsequent behavior of the anchor was evaluated in terms of change in lateral earth pressure. Basically, the construction of an underreamed anchor is carried out by the following steps: borehole drilling, cement grouting, and curing. Inevitably, some disturbances caused by the anchor installation may occur to the surrounding soil. During borehole drilling, the sand around the borehole is subjected to lateral unloading. However, when the cement grout is injected into the borehole, sand is pushed back to some extent by the cement grout. After curing, cement grout may be subject to about 0.1 % shrinkage in volume. So, the sand is laterally unloaded again. The effect of the above process has been simulated numerically (Shu, 1996). If only the change in lateral pressure is considered, the pull out resistances between anchors constructed in the field and those prepared in the laboratory are virtually the same. This shows that the raining method is one of the most suitable ways to prepare the sand for laboratory model anchor testing.

After the sand and the anchor were placed in the test tank, the anchor was uplifted vertically with the load frame shown in Fig. 2 at a rate of 3 mm/min. The load acting on the shaft of the cylindrical anchor was determined by subtracting the load measured at the top of the anchor from the overall pull out resistance. During the uplift loading, the pull out resistance, the end resistance, and the anchor movement were recorded simultaneously with a data logger.

BEHAVIOR OF INDEPENDENT ANCHOR

The behavior of independent anchor was studied in terms of the pull out resistance, the end resistance and the shaft resistance. However, the literature (Meyerhof & Adam 1968, Vermeer & Sutjiadi 1985, Mitsch & Clemence 1985, and Su & Fragaszy 1988) has shown that the anchorage behavior is significantly affected by the embedded

depth. So, the effect of embedded depth on the independent behavior of cylindrical anchor was also evaluated.

Pull Out Resistance

The laboratory test results confirm that the cylindrical anchor behaves quite differently as the shallow anchor when compared with a deep anchor. For anchors with the embedded depth (Z) of $4D$, the pull out resistance - displacement curve reaches a distinct peak value at small displacement ($\sim 10\% D$) (Fig. 3). But the pull out resistance decreases quite rapidly to a residual value as the anchor moves further. In comparison, for anchors embedded at a depth of $10D$, there is no obvious peak value on the pull out resistance - displacement curve (Fig. 4). If an anchor has a distinct peak pull out resistance, it is classified as a shallow anchor in this paper. If it has no clear peak pull out resistance, it is classified as a deep anchor. For the test sand used, the critical depth which distinguishes the shallow anchor from the deep anchor was about $6 \sim 8D$.

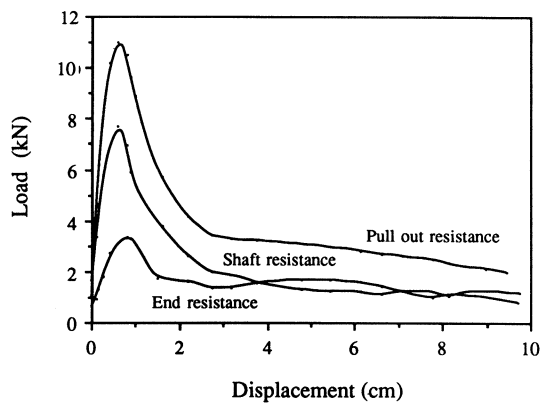


Fig. 3 Test Results of Shallow Anchor ($Z/D = 4$)

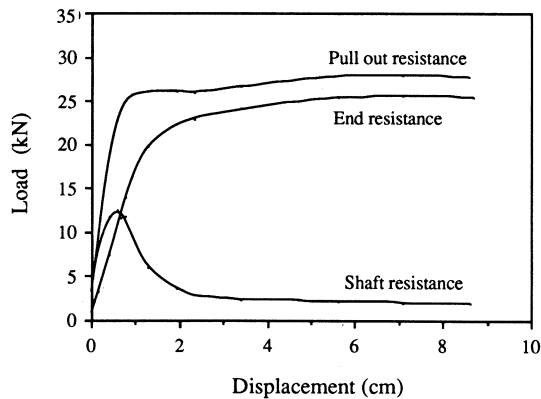


Fig. 4 Test Results of Deep Anchor ($Z/D = 10$)

End Resistance

The development of end resistance with the anchor displacement is rather different between the shallow and the deep anchors. For deep anchors, the end resistance reaches a value considerably larger than the peak shaft resistance. After the end resistance reaches its ultimate state, a steady resistance is maintained. No significant drop in the end resistance is observed (Fig. 4). The results show that an end bearing zone has been fully developed above the uplifted anchor. However, if the anchor is shallowly embedded, then there is not sufficient volume of soil above the anchor for the end bearing zone to fully develop. So, the end resistance of the shallow anchor is smaller than that of the deep anchor. However, the end resistance increases quite rapidly with depth before a critical depth of about 7 D is reached. Beyond this critical depth, the end resistance increases almost linearly with embedded depth (Fig. 5).

To understand the range of influence induced by the uplifting anchor, a numerical study was carried out on an anchor with a diameter of 50 mm, length-to-diameter ratio of 5 and embedded depth-to-diameter ratio of 8. This anchor was placed in a sand with relative density of 70 %. The soil model used is capable of simulating the strain softening and the volume dilatancy behaviors of sand (Shu, 1996). The calculated vertical stress around the anchor at peak pull out resistance is shown in Fig. 6. The sand just above the anchor was subjected to a significant stress concentration. But the vertical stress remains virtually unchanged for sand at some distance away from the anchor. Vertically, the vertical stress for sand located four times the anchor diameter above the anchor is not affected by the uplifting anchor. Horizontally, the sand located beyond five times the anchor diameter from the center line of anchor also shows no increase in vertical stress. This indicates that the zone influenced by an uplifting anchor is around 4D above the top of anchor and 5D horizontally away from the anchor.

Due to the void forming below the cylindrical anchor, the soil around the bottom of the anchor is undergoing some kind of stress relaxation (Fig. 6). The end resistance

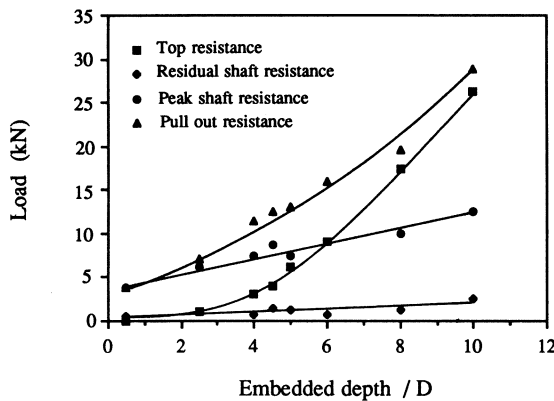


Fig. 5 Anchor Resistances at Different Depths

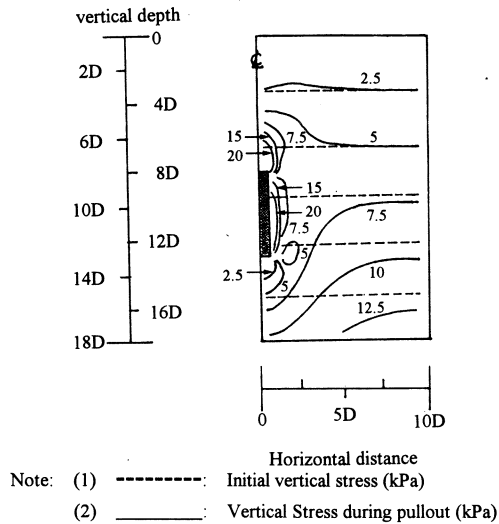


Fig. 6 Vertical Stress Around an Uplifting Cylindrical Anchor at Peak Pull Out Resistance

of the anchor may decrease as a result of the reduction in the stress level of surrounding soil. However, if the end bearing zone above the anchor can be kept some distance away from the void by increasing the length of the anchor shaft, then the end resistance of the anchor will be less affected by the void beneath the anchor. Therefore, the end resistance of the cylindrical anchor will be larger than that of the plate anchor (Fig. 7). As a matter of fact, since the end bearing zone develops some distance below the top of the anchor and extends toward the ground surface (Su & Fragaszy 1988), the existence of the anchor shaft can not only reduce the effect of stress relaxation but also provide the space needed for the end bearing zone to develop fully. This is the main advantage of the cylindrical anchor over the plate anchor in terms of the anchorage capacity.

Shaft Resistance

The development of pre-peak shaft resistances with the anchor movement for the shallow anchor is very similar to that of the deep anchor (Figs. 3 & 4). It reaches the peak value at small displacement ($\sim 8\% D$) and then decrease rapidly to a residual value. The dramatic drop in shaft resistance from the peak to the residual is basically the result of the movement of sand particles into the void left behind by the uplifting anchor. After the peak value is reached, the effect of void induced stress relaxation becomes evident and the confining pressure around the lower portion of the anchor begins to decrease. Finally, the shaft resistance approaches a constant residual value.

INTERACTIVE BEHAVIOR OF CYLINDRICAL ANCHORS

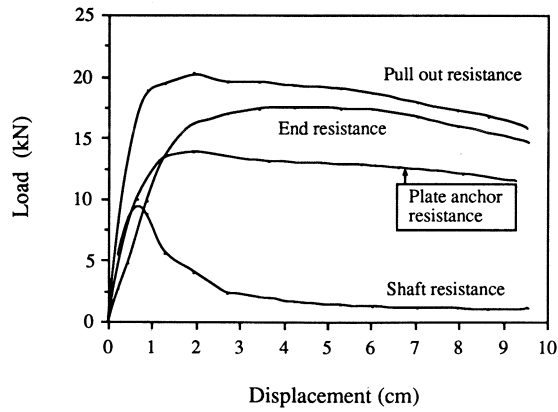


Fig. 7 Resistances of Cylindrical Anchor and Plate Anchor ($Z/D = 8$)

The shaft resistance of the cylindrical anchor is commonly determined from the following equations:

$$Q_{\tau} = K_f \sigma'_v \tan \phi' A_{\tau} \quad (1)$$

or
$$Q_{tr} = K_r \sigma'_v \tan \phi' A_{\tau} \quad (2)$$

where Q_{τ}, Q_{tr} = the peak and the residual shaft resistances of the anchor

K_f, K_r = coefficients of the lateral earth pressure at peak and at residual shaft resistances

σ'_v = effective overburden pressure

ϕ' = effective friction angle of soil

A_{τ} = surface area of the shaft

It can be seen in Fig. 8 that the coefficients of the lateral earth pressure (K_f and K_r) for the model anchor decrease gradually with the embedded depth and approach a constant value when the depth is greater than $10D$. But the K_f value is considerably larger than the coefficient of lateral earth pressure at rest, $K_0 (=1 - \sin\phi')$. This is mainly the result of the increase in stress level within the surrounding soil as the anchor is being pulled out (Fig. 6). So, the lateral pressure ($K \sigma'_v$) acting on the anchor shaft is increased. If the initial effective overburden pressure is substituted to Eq. 1 to determine the peak end resistance, then it will generate a larger K_f value than the K_0 . If the anchor is uplifted further some stress relaxation around the bottom of the anchor will result due to the void forming beneath the anchor. Consequently, the lateral pressure acting on the anchor will decrease. Similarly the coefficient of the lateral earth pressure will decrease. Since the shaft length of the model anchor is only $4.5D$, the effect of the void induced stress relaxation has great influence on the shaft

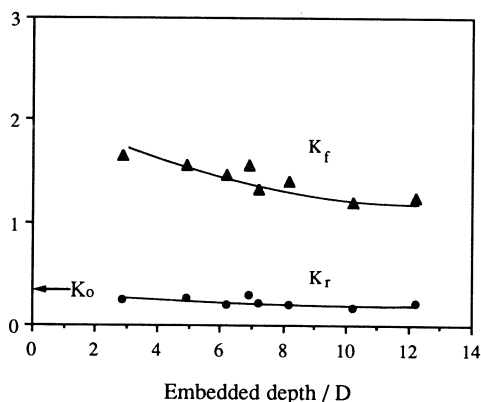


Fig. 8 K_f and K_r at Different Embedded Depths

resistance. As a result, the coefficient of lateral earth pressure decreases gradually to the K_o value or even smaller. Therefore, K_o is more suitable to estimate the residual shaft resistance of the cylindrical anchor, but it tends to significantly underestimate the peak shaft resistance.

INTERACTIVE BEHAVIOR OF ANCHORS

Similar to the group effect of piles, certain reduction in the anchorage capacity of closely spaced anchors is expected. Although some research has been done to investigate spacing effect for the plate anchor, it has been demonstrated by Su & Fragaszy (1988) that the influence zone above a uplifting plate anchor is smaller than that of a cylindrical anchor. To further investigate the effect of spacing on the anchorage behavior of the cylindrical anchor, a series of tests was performed on a pair of anchors with various horizontal and vertical spacings (Table 1).

Effect of Horizontal Spacing

To examine the effect of horizontal spacing on the anchorage behavior, the anchors were buried at the same depth but with different horizontal spacings. Theoretically, since these two anchors were pulled out symmetrically with the testing apparatus shown in Fig. 2, it was expected to generate the same anchorage behavior. However, due to experimental error during testing, there was about 5 % difference in the load-displacement curves for these two anchors. To compare with the behavior of the independent anchor, an average behavior of these two anchors was used for the following analysis.

Basically, the average load-displacement curve for these two horizontally spaced anchors is very similar to that of the independent anchor in shape but is smaller in

INTERACTIVE BEHAVIOR OF CYLINDRICAL ANCHORS

magnitude. As the horizontal spacing increases, the resistances of anchor are approaching to those of the independent anchor (Figs. 9 & 10). In general, the anchorage resistance of the paired anchors is smaller than that of the independent anchor until a certain critical value of horizontal spacing ($7D$ for shallow anchor and $10D$ for deep anchor) is reached. The pull out resistance shows a 50% increase when the horizontal anchor spacing increases from $2D$ to the critical value. However, it should be noted that the critical spacing mentioned above is about 75 % larger than the diameter of the circle of heaving soil at the surface ($\sim 4D$) caused by an uplifted shallow anchor. In other words, if the diameter of the heaving circle is used, it will underestimate the influence range of the anchor.

As indicated by Su & Fragaszy (1988), when the shaft resistance reaches its peak value, the failure surface is close to the soil-shaft interface and can be defined by a cylindrical surface. Therefore, the influence zone is small when the peak shaft resis-

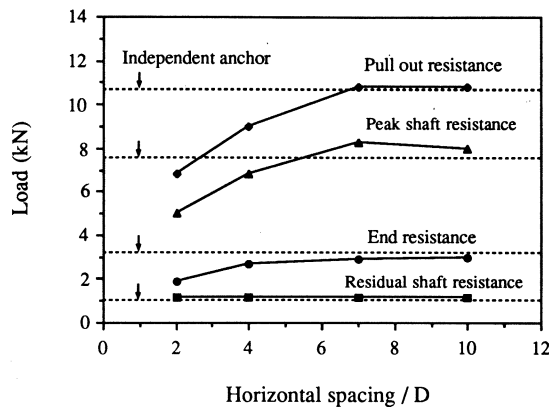


Fig. 9 Resistances of Anchor at Different Horizontal Spacings ($Z/D = 4$)

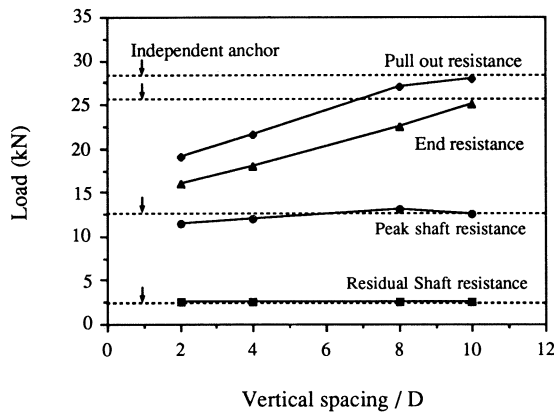


Fig. 10 Resistances of Lower Anchor at Different Vertical Spacings ($Z/D = 10$)

tance is reached. As the end resistance reaches its peak value, a spherical or a conical failure zone will be formed above the anchor and extends some distance into the soil. Therefore, the influence zone of the end resistance is larger than that of the shaft resistance in dimension. As a result, the minimum horizontal spacing which is free of interference for a deep anchor (end resistance control) will be larger than that for a shallow anchor (shaft resistance control).

Effect of Vertical Spacing

If maintaining the minimum horizontal spacing between the anchors is not possible due to the restriction of site, the anchors can be installed at different dip angles to increase the spacing of the fixed anchor length and to minimize the group effect. In other words, the anchorage bodies of anchors are not installed at the same elevation and are vertically spaced. To study the interactive effect between vertically spaced anchors, two anchors which were embedded at different depths were uplifted simultaneously and their load-displacement curves are compared with that of a single anchor.

The upper anchor of the pair was placed at a depth shallower than the critical depth and the lower anchor was placed at a depth of $10D$ ($>$ critical depth) during the laboratory tests. The lower and the upper anchors behave like the deep and the shallow anchors, respectively (Figs. 4 & 11 and Figs. 3 & 12). But the lower anchor yields a smaller pull out resistance than a single deep anchor while the upper anchor shows a larger pull out resistance than a single shallow anchor. The decrease in pull out resistance of the lower anchor is resulted mainly from the void generated below the upper anchor. If the vertical spacing between these two anchors is not large enough, then the end resistance as well as the pull out resistance of the lower anchor will be reduced due to the void induced stress relaxation by the upper anchor. For anchors with a horizontal spacing S_h equal to $1D$, a vertical spacing S_v of $9.5D$ can be free of the interference of the upper anchor (Fig. 13). If the upper anchor is placed within the influence zone

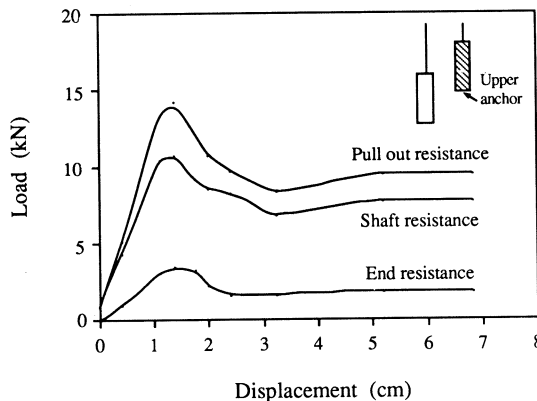


Fig. 11 Resistances of Upper Anchor ($Z/D = 4.5$, $S_h = D$, $S_v = 5.5D$)

INTERACTIVE BEHAVIOR OF CYLINDRICAL ANCHORS

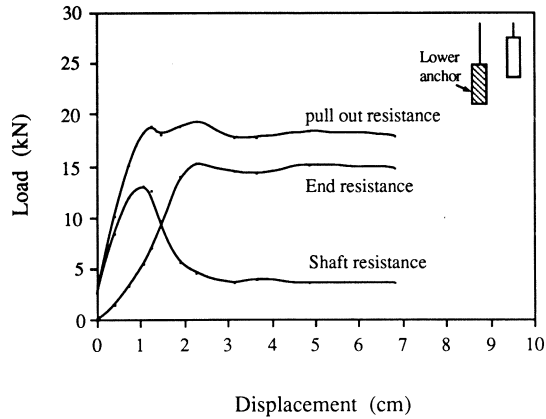


Fig. 12 Resistances of Lower Anchor ($Z/D = 10$, $S_h = D$, $S_v = 5.5D$)

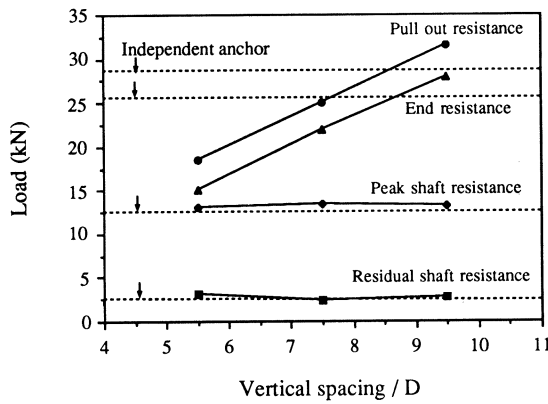


Fig. 13 Resistances of Lower Anchor at Different Vertical Spacings ($S_h = D$)

of the lower anchor, then the lateral pressure acting on the shaft of the upper anchor will be larger than that of the independent anchor. So, a higher shaft resistance and a higher pull out resistance are expected for the upper anchor. However, since the failure surface of the shaft resistance is close to the soil-shaft interface, the peak shaft resistance of the lower anchor is virtually un-affected by the existence of the upper anchor (Fig.13).

Zone of Interference

Since the model anchor test has shown a distinctive group effect between closely spaced anchors, it is of interest to define the zone of interference between cylindrical anchors and to suggest the allowable vertical and horizontal spacings which are free of

interference. The pull out resistance of the paired anchors with different spacings are shown in Fig. 14. To facilitate the analysis, the horizontal and the net vertical spacings between two test anchors (the upper one is acting as the disturbing anchor, the lower one is as the target anchor) are represented by the data points in Fig. 14. The net vertical spacing (S_{vn}) is defined as the distance between the bottom of the upper anchor and the top of the lower anchor; the horizontal spacing (S_h) is defined as the horizontal distance between the center lines of neighbouring anchors (Fig. 14). The reason for using S_{vn} as the vertical spacing for analysis is because the void formed below the disturbing anchor has a very significant effect on the pull out resistance of the target anchor. Following this definition, two anchors which are placed side by side on the same level will have the net vertical spacing S_{vn} equal to $-4.5D$ (Note: the length of model anchor is equal to $4.5D$). The interaction effect is defined as the ratio between the pull out resistance of the lower or the upper anchor and that of the equivalent independent anchor. If the interaction effect is equal to 100%, it indicates that the average behavior of the paired anchors is equal to that of the independent anchor and there is no interference between the anchors. The number shown next to the data points of Fig. 14 represents the interaction effect on the target anchor. For example, a number of 68.8 next to the point of $S_h = D$ and $S_{vn} = D$ indicates that a pull out resistance of only 68.8% of that of the independent anchor was observed on the target anchor if the disturbing anchor is placed $1D$ horizontally and $1D$ vertically away from the target anchor.

As shown in Fig.14, if the value of S_{vn} is less than $-1.5D$, then the contour of a given interaction effect follows a near vertical path. It indicates that if the void forming beneath the disturbing anchor can be kept $1.5D$ below the top of target anchor, then the void has virtually no further effect on the pull out resistance of the target anchor. Also shown in Fig. 14, the interaction effect between two neighbouring anchors can be

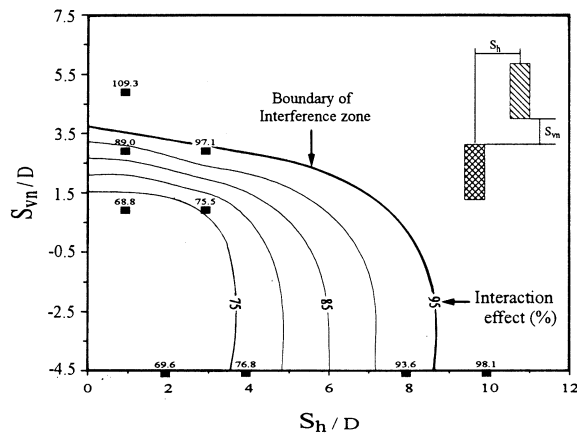


Fig. 14 Change of Interaction Effect with Horizontal Spacing and Net Vertical Spacing

INTERACTIVE BEHAVIOR OF CYLINDRICAL ANCHORS

kept above 95% if the disturbing anchor is placed outside of the 95% contour. Practically, two anchors have the interaction effect of 95% can be considered to be no interference between them. So, the 95% contour can be taken as the boundary of anchor interference. Based on this boundary, there will be virtually no interference if anchors are placed 9D horizontally apart or 4D vertically apart. The boundary of interference zone shown in Fig. 14 is in good agreement with the zone of vertical stress change around an uplifting anchor (Fig. 6). Finally, it should be noted that the boundary of no interference zone indicated in Fig. 14 is considerably larger than the 4D spacing commonly adopted for the shaft anchor and the 6D spacing proposed for the plate anchors by Hanna (1982).

CONCLUSIONS

Based on the model test results for the cylindrical anchor ($L/D = 4.5$) in dense sand, the following conclusions can be advanced:

1. The embedded depth of $6 \sim 8D$ can be adopted to distinguish the shallow anchor from the deep anchor. The capacity of the shallow anchor is controlled by the shaft resistance while the capacity of the deep anchor is controlled by the end resistance. However, the peak shaft resistance and the peak end resistance do not occur simultaneously for either shallow or deep anchor.
2. The failure zone is close to the soil-shaft interface when the shaft resistance reaches its peak value. But a spherical or a conical failure zone is formed above the anchor and extends some distance into soil when the peak end resistance is reached. Therefore, the minimum horizontal spacing allowed for the deep anchor (end resistance control) is larger than that for the shallow anchor (shaft resistance control).
3. Due to the void forming beneath the uplifting anchor, some stress relaxation is resulted around the bottom of the anchor. The stress relaxation has significant effect on the anchor beneath it, if the top of lower anchor is located within a distance of 4D from the bottom of upper anchor.
4. Since the anchorage behavior of the deep cylindrical anchor is controlled by the end bearing behavior, the allowable minimum spacings proposed here are considerably larger than those of the shaft anchor. The boundary of anchor interference has been established for deep cylindrical anchors in terms of the net vertical spacing and the horizontal spacing between the neighboring anchors (Fig. 14).

ACKNOWLEDGEMENT

The Authors wish to thank the National Science Council of the R. O. C. for providing financial support for this research (NSC80-0410-E011-16).

REFERENCES

- AMERICAN ASSOCIATION OF STATE HIGHWAY AND TRANSPORTATION OFFICIALS (AASHTO). (1991). Standard specifications for highway bridges, 15th Edition, Washington.
- BRITISH STANDARDS INSTITUTION (BSI). (1989). British standard code of practice for ground anchorages (BS 8081), London.
- DEUTSCHE INDUSTRIE NORM (DIN 4125). (1988). Ground anchorages - design, construction and testing, Beuth Verlag GmbH, Berlin.
- FEDERATION INTERNATIONALE DE LA PRECONTRAINTE (FIP). (1982). Recommendations for the design and construction of prestressed concrete ground anchors. Slough.
- HANNA, T. H. (1982). Foundations in tension - ground anchors. Trans Tech Publications, Clausthal, Germany.
- HANNA, T. H., SPARKS, R., and YILMAZ, M. (1972). "Anchor behavior in sand", Journal of the Soil Mechanics and Foundation Division, ASCE, 98 (11): 1187-1208.
- LARNACH, W. J. and MACMULLAN, D. J. (1975). "Behavior of inclined groups of plate anchors in dry sand", Diaphragm Wall and Anchorages. Institution of Civil Engineers, London, pp. 153-156.
- LIAO, H. J. and OU, C. D. (1990). "Behavior of mechanically underreamed anchor in mudstone", Proceedings of 10th Southeast Asian Geotechnical Conference, Taipei, Vol. 1, pp. 181-185.
- MEYERHOF, G. G. and ADAMS, J. I. (1968). "The ultimate uplift capacity of foundations", Canadian Geotechnical Journal, 5 (4): 225-244.
- MITSCH, M. P. and CLEMENCE, S. P. (1985). "The uplift capacity of Helix anchors in Sand", Proceedings of a session sponsored by the Geotechnical Engineering Division, ASCE. New York. pp. 26-47.
- SHU, S. C. (1996). Anchorage behavior of vertical anchors in sand, Ph. D thesis, National Taiwan Institute of Technology, Taipei.
- SU, W. and FRAGASZY, R. J. (1988). "Uplift testing of model anchors", Journal of Geotechnical Engineering, ASCE, 114 (9): 961-981.
- VERMEER, P. A. and SUTJIADI, W. (1985). "The uplift resistance of shallow embedded anchors", Proceedings of 11th International Conference on Soil Mechanics and Foundation Engineering, San Francisco, Vol. 3. pp. 1635-1638.

ANALYSIS AND DESIGN OF A TIED BACK-TO-BACK GEOSYNTHETIC REINFORCED SOIL WALL

S.C.R. Lo¹, S.Q. Li², M. Gopalan³ and Z. Gao⁴

SYNOPSIS

The design of a tied back to back geosynthetic wall subjected to heavy set-back surcharge from railway loading has been examined. Simplified rules were used in the detailed design of these walls and the critical sections were studied using non-linear finite element analysis. The stress and strain fields of a tied back-to-back wall were found to be quite different from a conventional reinforced soil wall. However, the simplified design rules gave reasonable to conservative reinforcement tension and connection force ratio relative to the finite element results, provided the geosynthetic reinforcement within the quoted range of stiffness was used. The finite element analysis predicted considerable higher reinforcement tension if metallic reinforcement was used. This difference is due to the dependence of a tied back-to-back wall on the reinforcement stiffness..

INTRODUCTION

The Dutton Park Section of the Dutton Park to Port of Brisbane Rail Link is a \$9 million project undertaken by Queensland Rail. This project included 1650 m² of reinforced soil walls to support an elevated section of the railway. The construction of the reinforced soil walls was sub-contracted to a specialist sub-contractor on a design-and-construct basis. This sub-contracting system encouraged cost-effective design and allowed competition between different reinforced soil systems on an objective basis. The residual soil provided a competent foundation for the reinforced soil wall. An allowable bearing pressure of 250 kPa was guaranteed in the contract. Hence the cost-effectiveness of the design was driven by a reinforced soil structure.

Two of the reinforced soil walls, referred to as Wall 1 and Wall 2 respectively, were aligned parallel at a distance of about 6m apart as shown in Fig. 1. These two walls constituted approximately 80% of the reinforced soil structure. The small distance between the Wall 1 and wall 2 led to an overlapping of the two reinforced zones.

¹ Senior Lecturer, Department of Civil Engineering, University College, University of New South Wales, Australian Defense Force Academy, Australia.

² Senior Engineer, Golder and Associates, Australia.

³ Research Officer, Department of Civil Engineering, University College, University of New South Wales, Australian Defense Force Academy, Australia.

⁴ Research Officer, Department of Civil Engineering, University College, University of New South Wales, Australian Defense Force Academy, Australia.

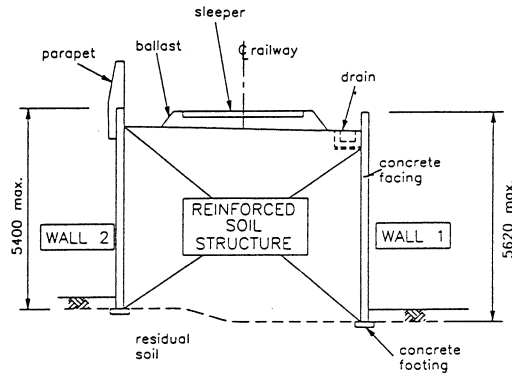


Fig. 1 General Arrangements

Normal design practice (FHWA 1991) is to design the two walls separately and independently with the reinforced block not subject to any active thrust. This implied overlapping of reinforcements. A possibly more economical use of the reinforcing material was to connect the two walls with the same reinforcement. Such a configuration is referred to as a Tied Back-to-back (TBB) wall in this paper. This arrangement may change the strain field of the reinforced zone drastically. FHWA (1991) suggests that the reinforcement tension of a TBB wall may be considerably higher than that predicted by conventional design procedure. Difficulties in constructing a TBB wall are also mentioned.

The final design adopted was based on a geosynthetic reinforcement system referred to as the Freyssisol system. The reinforcing elements of this system were 85 to 90 mm wide straps. The structure of the reinforcing strap is shown in Fig. 2a. It consisted of a number of groups of high tenacity polyester fibres individually encapsulated by a modified polyethylene, and manufactured in rolls of 100m length. The straps came in nominal strength grades of 20, 30, 50 and 100kN. The standard vertical spacing between reinforcement levels was 800mm, but three standard horizontal spacings of 667mm, 800mm and 1000mm could be used. The straps were connected to the wall facing by attachment loops and pins (Fig. 2b). The wall facing was constructed from Tee-shaped precast concrete panels (Fig. 2c). The Freyssisol system could overcome the difficulties associated with the construction of a TBB wall by running the straps between the two walls in a zig-zag fashion as illustrated in Fig. 3. It was also hypothesised that the reported higher reinforcement tension associated with a TBB wall was largely due to the quasi-inextensible nature of metallic reinforcement used in those studies. The ability of the Freyssisol strap to accommodate some extension would thus lead to a significant diminution of the "additional" tension due to the use of a TBB configuration. In view of the higher material cost associated with the Freyssisol straps in overlapping the reinforced zone, a TBB wall configuration was adopted for the project.

ANALYSIS AND DESIGN OF TIED BACK-TO-BACK WALL

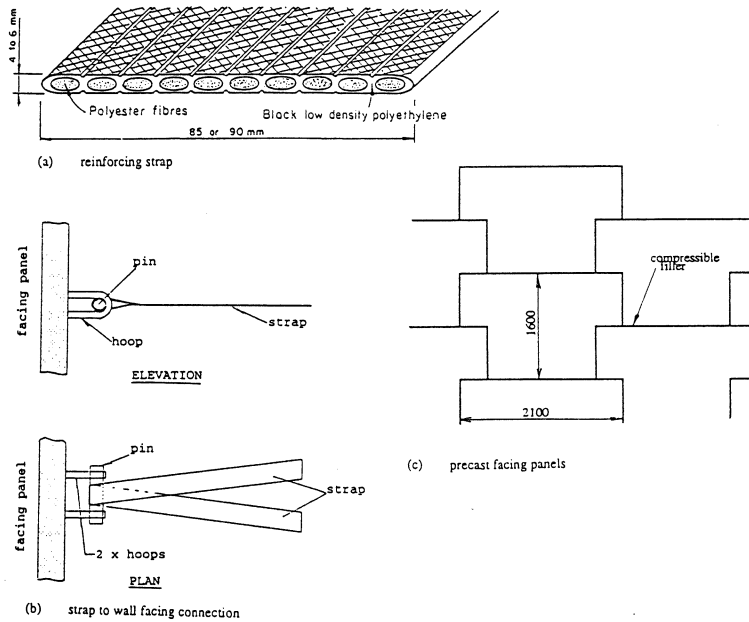


Fig. 2 Freyssisol Wall

- (a) Reinforcing Strap
- (b) Strap to Wall Facing Connection
- (c) Precast Facing Panels

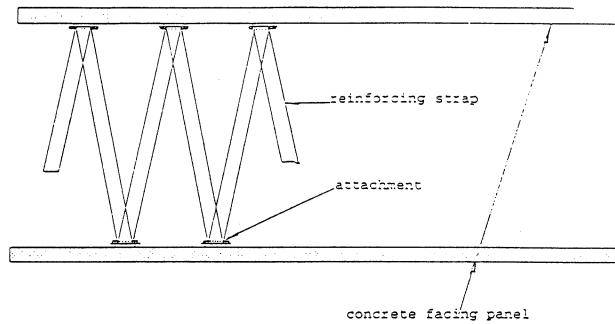


Fig. 3 Reinforcement Layout of TBB Freyssisol Wall

However, the behaviour of a TBB Freyssisol wall could be quite different from that of a normal Freyssisol wall, and hence the conventional design procedure may not be appropriate. The heavy set-back surcharge from the railway loading further complicated the design. The design challenge was met by a combination of simplified procedures and non-linear finite element analysis as described below.

DESIGN METHODOLOGY

The finite element method, (FEA), is a powerful tool for modelling complicated geotechnical systems. However, successful prediction of the behaviour of a geosynthetic reinforced soil structure by FEA is still a difficult task (Wu et al 1991, Lo and Li 1993). Proper modelling of the highly non-linear soil behaviour and the construction sequence are essential for making reliable predictions. The former leads to selection of soil models and soil parameters and the latter leads to large computational time. FEA, on its own, is still not a very practical tool for the routine design where the configuration has yet to be worked out. Hence the strategy adopted was to conduct a series of non-linear FEA on subjectively chosen "representative" sections as a means of developing a simplified design procedure for the initial design. The choice of "representative" section required engineering judgement in addition to the experience on the design and construction of reinforced soil walls. The influence of selecting different soil models, different soil parameters and different distribution of reinforcement on the pertinent design values, such as maximum reinforcement tension, were included in such an exercise. The resultant simplified design rules would then allow the engineer to work out design sections. The critical sections so derived, which had dimensions and reinforcement distribution different from the "representative" sections, were further checked by another round of FEA.

The simplified design equation for $T_{\max}(i)$, the maximum reinforcement tension at i -th reinforcement level, is:

$$T_{\max}(i) = K_a \cdot (s_v(i) + q + a(i) \cdot \Delta s_v(i)) \cdot s_v \cdot s_h \quad (1)$$

where K_a = Rankine active pressure coefficient

$s_v(i)$ = average overburden stress (due to the self weight of the fill) at the i -th level

q = uniform surcharge

$\Delta s_v(i)$ = additional vertical stress at the i -th level calculated by the conventional 2 to 1 stress spreading

$a(i)$ = a reduction coefficient

s_v = vertical reinforcement spacing

s_h = horizontal reinforcement spacing

The reduction factor $a(i)$ is given by

$$a(i) = wb(i)/w0(i) < 1$$

$wb(i)$ and $w0(i)$ are defined in Fig. 4. The first term of the equation implies that, due to the extensibility of the reinforcement strap, the conventional design rule is adequate for a TBB Freyssisol wall. The calculation of the third term, however, is somewhat different from the conventional procedure. It implies the reinforcement tension due to a setback loading is less than that due to a similar load on the active region of a conventional reinforced soil structure. It needs to be emphasized that Eqn (1) is

ANALYSIS AND DESIGN OF TIED BACK-TO-BACK WALL

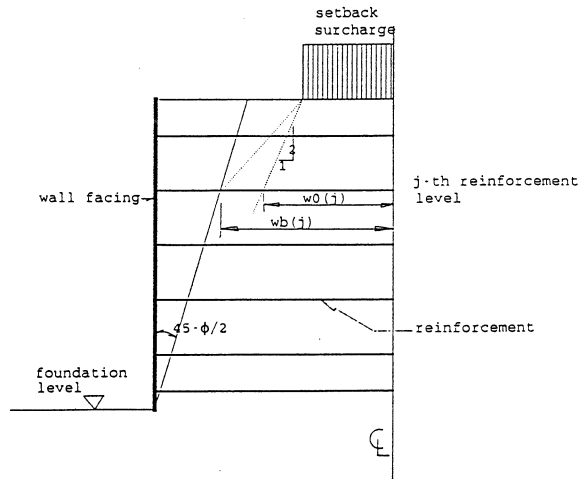


Fig. 4 Set-back Surcharge

developed for geosynthetic reinforcement with a stiffness similar to that of the Freyssisol straps.

The attachment of a strap to the wall panel should be designed to resist the reinforcement tension immediately behind the wall panel. This force, referred to as the connection force, (CF), is in general, less than the maximum reinforcement tension at the same level. The CF was conventionally normalised with respect to the maximum reinforcement tension at the same level, thus giving a CF ratio. The design assumed the CF ratio reduced linearly from unity at the toe of the wall to 0.75 at the crest of the wall.

The maximum tension locus of a TBB Freyssisol wall was quite different from that of a normal wall. However, this difference had no design implication because reinforcement pull-out was not possible in a TBB wall.

FINITE ELEMENT ANALYSIS

The most critical design section is presented in Fig. 5. The fill material used was a completely decomposed granite. The results of the final round of a non-linear FEA of this section are presented in this paper.

Numerical Strategy

An important aspect of the analysis was the modelling of the construction sequence. Each level of reinforcement was represented by a construction stage as illustrated in Fig. 6. The global stiffness matrix was re-assembled at each and every construction stage. This avoided the possibility of numerical problems associated with the use of phantom elements to represent soils or reinforcement yet to be placed. The gravity load in each

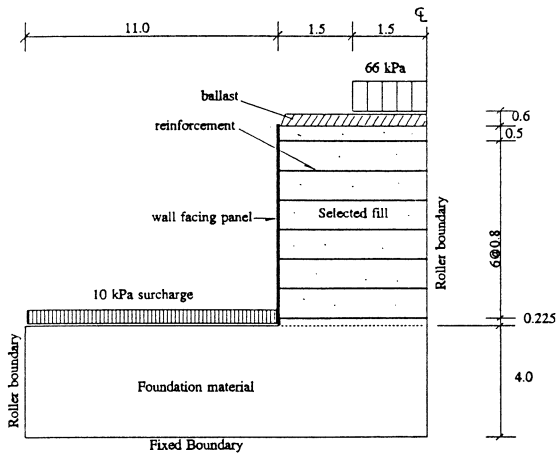


Fig. 5 Idealised Critical Section

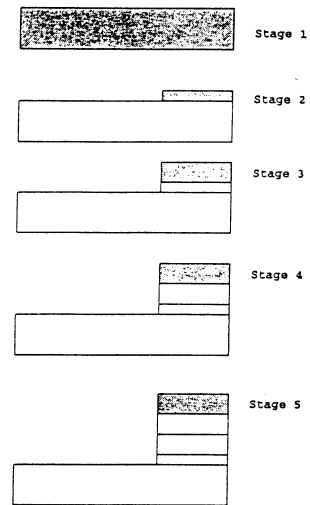


Fig. 6 Finite Element Modelling of Construction Sequence

construction stage was "turned on" in 5 to 10 increments. The stiffness matrix was re-assembled and inverted at every load increment. The effect of embedment was modelled by an overburden stress of 10 kPa.

Modelling of Facing

The modelling of the facing required special considerations. As the facing consisted of precast concrete panels separated by compressible strips the axial stiffness and to a lesser extent the flexural stiffness of the facing was less than that of a continuous concrete wall. Indeed, the concrete facing in a global sense, was highly compressible in the axial direction. The method adopted was to replace the 150mm thick panel with an equivalent wall of low axial stiffness and a flexural stiffness equal to about half of that of the 150mm thick panel. This can be achieved by using a low equivalent Young's modulus and an equivalent thickness. The FE results were only marginally affected by the value of the equivalent Young's modulus, provided that it was comparable to that of soil. A detailed parametric study indicated that this approach was acceptable.

Material Models

Both the foundation soil and the backfill was modelled by the Duncan and Chang (1971) hyperbolic model where the tangential Young's modulus, E_t , is given by:

$$E_t = K.(s_3/p_a)^n.p_a.(1-S)^2 \quad (2)$$

$$S = \frac{r_r.(1-\sin(\phi))(\sigma_1-\sigma_3)}{2c.\cos(\phi) + 2\phi_3.\sin(\phi)} \quad (2a)$$

ANALYSIS AND DESIGN OF TIED BACK-TO-BACK WALL

where K , n , r_f = are non-dimensional constants
 p_a = atmospheric pressure in consistent unit
 f = friction angle
 c = cohesion

Note that the values of r_f and n are always less than or equal to unity. At low confining pressure, which may occur at the initial steps in turning on the gravity, the above equation may lead to the value of E_t approaching zero. This will lead to numerical problems. To prevent this from happening, elements in the process of being constructed were assigned a minimum E_t value of 4000kPa. The material parameters adopted are presented in Table 1. These parameters were conservatively estimated based on published data. The sensitivity of the FEA results to choice of material parameters and material models is examined in a separate section.

Table 1

Soil Parameters for Finite Element Analysis		
Parameter	Foundation	Fill
ϕ (deg)	30	35
C (kpa)	50	0
K	600	1500
n	0.5	0.5
r_f	0.78	0.78
ν	0.3	0.3

The geosynthetic reinforcements were modelled as elastic bar elements with stiffness values proportional to the strength grade and inversely proportional to the strap spacing in the horizontal direction. Since the design was based on a high safety factor against reinforcement rupture, the working stress in the reinforcement was deemed low and the modelling of non-linearity load extension behaviour was not considered necessary.

RESULTS

Reinforced Soil Action and Maximum Tension Zone

The variation of reinforcement tension along the length of a reinforcement, for both the "no surcharge" and "with surcharge" conditions (ie with and without the 66 kPa railway loading applied), is presented in Fig. 7. The maximum tension, in general, did not occur behind the wall panel but was a function of distance into the reinforced soil block. This implied that the geosynthetic straps were not functioning as ties, but as soil

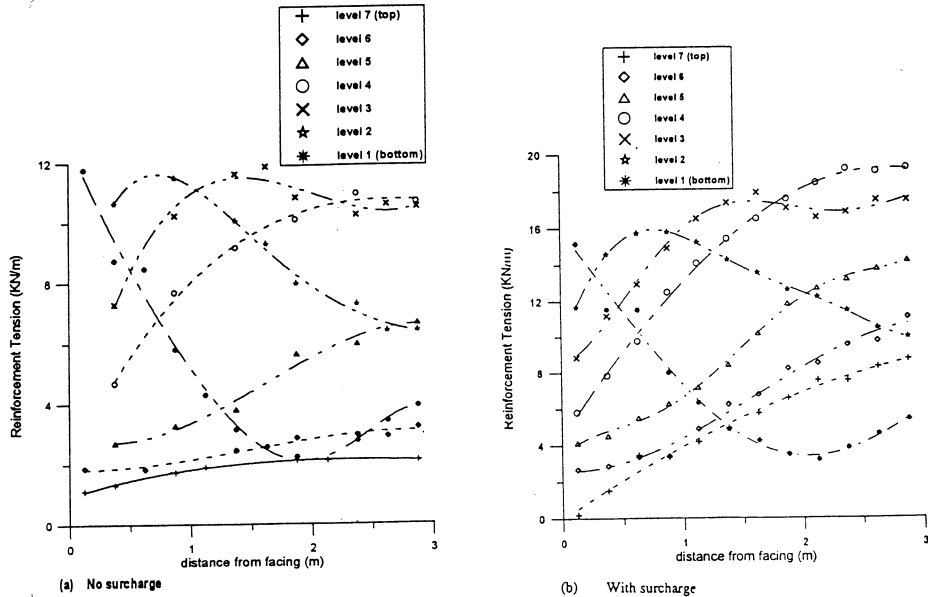


Fig. 7 Distribution of Reinforcement Tension
(a) No Surcharge
(b) With Surcharge

reinforcement despite the opposing wall panels were tied together by straps. A distinct peak in the reinforcement tension was observed in the lower layers. The locations of maximum reinforcement tension, however, were not distinctly defined in the upper reinforcement layers. This was best illustrated by plotting the maximum tension zone as presented in Fig. 8. The maximum tension zone in the i -th level is defined by a variation of 5% from the maximum reinforcement tension at the same level. At the lower levels, the maximum tension zone was relatively narrow, thus indicating a distinct peak in the reinforcement tension. But there was a significant increase in width of the zone at higher reinforcement levels. The maximum tension zone for the "no surcharge" condition was very similar to that of the "with surcharge" condition.

Maximum Reinforcement Tension

The maximum reinforcement forces obtained by the FEA were compared with the design values as given by Eqn (1). For the "no surcharge" condition, good agreement was achieved for the top four layers of reinforcement (Fig. 9). Evident discrepancies, with the FEA predicting lower reinforcement tension, was observed for the bottom three layers of reinforcement. The discrepancy was a maximum at the bottom-most level. This is believed to be due to foundation restraint, a characteristic that is not accounted for in Eqn. (1). For the "with surcharge" condition, the FEA consistently predicted a lower reinforcement tension relative to that given by Eqn (1). This implied

ANALYSIS AND DESIGN OF TIED BACK-TO-BACK WALL

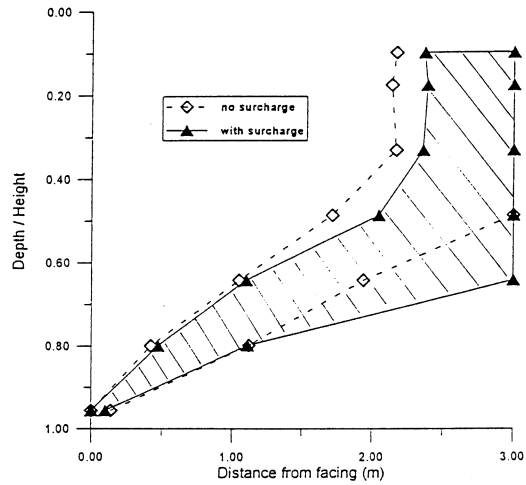


Fig. 8 Maximum Tension Zone.

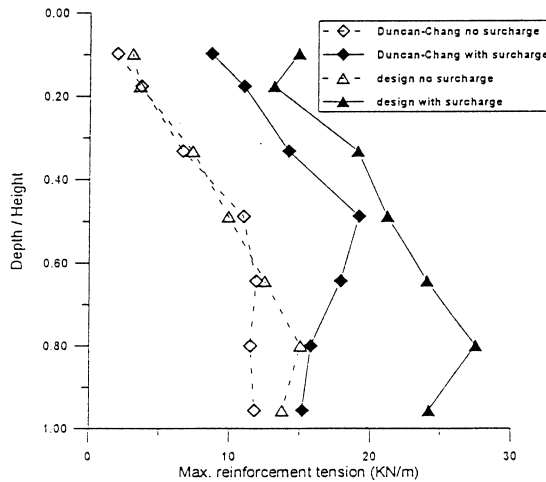


Fig. 9 Variation of Maximum Reinforcement Tension with Depth

that the second term of Eqn (1) over-predicted the additional reinforcement tension due to the 66 kPa set-back surcharge.

Connection Forces

The CF ratio is presented as a function of depth in Fig. 10. The CF ratio governs the design of the structural elements connecting the strap to the wall panels. For both the "no surcharge" and "with surcharge" conditions, the CF ratio predicted by the FEA approached unity at the bottom-most level, but reduced with increase in elevation. This pattern was consistent with that assumed in the design, but CF ratio predicted by the

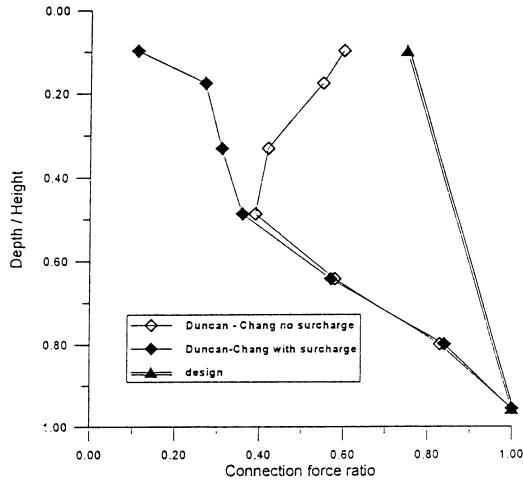


Fig. 10 Connection Force Ratio

FEA was always lower than that assumed in conventional design. The reduction in the CF ratio was more pronounced for the "with surcharge" condition. This suggested that the set-back surcharge, had a much smaller effect on the reinforcement tension immediately behind the wall panels relative to $T_{max}(i)$, the maximum reinforcement tension at the same level.

Lateral Displacement Profile

The lateral displacement profiles for both the "no surcharge" and "with surcharge" conditions are presented in Fig. 11. The lateral displacements were normalised against

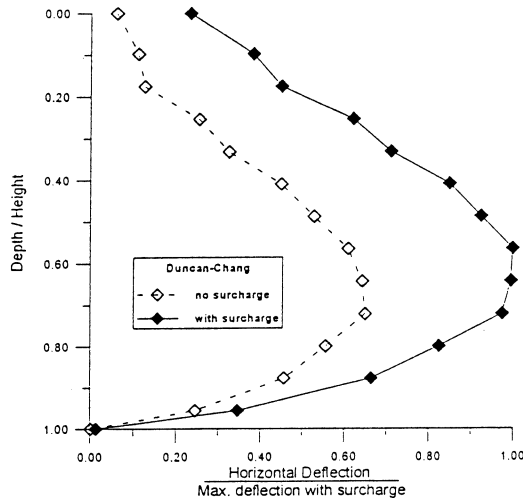


Fig. 11 Lateral Displacement Profile

ANALYSIS AND DESIGN OF TIED BACK-TO-BACK WALL

the maximum displacement for the "with surcharge" condition. The plots indicate that the heavy set-back surcharge produced a 40% increase in lateral displacement. The lateral displacement attained a maximum value at an elevation of about one third to half of the height of the wall. It decreased to a very low value at the foundation level. This pattern is believed to be due to the lateral restraint offered by the foundation and is consistent with the variation of maximum reinforcement tension with depth as presented in Fig. 9.

SENSITIVITY STUDIES

Influence of Reinforcement Stiffness

It was hypothesized that the very high reinforcement tension in a TBB wall as suggested in FHWA (1991) was associated with the high stiffness of metallic soil reinforcement system. Hence, the FEA should be able to predict a significantly higher reinforcement tension if the stiffness of the reinforcement was of the same order as that of metallic reinforcement. Thus the analysis was repeated with the reinforcement stiffness increased to 15,000 kN/m. This stiffness was about half of that of a typical steel system. As illustrated in Fig. 12, the FEA do predict reinforcement tension considerably higher than that given by the Eqn (1). This exercise added confidence to the analysis and supported the hypothesis that the extensibility of the Freyssisol straps contributed to the effectiveness of a TBB wall.

Influence of Soil Parameters

It is recognised that there are uncertainties in the input soil parameters, and it is most important to investigate the sensitivity of the wall behaviour to variations in soil

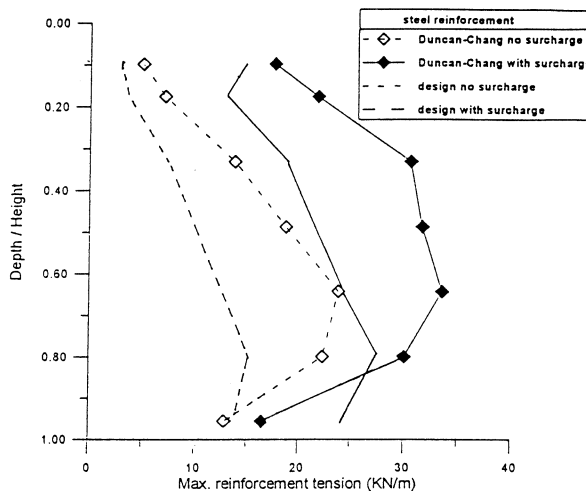


Fig. 12 Reinforcement Tension for Steel System

parameters. Thus, the effect of varying the input soil parameters were studied by repeating the analysis with

- i) reducing the K value of the fill to 500.
- ii) reducing the foundation parameters to $\phi = 30^\circ$, $c = 10$ kPa, and $K = 500$.

Although the above variations in input parameters did produce some minor changes in the FEA results, its effect on relevant design issues such as the maximum reinforcement tension was insignificant. Thus it can be concluded that the behaviour of the Freyssiosol TBB wall was not sensitive to changes in soil parameters.

Influence of Soil Model

The choice of soil models for a finite element analysis is not unique. Hence, some of the analyses were repeated using the Mohr-Coulomb elastic-plastic model. A constant Young's modulus (prior to failure) of 20 MPa was assumed for both the foundation and the backfill. The maximum reinforcement tension predicted by the Mohr-Coulomb model was compared to that of the Duncan-Chang model as given in Fig. 13. With the exception of the bottom two levels, good agreement was obtained. The Mohr-Coulomb model predicted a slightly lower reinforcement tension for the upper levels, but gave a significantly higher reinforcement tension for the bottom two levels. The result was indicative of a lower foundation restraint implied by the Mohr-Coulomb model. A similar comparison for the "no surcharge" was not presented because good agreement was achieved for all levels of reinforcement. This indicated that the sensitivity to the choice of soil model increased with the complexity of loading. Both models, however, predicted a maximum reinforcement tension lower than that given by the design Eqn (1). A comparison of the CF ratio for the "with surcharge" condition is presented in Fig. 14. The Mohr-Coulomb model predicted a higher CF

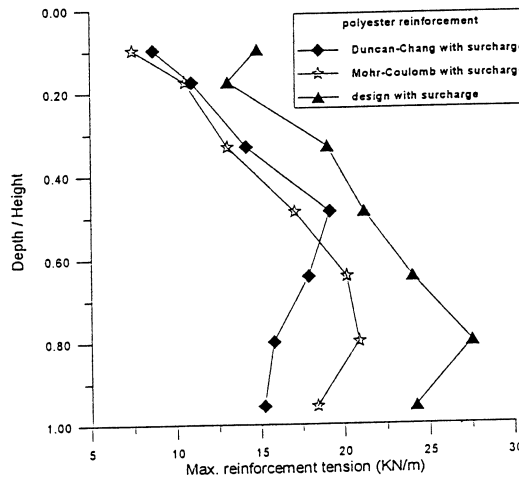


Fig. 13 Influence of Soil Model on Reinforcement Tension

ANALYSIS AND DESIGN OF TIED BACK-TO-BACK WALL

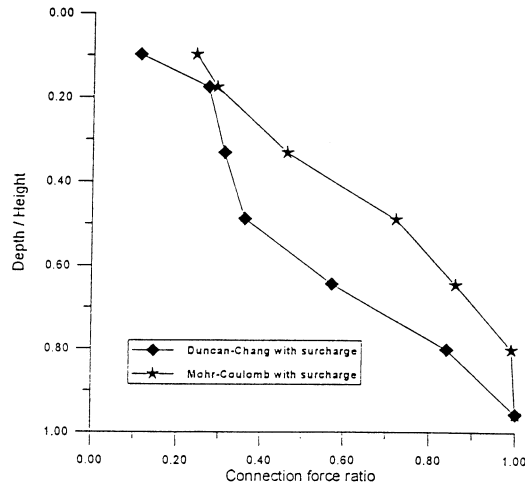


Fig. 14 Influence of Soil Model on Connection Force Ratio

ratio. This is believed to be due to the higher dilation implied by the Mohr-Coulomb model. However, the CF ratio predicted by the FEA was always lower than that assumed in the design. A comparison of the lateral deflection profile for the "with surcharge" condition is presented in Fig. 15. Note that the lateral deflection was normalised by the maximum deflection predicted by the same model. Despite the significant difference in modelling soil stiffness by the two models, similar deflection profile was obtained. This implied that the absolute values of lateral deflections was dependent on the choice of soil model, but the movement pattern was not.

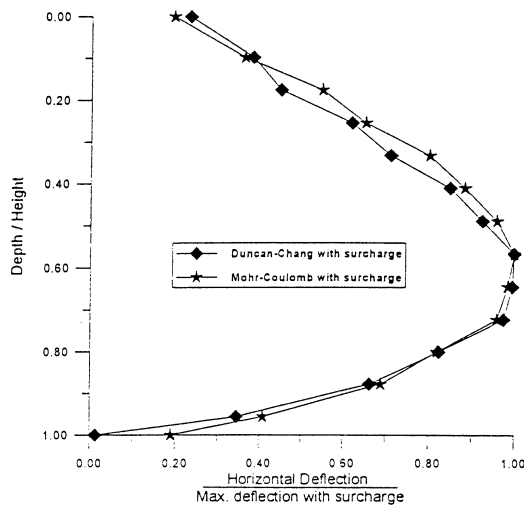


Fig. 15 Influence of Soil Model on Lateral Displacement Profile

SUMMARY AND CONCLUSIONS

The design and analysis of a Freyssisol TBB wall with heavy set-back surcharge has been presented. In view of the wall configuration and complicated loading conditions, non-linear finite analysis with modelling of construction sequence was used to study the behaviour of the wall. The analysis indicated that the reported (very) high reinforcement tension associated with TBB wall was not applicable for Freyssisol TBB walls and the design equation adopted for the project yielded conservative results. At the time of writing this paper, the wall construction was near completion. No particular construction difficulties were encountered. This is due to the construction logistics of a Freyssisol wall. Thus the TBB wall may be adopted as a competitive and viable configuration for Freyssisol reinforced soil.

ACKNOWLEDGEMENT

This project forms part of a continuing research program on reinforced soil systems conducted at University college, University of New South Wales, Canberra. Part of the research reported in this paper was supported by Austress-Freyssinet Pty Ltd. The opinions expressed in this paper, however, are solely those of the authors.

REFERENCES

- DUNCAN, J.M. & CHANG, C.Y. (1970) "Nonlinear analysis of stress and strain in soils", *Joul. Soil Mech. and Foundation Div. ASCE*, 96 (5), pp 1629-1653.
- FHWA (1991) "Reinforced soil structures Vol. 1, Design and construction guidelines", Publication No. FHWA-RD-89-043, Nov.
- LO, S.C.R. and LI, S-Q. (1993) "Behaviour of a breakwater on soft sediments - failure and success" *Third Intl. Conference on Case Histories in Geotechnical Engineering*, St. Louis, Missouri, June , pp 383-388.
- WU, T.H., QI, X., CHEN, N., KSOUN, I., HELWANI, M.B. & HUANG, G.C. (1991) "Comparison of Predictions for the Denver Walls", *Proc. of the Intl. Symp. on Geosynthetic Reinforced Soil Retaining Walls*, Denver, Colorado, Aug. , pp 43-60

CASE STUDIES OF ROCK-SOCKETED PILES

C. F. Leung¹

SYNOPSIS

This paper presents the results of load tests on a large number of instrumented bored piles socketed in sedimentary rocks and granite in Singapore. Many of these piles were load tested to at least 2.5 times the respective working load. The ultimate unit shaft friction values obtained in the rocks are correlated to the unconfined compressive strength of the rock by means of the rock socket adhesion factor. In cases where unconfined compressive strength of the rocks is not available, the unconfined compressive strength is obtained indirectly from other rock parameters such as pressuremeter test data, standard penetration resistance values and point load strength values. Illustrative examples presented in this paper show that pressuremeter test can be a viable alternative to determine the strength of fractured rocks. For weak rock with unconfined compressive strength below 5 MPa, the measured adhesion factors agree reasonably well with those proposed by several existing design methods. For rocks with unconfined compressive strength above 5 MPa, the measured adhesion factors are considerably lower than those proposed by existing design methods. It is believed such rocks have been significantly weakened by chiselling during pile installation.

INTRODUCTION

It is often necessary to install pile foundations deep into the bedrock in order that the desirable load carrying capacity can be achieved. For a pile having a rock socket of considerable length, a large percentage of the pile capacity is derived from the base resistance as well as from the resistance along the socket shaft. In a pile design, adequate factor of safety has to be provided against bearing capacity failure. Thus under working load condition whereby the applied load is less than half of the ultimate pile capacity, only a small portion of the ultimate resistance is mobilised while a much larger proportion of the ultimate socket shaft resistance is mobilised. Hence it would be beneficial to the pile designer if the socket shaft resistance can be determined with a good degree of confidence. Similar in principle to the use of adhesion factor in the determination of ultimate shaft resistance for soil, conventional design methods (for example Rosenberg and Journeaux, 1976; Horvath and Kenny, 1979; Williams and Pells, 1981; Rowe and Armitage, 1987) on rock-socketed piles also related the ultimate shaft resistance of the rock socket to the unconfined compressive strength of the rock by an empirical rock socket adhesion factor α . As researchers derived the α values by back-analysing various case studies on rock-socketed piles, it is not surprising that the magnitudes of suggested α values by various design methods are different. Moreover,

¹ Senior Lecturer, Department of Civil Engineering, National University of Singapore, Singapore.

the α values may not be applicable to rock-socketed piles in this region as all the case studies back analysed by these researchers were from outside Southeast Asia.

In the past decade, the Author has reported the results of several case studies on rock-socketed piles in Singapore (see for example Radhakrishnan, Leung and Subrahmanyam, 1985; Leung et al., 1985 and 1988; Radhakrishnan and Leung, 1989; Tan, Wong and Leung, 1994). Other researchers have also published the findings of the performance of rock-socketed piles in Singapore (see for example Buttlig, 1986; Chang et al., 1989; Chang and Broms, 1991; Poh and Chiam, 1993) and other parts of Southeast Asia (see for example Toh et al., 1989; Jeng et al., 1993; Moh et al., 1993). Based on the field data reported earlier and a good number of unpublished case studies in both sedimentary rocks and granite obtained by the Author recently, the α values deduced from these studies are evaluated against those suggested by existing design methods. In the first half of this paper, the performance of piles socketed in weak and moderately weak sedimentary rocks in Singapore will be examined. In the second half of this paper, the behaviour of piles socketed in Singapore granite will be reviewed.

SEDIMENTARY ROCKS

The sedimentary rock formation in Singapore is geologically termed as the Jurong formation. It comprises sedimentary series of sandstone, siltstone, shales and conglomerates formed in the Triassic period. These beds are severely folded and some faults have developed in the formation. Pitts (1984) provided a concise account on the geology of the formation. Very deep weathering is a feature of the sedimentary rocks which underlie the southern and western parts of Singapore. The weathering can produce highly weathered rocks down to 50 m, and sometimes greater. In the western part of Singapore, the rock is typically close to the ground surface with a subsurface profile consisting of several metres of completely weathered and decomposed rocks and residual soils, underlain by highly weathered and fractured rocks of undetermined thickness. In the southern part of Singapore, the rock formation is usually overlain by deposits of soft marine clay of variable thickness ranging from 1 m to 20 m. In addition, sandstone boulder up to 2 m³ in size are found embedded in a matrix of stiff to hard silty and sandy clay.

Leung and Radhakrishnan (1990) provided a concise account on the geotechnical properties of weathered sedimentary rocks in Singapore. Standard penetration tests are by far the most frequent in-situ tests carried out in the rock. The standard penetration resistance N values and the rock quality designation RQD values are often the only two rock parameters available in most cases. Fig.1(a) and (b) show the variations of N and RQD values respectively with depth obtained from a site located in the western part of Singapore. The standard penetration tests were terminated when the number of blows exceeded 100. An extrapolated N value is adopted in the present study such that 100 blows/150 mm penetration is equivalent to an extrapolated N value of 200. As illustrated in Fig. 1(a) and (b), both the N and RQD values are highly scattered making it difficult to evaluate the rock strength accurately from these parameters. For some

CASE STUDIES OF ROCK-SOCKETED PILES

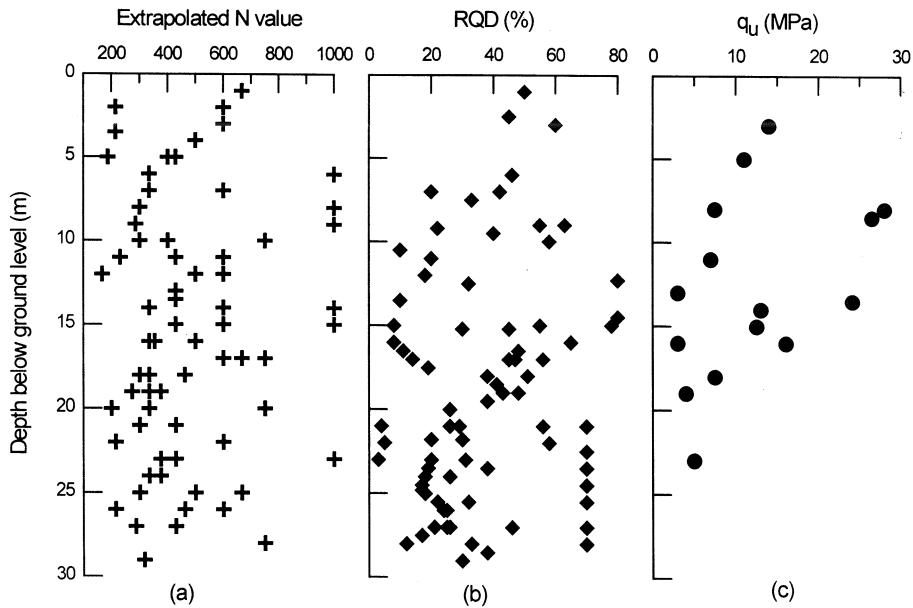


Fig. 1 Variations of (a) Extrapolated N Values, (b) RQD and (c) Unconfined Compressive Strength of Sedimentary Rocks with Depth

large projects, in-situ pressuremeter tests are performed in the rock and laboratory unconfined compression tests and point load tests are performed on the rock samples. The variation of the unconfined compressive strength, q_u , of the intact rock cores against depth obtained from the same site is given in Fig. 1(c) which illustrates that the rock strength is highly variable with q_u values ranging from 2 MPa to 28 MPa. It is often impossible to carry out many unconfined compression tests at a given site as the rock samples obtained are often highly fractured with core length that is too short for compression testing. Unconfined compressive strength, q_u , is the most commonly used parameter employed in conventional design methods for rock-socketed piles. In view of this, Leung and Radhakrishnan (1990) analysed a large number of rock test data and proposed the following approximate correlation relationships between q_u and point load strength $I_s(50)$ and between q_u and extrapolated N values. These correlation relationships are re-stated below:

$$q_u = 6.12I_s(50) \quad (1)$$

$$q_u = 10^{-3.29 + 1.45\log_{10}(N)} \quad (2)$$

Mair and Wood (1987) gave a concise account on the determination of shear strength of rock from the pressure-deformation response obtained from a pressuremeter test. They showed that by replotting the test data in the form of pressure P versus $\log_e(\Delta V/V)$ where V is the volume of cavity at any stage and ΔV is the change in volume,

a linear relationship exists after the rock has yielded and the gradient of the line is the undrained shear strength of the material. The data obtained from a sample pressuremeter test conducted on a fractured sedimentary rock is replotted using the above approach and shown in Fig. 2. It is evident that the plot follows precisely the expected manner described earlier. The unconfined compressive strength of the rock, which is equal to two times the gradient of the straight line given in Fig. 2, is found to be 8.8 MPa which is within the range of strength shown in Fig. 1(c). This illustrates that pressuremeter test can be a viable alternative in evaluating the shear strength of fractured rock.

BORED PILES IN SEDIMENTARY ROCKS

In the course of foundation construction for a good number of construction projects involved by the Author, many large diameter bored piles socketed in sedimentary rocks were load tested to at least 2.5 times the respective pile working load. All these piles were instrumented with vibrating wire strain gauges to measure the load transfer characteristics along the pile shaft during the load tests. Other instruments such as Carlson meter and rod extensometers were also provided in a limited number of test piles. The pile diameter ranges from 0.5 m to 1.8 m and the pile length varies from 7 m to 30 m with socket length ranging from 2 to 13 times pile diameter.

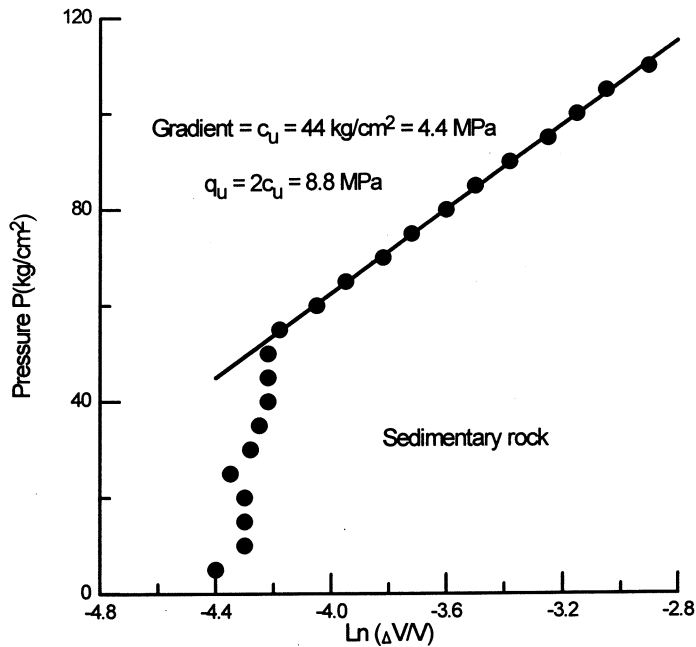


Fig. 2 Plot of Pressure Versus $\text{Ln}(\Delta V/V)$ Based on Pressuremeter Test Data on Sedimentary Rocks

CASE STUDIES OF ROCK-SOCKETED PILES

In all the case studies presented in this paper, boring was carried out by crane-mounted flight augers and chisels up to a maximum weight of 100 kN were used for breaking up the hard formation. It was observed that chiselling of the hole had produced highly roughened walls and larger shaft diameter than actually required. In addition, the pile walls were noted to be irregular and rougher compared to augered holes. Even though the water table was located close to the ground surface, there was very little inflow of water into the hole. It was therefore possible to install most of the piles in the dry. After boring and chiselling had been carried out to the required depth, the remaining loose material at the bottom of the bored hole was cleaned by a clean-out bucket. Occasionally when the muck and slimy dirt still remained after the use of the clean-out bucket, a cage was hoisted down to the bottom of the bored hole and manpower was used to clean out the loose material. Strict control was exercised to ensure adequate cleaning of the pile base to enable good contact between the pile and the rock beneath. Concreting of the shaft using grade 30 or grade 35 concrete was done in one continuous pour. In bored holes where the ingress of water was substantial or where there is a layer of soft soil overburden, temporary steel casings were installed. The tremie method was employed in concreting of these piles.

CASE STUDIES

This paper presents the results of back-analysis on a good number of load tests conducted on piles socketed in sedimentary rocks. The results obtained from a test pile installed in the southern part of Singapore are presented as an illustrative example. This pile is a 1.4-m diameter pile with a penetration length of 16 m below the ground level. Fig. 3(a) shows the simplified subsurface profile of the pile which consists of 3 m of fill, 2 m of soft marine clay, 3 m of firm silty clay followed by dense clayey silt of about 2.5 m thick. The bottom part of the pile is located in a 5.5-m deep rock socket of highly fractured, very weak to weak siltstone. The unconfined compressive strength for the upper and lower parts of the rock socket is 3.5 MPa and 6.5 MPa respectively. A maximum test load of 20 MN was applied on the pile using the maintained load method with the reaction provided by a series of ground anchors. The applied load was measured by means of a hydraulic load cell placed between the loading system and the pile top. The settlement at the pile top was monitored by means of dial gauges with a sensitivity of 0.01 mm/division mounted on an independent support system. Fig. 4 shows the load-settlement curve of the pile under the final loading/unloading cycle. It is evident that the load-settlement response is fairly linear up to an applied load of 7 MN. This is in line with Osterberg and Gill's (1973) and Radhakrishnan and Leung's (1989) observation that the load-settlement response of a rock-socketed pile is linear under working load. At the maximum test load of 20 MN, the settlement is noted to be about 16 mm.

The pile was instrumented with vibrating wire strain gauges at five elevations along the pile shaft with four gauges at a given elevation. The load distribution along the pile shaft and the unit shaft friction versus depth relationships are shown in Fig. 3(b) and 3(c) respectively. As expected, very little resistance is provided by the fill, marine clay and

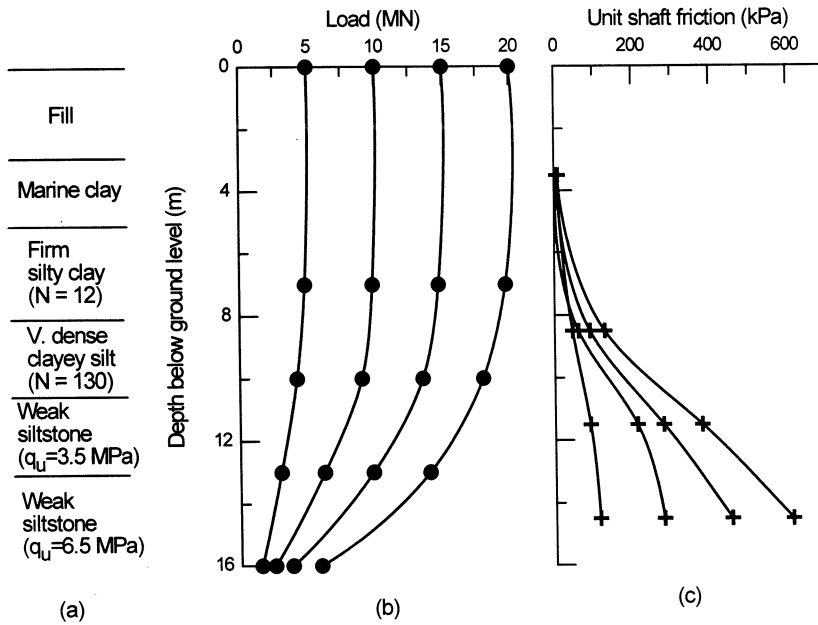


Fig. 3 (a) Simplified Subsurface Profile, (b) Load Distribution and (c) Unit Shaft Friction Distribution Along the Shaft of a Typical Pile Socketed in Sedimentary Rocks

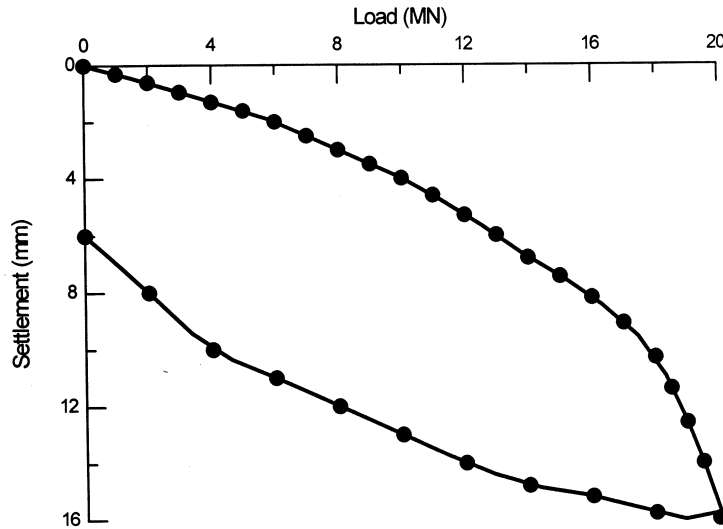


Fig. 4 Load-Settlement Response

CASE STUDIES OF ROCK-SOCKETED PILES

firm silty clay strata. The maximum unit shaft friction is noted to be about 120 kPa for the very dense clayey silt. It is evident that much of the pile resistance is derived from the rock socket as the observed unit shaft friction values in the rock are substantially larger than those observed in the soil strata. A maximum unit shaft friction of 390 kPa and 620 kPa is observed in the upper and the lower rock socket respectively. The rock socket adhesion factor α is hence determined to be 0.11 for the upper socket and 0.095 for the lower socket. The unit shaft friction/shaft movement curves at different elevations along the pile shaft are shown in Fig. 5 which indicates that the shaft resistances have been fully mobilised for all the soil strata. In the rock socket, the initial unit shaft resistance/shaft movement response is fairly linear. A shaft movement of about 10 mm is required to mobilise the maximum unit shaft friction of 390 kPa in the upper socket while a shaft movement of about 9 mm is required to mobilise the maximum unit shaft friction of 620 kPa in the lower socket. At maximum test load, about 35% of the applied load is transmitted to the pile base. The maximum unit base resistance is noted to be about 4.5 MPa which is only 77% of the q_u of the rock. This indicates that only a small portion of the base resistance has been mobilised.

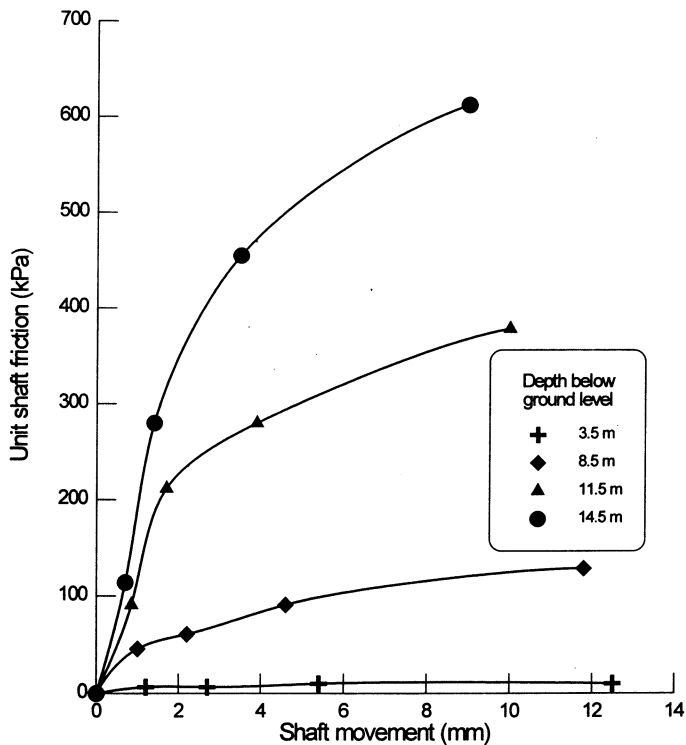


Fig. 5 Unit Shaft Friction/Shaft Movement Curves

Radhakrishnan and Leung (1989) reported the findings of load tests on four large diameter piles socketed in moderately weak sedimentary rocks and the observations are summarised in Table 1. Pile 430, which is embedded in rock having average q_u of 9 MPa, has been load tested to ultimate failure. The ultimate unit shaft friction is noted to be 700 kPa and hence the rock socket adhesion factor α is 0.078. This observed α value is quite similar to the magnitude of 0.088 obtained for pile 317 which is socketed in rock of the same average strength and has not been load tested to ultimate failure. The results indicate that when a pile is load tested to at least 2.5 times the respective working load, the mobilised shaft friction in the rock socket can be expected to reach or very close to the ultimate state. The results shown in Table 1 and the data obtained from the example test pile presented earlier illustrate that the α value generally decreases with increase in q_u . This trend is in agreement with existing design methods on rock-socketed piles such as that by Williams and Pells (1981). The observed unit base resistance of pile 430 is 13.1 MPa which is about 1.46 times the q_u of the rock. This is substantially higher than the corresponding value of about 0.15 times q_u for the other three test piles which have not been load tested to ultimate failure, see Table 1. This observation confirms that for a large diameter bored pile, the shaft friction would be mobilised first and much of the base resistance would be mobilised only after the entire shaft resistance has been fully mobilised, as suggested by Tomlinson (1995).

Table 1 Summary of Observations of Load Tests on Rock-Socketed Piles Reported by Radhakrishnan and Leung (1989)

Pile No.	Pile dia. (m)	q_u of rock socket (MPa)	Maximum test load (MN)	Maximum unit shaft friction (kPa)	Rock socket adhesion factor α	Maximum unit base resistance (MPa)	Ratio of Unit base resistance/ q_u
430*	0.705	9	10	700	0.078	13.10	1.46
TP1	0.81	6	10	560	0.093	0.97	0.16
67	1.35	7	12	600	0.086	1.05	0.15
317	1.5	9	15	800	0.088	1.36	0.15

* Pile tested to ultimate failure

ROCK SOCKET ADHESION FACTOR

For all the test piles examined in the present study, the values of ultimate unit shaft friction obtained from rock sockets of various strengths are established based on the load distribution along the rock socket under at least 2.5 times working load. The measured values are then correlated to the unconfined compressive strength of the rock based on the data obtained from the borehole nearest to the test pile. If q_u is not available, then other rock test data are considered and correlated to q_u using the methods

CASE STUDIES OF ROCK-SOCKETED PILES

described in an earlier section. These include the determination of q_u from pressuremeter test data using the approach illustrated in Fig. 2, from point load strength data using Equation (1), and from extrapolated N values using Equation (2). It should be noted that the q_u values obtained in this manner may be subjected to some degree of inaccuracy. The values of rock socket adhesion factor α hence obtained are plotted against q_u and shown in Fig. 6.

The suggested α values from four design methods on rock-socketed piles are also shown in Fig. 6. It is evident that for weak rock with q_u less than 5 MPa, majority of the measured α values are fairly close to those proposed by Rosenberg and Journeaux (1976), and Horvath and Kenny (1979). On the other hand, the measured values are considerably lower than those proposed by Williams and Pells (1981), and Rowe and Armitage (1987). For fractured rocks, Williams and Pells suggested that a rock socket reduction factor β should be applied to α to take into account the fracture state of the rock. The sedimentary rocks at the sites generally have very closely spaced fissures and a value of 0.6 for β can be deduced according to Williams and Pells' interpretation. It is evident that if Williams and Pells' α values are multiplied by a factor of 0.6, they would be much closer to the measured values. For moderately weak rock with q_u larger than 5 MPa, majority of the measured α values are considerably lower than the suggested values from the four design methods, as shown in Fig. 6. It is often necessary to use a heavier chisel or a higher number of chisel drops to advance a bored hole in moderately weak rock as compared to weak rock. Thus it is postulated that the shaft resistance has been significantly affected by the chiselling process which loosens and significantly weakens the moderately weak rock during pile installation. This indicates that the method of pile installation may significantly affect the shaft resistance of moderately weak rocks.

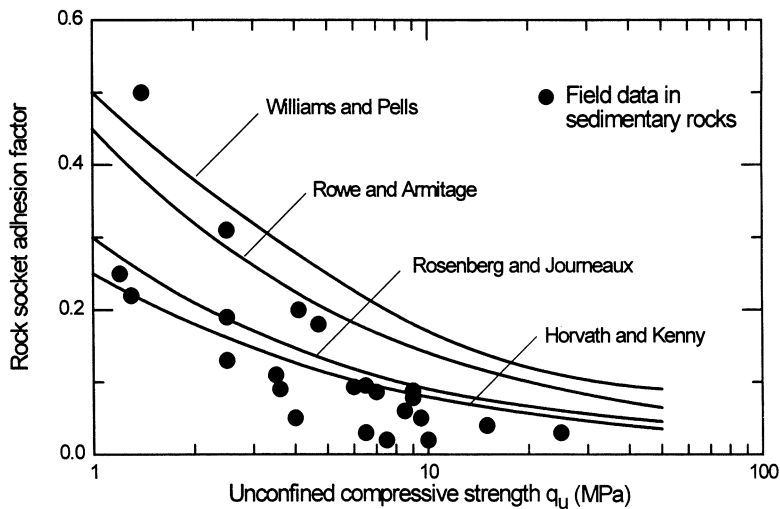


Fig. 6 Plot of Rock Socket Adhesion Factor Versus Unconfined Compressive Strength of Sedimentary Rocks

GRANITE

The granite formation in Singapore, which occurs in the central and northern part of the island, is geologically termed as the Bukit Timah formation. The degree of weathering of the granite varies with depth ranging from completely weathered residual soils to slightly weathered granite rock. The weathering grade may change gradually to the bedrock or rapidly from Grade IV to Grade II based on Anon's (1970 and 1972) classification. In addition, boulders of grades I, II and III material with size exceeding 400 mm average diameter are found within the more weathered strata. Poh et al. (1987) provided a brief review on the weathering classification of Singapore granite. The depth of the bedrock also varies greatly from close to the ground surface to depth of more than 40 m. The granite is generally greyish in colour with unconfined compressive strength as high as 280 MPa. It is worthy to note that a layer of dense silty sand often exists at the soil/rock interface. This dense sand is very stiff as it has a N value in excess of 100 and is highly permeable.

Fig. 7(a) and (b) show the variations of extrapolated N and q_u values respectively against depth obtained from several sites located in the northern part of Singapore. The rocks at these sites can be classified into two main classes: weak rock with q_u less than 5 MPa and moderately strong rock with q_u higher than 12.5 MPa. It is impossible to carry out standard penetration tests in moderately strong rock as refusal is often encountered when carrying out the test in a borehole. In contrary to the range of N values for sedimentary rocks shown in Fig. 1(a), only a handful of N values in granite are greater than 300 reflecting the rather infrequent occurrences of moderately weak rock (q_u between 5 MPa and 12.5 MPa). It is almost

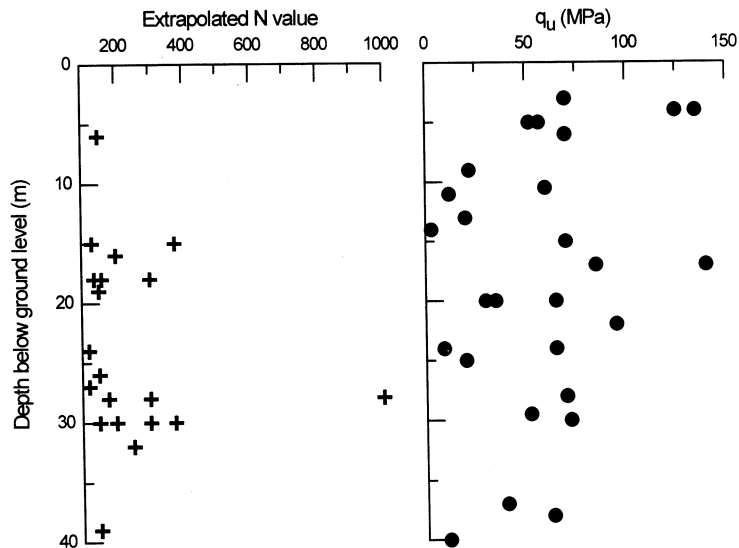


Fig. 7 Variations of (a) RQD and (b) Unconfined Compressive Strength of Granite with Depth

CASE STUDIES OF ROCK-SOCKETED PILES

impossible to carry out unconfined compression tests on weak granite as the rocks are completely or highly fractured with core length too short for compressive testing. Thus very few rock samples with q_u less than 5 MPa are shown in Fig. 7(b). Majority of the q_u values range from 12 to 100 MPa with a few samples having very high strength of 120 to 145 MPa. The RQD of the rock ranges widely across the entire spectrum of 0% to 100%. Similar to sedimentary rocks, the unconfined compressive strength can also be determined from pressuremeter test data using the approach shown in Fig. 2. The result of a typical test is shown in Fig. 8 in which the q_u is determined to be 12.5 MPa which falls within the range of q_u values shown in Fig. 7(b). This again illustrates that pressuremeter test can be a viable alternative to evaluate the shear strength of weak and fractured granite.

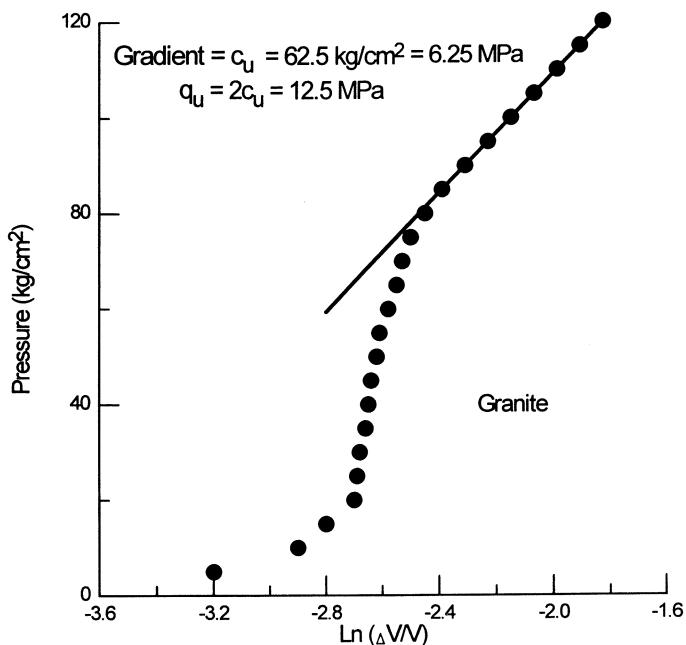


Fig. 8 Plot of Pressure Versus Ln($\Delta V/V$) Based on Pressuremeter Test Data on Granite

BORED PILES IN GRANITE

In all the case studies reported in this paper, the bored piles were installed using crane-mounted flight auger. In contrary to piles in sedimentary rocks, groundwater was frequently encountered during pile installation resulting in wet bored holes. This is probably attributed to the presence of dense sand layer at the soil/rock interface. The dense sand has a high coefficient of permeability and the significant inflow of water often caused the collapse of the borehole wall. The occurrence of soft toe was detected at the base of some bored holes. This is one of the major problem for installing piles in granite. Very often, casing or bentonite fluid

was required to stabilise the borehole wall. When granite bedrock was encountered, rock coring bucket and chisel weighing 30 to 60 kN were used to drill the rock socket. When the required pile length was achieved, coring bucket was used to attempt to flatten the pile base and cleaning bucket was used to clean the pile base before lowering down the reinforcement cage. For piles with diameter 600 mm or smaller or if the bedrock is shallow, down-the-hole hammer was found to be effective in advancing the bored holes. As most of the bored holes were wet, the tremie method was employed for concreting the pile.

CASE STUDIES

More than 20 load tests have been conducted on piles with granite sockets. The results obtained from a test pile are presented as an illustrate example. This pile is a 1-m diameter pile with a penetration length of 30 m below the ground level. The simplified subsurface profile of this pile is shown in Fig. 9(a). The strata below the ground level consists of a 24-m thick clayey silt followed by a 5-m thick dense silty sand. The granite rock socket is 1 m deep having q_u value of 12.5 MPa. A maximum test load of 9 MN was applied using the maintained load method with the reaction provided by dead-weights. Fig. 10 shows the load-settlement response of the final loading/unloading cycle. The load-settlement response is noted to be fairly linear up to an applied load of 3.6 MN. The settlement is observed to be about 21 mm at the maximum test load of 9 MN.

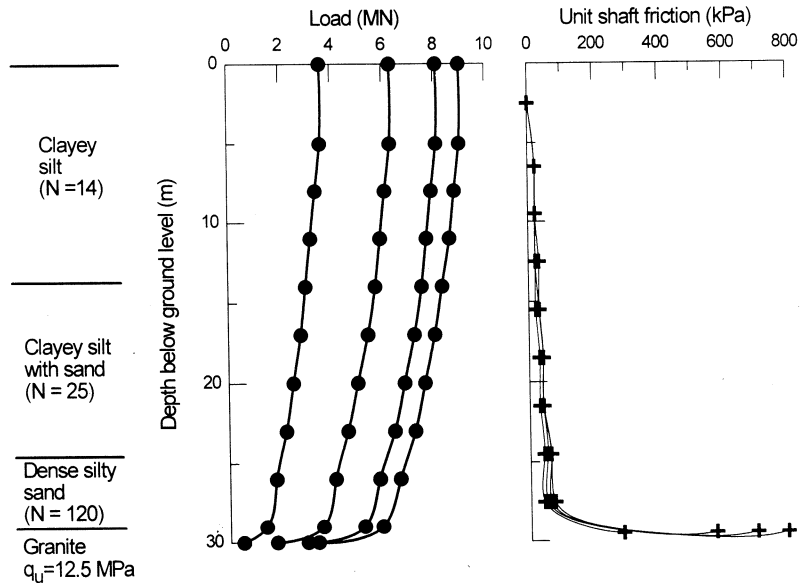


Fig. 9 (a) Simplified Subsurface Profile, (b) Load Distribution and (c) Unit Shaft Friction Distribution Along the Shaft of a Typical Pile Socketed in Granite

CASE STUDIES OF ROCK-SOCKETED PILES

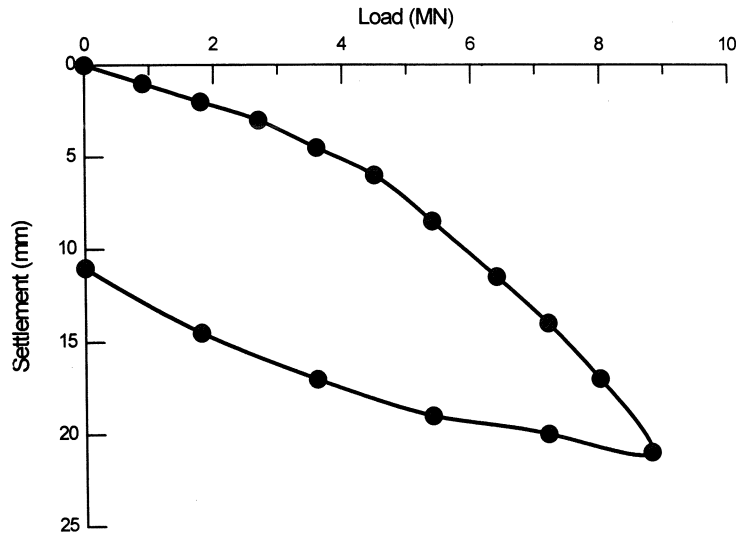


Fig. 10 Load-Settlement Response

The pile was instrumented with vibrating wire strain gauges at eleven elevations along the pile shaft with two or four gauges at each elevation. The load distribution along the pile shaft and the unit shaft friction versus depth relationships are shown in Fig. 9(b) and (c) respectively which clearly illustrate that much of pile resistance is derived from the rock socket. For the dense silty sand with a N value of 120, the observed maximum unit shaft friction is noted to be only about 80 kPa. It is suspected that the sand may have been significantly weakened during pile installation. The maximum unit shaft resistance of the granite is about 800 kPa and hence the rock socket reduction factor is determined to be about 0.064. The unit shaft friction/shaft movement relationships at different depths along the pile shaft are shown in Fig. 11 which clearly reveals that the shaft friction in the soil strata has been fully mobilised. In the granite socket, a shaft movement of about 10 mm is required to mobilise the maximum unit shaft friction of 800 kPa. At maximum test load, about 42% of the applied load was transmitted to the pile base. The maximum unit base resistance is noted to be about 5 MPa which is only about 45% of q_u of the granite. This again confirms that little base resistance has been mobilised at maximum test load.

Similar to the back-analysis conducted on piles in sedimentary rocks, the measured α values obtained from the test piles socketed in granite are correlated to q_u . If q_u is not available, other rock test data such as N value and pressuremeter test data are considered and correlated to q_u using the methods described earlier. The α values hence obtained are plotted against q_u and compared with those proposed by existing design methods and the results are shown in Fig. 12. For weak rock with q_u less than 5 MPa, about half of the measured values are comparable to those proposed by Rosenberg and Journeaux (1976) and Horvath and Kenny (1979). The remaining half are considerably

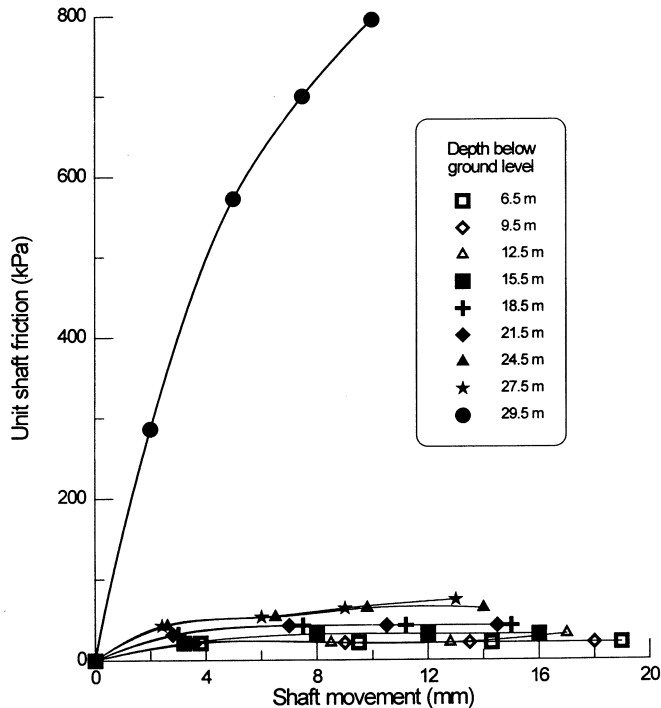


Fig. 11 Unit Shaft Friction/Shaft Movement Curves

lower than the suggested values. There are no data obtained for moderately weak rocks with q_u between 5 MPa and 12.5 MPa. For moderately strong rocks with q_u larger than 12.5 MPa, all except one of the measured α values are much lower than the suggested values. The measured α values for moderately strong granite are generally smaller than the corresponding measured α values for moderately weak sedimentary rocks. This is probably due to more chiselling is required to break the moderately strong rocks.

CONCLUSIONS

Back analyses are conducted to evaluate the performance of large diameter bored piles with sockets in sedimentary rocks and granite in Singapore. In these case studies, majority of piles in sedimentary rocks were installed in dry bored holes. On the other hand, piles in granite were often installed in wet bored holes. In addition, a layer of dense sand of high permeability often exists at the soil/granite interface and bentonite fluid was often required to prevent the collapse of borehole wall during pile installation. The rock parameters obtained from various in-situ and laboratory tests on the rocks are also reviewed. In general, both the RQD and N values are noted to be highly scattered making it difficult to interpret the rock strength accurately from these parameters. Although unconfined compressive strength is the most commonly used rock parameters

CASE STUDIES OF ROCK-SOCKETED PILES

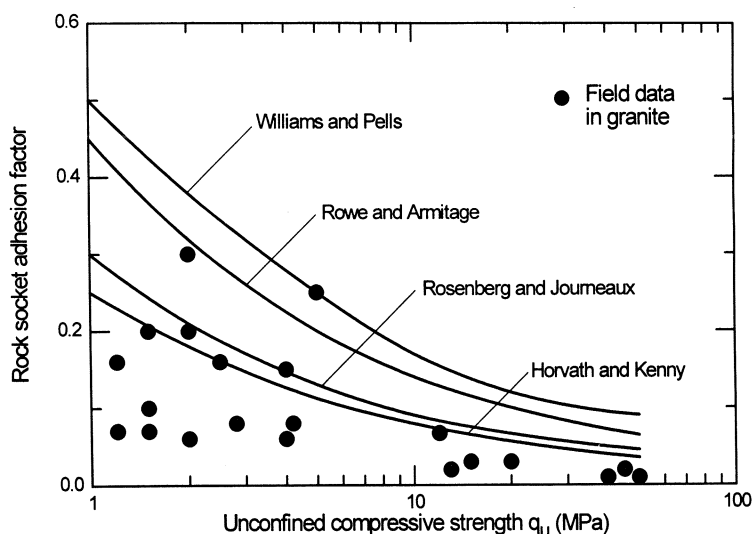


Fig. 12 Plot of Rock Socket Adhesion Factor Versus Unconfined Compressive Strength of Granite

in conventional design methods on rock-socketed piles, it is usually difficult to carry out many tests at a given site as the core samples of fractured rocks are generally too short for compression testing. As illustrated by the examples given in this paper, pressuremeter test data can be a viable alternative to evaluate the shear strength of fractured sedimentary rocks and granite. The results of pile load tests reveal that the shaft resistance is almost fully mobilised as long as the applied load is at least 2.5 times the respective pile working load. The rock socket adhesion factors obtained from the back-analyses indicate that for weak rock with unconfined compressive strength less than 5 MPa, the measured α values are reasonably close to those proposed by Rosenberg and Journeaux, Horvath and Kenny, and Williams and Pells. However, for rock with unconfined compressive strength larger than 5 MPa, the measured rock socket adhesion factors are considerably lower than the suggested values. It is believed that chiselling of rock during pile installation had significantly weakened the rocks.

ACKNOWLEDGEMENTS

The Author wishes to thank Mr R Radhakrishnan who has earlier provided many ideas and suggestions in the study of rock-socketed piles in sedimentary rocks. The Author also wishes to acknowledge the contribution of the following former students of the National University of Singapore; namely Mr W J H Lee, Mr T S Looi, Mr D Y Ng and Mr H P Quah; in assisting in the analyses of some of the field test data.

REFERENCES

- ANON, (1970). The logging of cores for engineering purposes. Geological Society Engineering Group Working Party Report, *Quarterly Journal of Engineering Geology*, vol. 3, pp 1-24.
- ANON, (1972). The preparation of maps and plans in terms of engineering geology. Geological Society Engineering Group Working Party Report, *Quarterly Journal of Engineering Geology*, vol. 5, pp 293-381.
- BUTTLING, S. (1986). Testing and instrumentation of bored piles. *Proceedings of Fourth International Geotechnical Seminar*, Nanyang Technological Institute, Singapore, November, pp 211-218.
- CHANG, M.F., BROMS B. B. & GOH, A.T.C. (1989). Design of bored piles in residual soils and weathered rocks in Singapore - review and recommendations. *Journal of Institution of Engineers Singapore*, vol. 29, No. 2, pp 53-61.
- CHANG, M.F. & BROMS, B.B. (1991). Design of bored piles in residual soils based on field-performance data. *Canadian Geotechnical Journal*, vol. 28, pp 200-209.
- HORVATH, R.G. & KENNY T.C. (1979). Shaft resistance of rock-socketed drilled piers. *Proceedings of the Symposium on Deep Foundations*, ASCE Convention, Atlanta, pp 182-214.
- JENG, C.J., CHOU, L.L., CHANG, H.W. & LI, J.C. (1993). Case study on friction behaviour of socketed piles. *Proceedings of Eleventh Southeast Asian Geotechnical Conference*, Singapore, pp 547-552.
- LEUNG, C.F. & RADHAKRISHNAN, R. (1985). The behaviour of pile-raft foundation in weak rock. *Proceedings of Eleventh International Conference on Soil Mechanics and Foundation Engineering*, San Francisco, pp 1429-1432.
- LEUNG, C.F., RADHAKRISHNAN, R. & WONG, Y.K. (1988). Observations of an instrumented pile-raft foundation in weak rock. *Proceedings of Institution of Civil Engineers*, Part 1, U.K., vol. 84, pp 693-711.
- LEUNG, C.F. & RADHAKRISHNAN, R. (1990). Geotechnical properties of weathered sedimentary rocks. *Geotechnical Engineering*, vol. 21, pp 29-48.
- MAIR, R.J. & WOODS, D.M. (1987). *Pressuremeter testing methods and interpretation*. Butterworths, London, 1987.
- MOH, Z.C., YU, K., TOH, P.H. & CHANG, M.F. (1993). Base and shaft resistance of bored piles founded in sedimentary rocks. *Proceedings of Eleventh Southeast Asian Geotechnical Conference*, Singapore, pp 571-576.
- PITTS, J.P. (1984). A survey of engineering geology in Singapore. *Geotechnical Engineering*, vol. 15, pp 1-20.
- POH, K.B., BUTTLING, S. & HWANG, R. (1987). Some experiences of the soils and geology of Singapore. *Proceedings of Singapore Mass Rapid Transit Conference*, Singapore, pp 177-191.

CASE STUDIES OF ROCK-SOCKETED PILES

- POH, K.B. & CHIAM, S.L. (1993). Performance of bored piles in fractured granite. *Proceedings of Eleventh Southeast Asian Geotechnical Conference*, Singapore, pp 577-582.
- RADHAKRISHNAN, R., LEUNG C.F. & SUBRAHMANYAM R. (1985). Load tests on instrumented large diameter bored piles in weak rock. *Proceedings of Eighth Southeast Asian Geotechnical Conference*, Kuala Lumpur, vol. 1, pp 2.50-2.53.
- RADHAKRISHNAN, R. & LEUNG, C.F. (1989). Load transfer behaviour of rock-socketed piles. *Journal of Geotechnical Engineering*, ASCE, vol. 115, No. 6, pp 755-768.
- ROSENBERG P. & JOURNEAUX N.L. (1976). Friction and end bearing tests on bedrock for high capacity socket design. *Canadian Geotechnical Journal*, vol. 13, pp 324-333.
- ROWE, R.K. & ARMITAGE, H.H. (1987). A design method for drilled piers in soft rock. *Canadian Geotechnical Journal*, vol. 24, pp 126-142.
- TAN, G.P., WONG, Y.K. & LEUNG C.F. (1994). Performance of bored piles socketed in weak rock. *Proceedings of Third International Conference on Deep Foundation Practice*, Singapore, pp 277-281.
- TOH, C.T., OOI, T.A., CHIU, H.K., CHEE, S.K. & TING, W.H. (1989). Design parameters for bored piles in a weathered sedimentary formation. *Proceedings of Twelfth International Conference on Soil Mechanics and Foundation Engineering*, Rio de Janeiro, vol. 2, pp 1073-1078.
- TOMLINSON, M.J. (1995). *Foundation Design and Construction (6th Edition)*. Longman, U.K, 536p.
- WILLIAMS, A. F. & PELLIS, P.J. N. (1981). Side resistance rock sockets in sandstone, mudstone and shale. *Canadian Geotechnical Journal*, vol. 18, pp 502-513.

EFFECTS OF SLIP BETWEEN A PILE AND SURROUNDING SOIL ON NEGATIVE SKIN FRICTION

P. Karasudhi¹, A. C. Wijeyewickrema² and S. Katawaethwarag³

SYNOPSIS

Settlement of the surrounding soils due to water withdrawal from artesian wells may give rise to negative skin friction developed in piles. In this paper, the problems of soil settlement and negative skin friction in piles are analyzed by discretizing the near field into finite elements, and the far field into infinite elements. Biot's theory for quasi-statics of porous isotropic elastic solids is assumed to govern the soil media. The governing equations in the Laplace transform domain are solved numerically first, then the approximate inverse Laplace transform of the settlement solution function is obtained by a curve-fitting method. Settlement results agree closely with those obtained by another researcher. The interface yielding behavior can be incorporated by using the 'initial stress' method, in which the development of downdrag force is considered incrementally. Yielding at the pile-soil interface is considered to occur once the induced negative skin friction stress exceeds the allowable yielding interface shear stress. The effect of pile-soil slip after yielding is included in the analysis by shortening the embedded pile length with the assumed slip values.

INTRODUCTION

Disregarding the effect of downdrag forces due to consolidation of the surrounding soil has led to damages of buildings and foundations. This effect should be incorporated in the design of pile foundations whenever the soil settlement around the piles is expected. The problems of negative skin friction in piles, due to fill surcharge and water withdrawal from deep artesian wells, have been the object of numerous investigations, e.g. Ng, Karasudhi and Lee (1976) and Lee, Chin and Chow (1990). The exact analytical solutions for such problems are feasible only in simple cases.

The general three dimensional consolidation theory, taking into account the coupling between the solid and fluid, was first formulated by Biot (1941). For multilayered saturated elastic half spaces, the analytical approach is very complicated and mathematically intractable. The most suitable and efficient way to solve such problems is to employ numerical techniques where there is no restriction on geometry, inhomogeneity, anisotropy and boundary conditions. Sandhu and Wilson (1969) adopted

¹ Chair Professor, School of Civil Engineering, Asian Institute of Technology, P.O. Box 2754, Bangkok, Thailand, 10501.

² Associate Professor, School of Civil Engineering, Asian Institute of Technology, P.O. Box 2754, Bangkok, Thailand, 10501.

³ Former Graduate Student, School of Civil Engineering, Asian Institute of Technology, P.O. Box 2754, Bangkok, Thailand, 10501.

the conventional finite element technique to solve complex problems of a saturated elastic half space, by truncating the semi-infinite domain into a large but finite domain which is then discretized into standard finite elements. This method leads to a higher computational effort and cost because of the large number of degrees of freedom.

To avoid this difficulty, Rajapakse and Karasudhi (1985) proposed three types of infinite elements for solving elastostatic multilayered half space problems, by investigating the elastostatic far field behavior of a homogeneous half space and a layered half space. This scheme discretizes the whole material domain into conventional finite elements in the near field and infinite elements in the far field. Karasudhi and Poonsawat (1994) adopted this scheme to calculate land subsidence and negative skin friction due to water withdrawal from deep artesian wells. The objective of this paper is to extend the work of Karasudhi and Poonsawat (1994) to a non-linear analysis in which local yielding at the pile-soil interface as well as the effects of slip between a pile and surrounding soils on negative skin friction is investigated.

METHOD OF ANALYSIS

Water withdrawal from deep artesian wells, symbolized by the point sink in Fig. 1a, can cause land subsidence, different consolidation at different depths in the soil mass, and negative skin friction in piles embedded in such soil media.

Problem composition

The problem of negative skin friction in piles is decomposed into three systems, namely;

- (1) free-field subsidence due to water withdrawal from artesian wells such as depicted in Fig. 1a,
- (2) the half space subjected to the 'bond' forces q_i as shown in Fig. 1b, and
- (3) the fictitious bar subjected to $-q_i$ as in Fig. 1b.

Land subsidence

The problem of free-field subsidence in system (1) is solved by discretizing the whole material domain into conventional finite elements in the near field and infinite elements in the far field. By variational principle and setting the first variation of functional ($\delta\tilde{\pi}$) equal to zero, we can obtain the characteristic matrix

$$\begin{bmatrix} K & C \\ C^T & -\frac{1}{P} L \\ & P \end{bmatrix} \begin{Bmatrix} \tilde{U} \\ \tilde{P} \end{Bmatrix} = \begin{Bmatrix} \tilde{R}_1 \\ -\frac{1}{P} \tilde{R}_2 \end{Bmatrix} \quad (1)$$

in which

$$\mathbf{K} = \sum_e \mathbf{K}^e \quad \mathbf{C} = \sum_e \mathbf{C}^e \quad \mathbf{L} = \sum_e \mathbf{L}^e \quad \tilde{\mathbf{U}} = \sum_e \tilde{\mathbf{U}}^e \quad (2a-d)$$

$$\tilde{\mathbf{R}}_1 = \sum_e \tilde{\mathbf{R}}_1^e \quad \tilde{\mathbf{R}}_2 = \sum_e \tilde{\mathbf{R}}_2^e \quad \tilde{\mathbf{P}} = \sum_e \tilde{\mathbf{P}}^e \quad (3a-c)$$

and

$$\mathbf{K}^e = \int_{V^e} \mathbf{B}^T \mathbf{D} \mathbf{B} dV \quad \mathbf{C}^e = \int_{V^e} \mathbf{A} \mathbf{N}^P f dV \quad (4a-b)$$

$$\mathbf{L}^e = \int_{V^e} \mathbf{k} \mathbf{A}^{P^T} \mathbf{A}^P dV \quad \tilde{\mathbf{R}}_1^e = \int_{S^e} \mathbf{N}^{u^T} \bar{\mathbf{X}} dS \quad \tilde{\mathbf{R}}_2^e = \int_{S^e} \mathbf{N}^{P^T} \bar{\mathbf{Q}} dS \quad (5a-c)$$

in which matrices \mathbf{B} , \mathbf{D} , \mathbf{A} , \mathbf{A}^P are given in Appendix. Here $\tilde{\mathbf{U}}$, $\tilde{\mathbf{P}}$, $\tilde{\mathbf{R}}_1$ and $\tilde{\mathbf{R}}_2$ are the nodal vectors of displacements, pore pressures, boundary tractions and outflow rates, respectively.

The first of Eq. (1) is the discretized equilibrium equation in which \mathbf{K} is the usual elastic stiffness of the medium, \mathbf{C} the coupling matrix, $\tilde{\mathbf{R}}_1$ the load vector due to boundary traction. The second equation of Eq. (1) represents the discretized flow equation which relates volumetric strain to the inflow due to the nodal pore pressure and the outflow rate $\tilde{\mathbf{R}}_2$. Equation (1) gives a set of equations to be solved to find the numerical solutions of the problem at the nodes. The symbol \sim denotes the Laplace transform, i.e.

$$\tilde{v}(p) = \int_{0-}^{\infty} \exp(-pt) v(t) dt. \quad (6)$$

The problem of land subsidence is solved in the Laplace domain and then inverted back into the time domain using an approximate method. Details of formulation of Eq. (1) to Eq. (5), approximate inverse Laplace transform, and infinite elements has been described in Karasudhi and Poonsawat (1994).

Negative skin friction

The fictitious bar has the same dimensions as the actual pile, but its stiffness is equal to the difference between those of the latter and the half space, i.e.

$$\mathbf{E}^{(3)}(z) = \mathbf{E}^{(p)} - \mathbf{E}^{(2)}(z) \quad (7)$$

where E denote a Young's modulus, a supernumerical within parentheses a system number, and the superscript p within parentheses the actual pile. This procedure where three related systems are considered was first proposed by Muki and Sternberg (1970). The axial deformation of the fictitious bar is equal to the summation of the vertical normal deformation in the consolidation soil layer of system (1) and vertical normal deformation over the cross section of the region (D) in system (2). Consider the fictitious pile as a uniaxial member and divide it into N elements with nodal points at z_i ; $i = 0$ to N ; $z_0 = 0$, $z_N =$ pile length (Fig. 1). Accordingly, the equilibrium of axial forces acting on the fictitious bar, and its axial displacements at various values of z_i can be written as

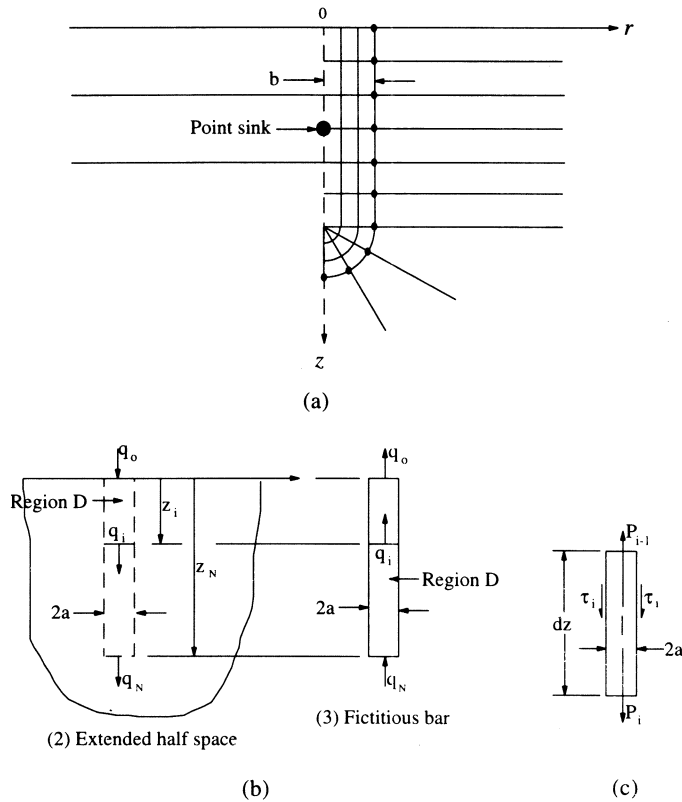


**Fig. 1 (a) System (1) with Point Sink;
 (b) Interacting Systems (2) and (3)
 (c) Small Segment of Actual Pile.**

$$\sum_{i=0}^N q_i = 0 \quad (8)$$

$$w_j^{(3)} = w_j^{(1)} + \sum_{i=0}^N b_{ji} q_i \quad (9)$$

where $b_{ji} = w_j^{(2)}$ due to unit q_i .

The fictitious bar is governed by strain-displacement relationship, equilibrium condition and the stress-strain relationship;

$$w_j^{(3)} = w_{j-1}^{(3)} + \frac{z_j - z_{j-1}}{E_j^{(3)}} \sum_{k=0}^{j-1} q_k \quad (j = 1, 2, \dots, N). \quad (10)$$

Equations (8)-(10) give $(N+2)$ equations, i.e.

$$\begin{bmatrix}
 b_{00} & b_{01} & \dots & b_{0N} & -1 \\
 (b_{10}-h_1/E_1^{(3)}) & b_{11} & \dots & b_{1N} & -1 \\
 \dots & \dots & \dots & \dots & \dots \\
 (b_{N0}-\sum_{i=1}^N h_i/E_i^{(3)}) & (b_{N1}-\sum_{i=2}^N h_i/E_i^{(3)}) & \dots & b_{NN} & -1 \\
 1 & 1 & \dots & 1 & 0
 \end{bmatrix}
 \begin{Bmatrix}
 q_0 \\
 q_1 \\
 \dots \\
 q_N \\
 w_0^{(3)}
 \end{Bmatrix}
 =
 \begin{Bmatrix}
 -w_0^{(1)} \\
 -w_1^{(1)} \\
 \dots \\
 -w_N^{(1)} \\
 0
 \end{Bmatrix}
 \quad (11)$$

to be solved to find the bond forces q_i and one displacement $w_0^{(3)}$. From the pile-soil interactive forces q_i acting at each instant in system (2), the vertical soil deformation $w^{(2)}$ and the vertical normal stress $\sigma_{zz}^{(2)}$ can be determined and then the vertical deformation of the pile nodes $w^{(3)}$ is easily obtained. Hence the axial stress in system (3), $\sigma_{zz}^{(3)}$, is determined by

$$\sigma_{zz}^{(3)} = \frac{dw^{(3)}}{dz} E^{(3)} \quad (12)$$

The stress of the actual pile $\sigma_{zz}^{(p)}$ will be obtained as follows,

$$\sigma_{zz}^{(p)} = \sigma_{zz}^{(1)} + \sigma_{zz}^{(2)} + \sigma_{zz}^{(3)} \quad (13)$$

The equilibrium of the axial forces and the negative skin friction acting upon the actual pile element where $z_{i-1} < z < z_i$ is

$$P_i - P_{i-1} + 2\pi ah_i \tau_i = 0 \quad (14)$$

where τ_i and P_i are the negative skin friction assumed constant along element i , and the axial force, respectively, at $z = z_i$, a the radius of the pile and $h_i = z_i - z_{i-1}$. We can obtain τ_i as follows,

$$\tau_i = - \frac{P_i - P_{i-1}}{2\pi ah_i} \quad (15)$$

Extension to include Effect of Pile-Soil Slip

The above analysis is based on the elastic response of pile-soil interaction. If the piles are installed through a soft clay layer, substantial slip may occur along the pile shaft. Accordingly, in these cases, a non-linear analysis would be required for better predictions.

The non-linear soil behavior can be incorporated using the 'initial stress' method by Lim et al. (1993), in which the development of downdrag force is considered incrementally by dividing the ground subsidence into small increments. The allowable

yielding interface shear stress can be evaluated by using the Coulomb expression. Slip at the pile-soil interface is considered to occur once the induced negative skin friction exceeds the limiting skin friction stress. The numerical procedure for non-linear analysis is outlined below.

- (1) Divide the subsidence from system (1) into small increments, $\{\Delta w^{(l)}\}$. From Eq. (11), the incremented form of element matrix equation is given by

$$[I_s]\{\Delta q\} = \{-\Delta w^{(1)}\} \quad (16)$$

where $[I_s]$ is the matrix in Eq. (11) and $\{\Delta q\}$ is the vector of incremental pile-soil interactive force including one term of incremental displacement of first node in system (3), i.e $\Delta w_0^{(3)}$.

- (2) For each increment, solve Eq. (16) to obtain the incremental pile-soil interactive force. Calculate the incremental skin friction stresses $\Delta \tau$ by the way of Eqs. (12) to (15) and the accumulated skin friction stresses from

$$\{\tau\} = \{\tau^i\} + \{\Delta \tau\} \quad (17)$$

where $\{\tau^i\}$ is the vector of accumulated induced skin friction stresses from the previous subsidence increment.

- (3) At each element, if the accumulated skin friction stress exceeds the allowable shear stress, the accumulated value of skin friction stress is set equal to allowable and Δq_i for that element is set equal to zero for next subsidence increment.
- (4) Proceed to next subsidence increment and repeat steps (2)-(3) until the subsidence of interest is reached.

RESULTS AND DISCUSSION

Prediction of Surface Subsidence in Central Bangkok

Groundwater withdrawal in Bangkok area is analyzed by the proposed method. The rates of withdrawal from different aquifers are shown in Table 1. The problem is considered in such a way that the pumping outflow rate is constant. Thickness and depth of aquifers are tabulated in Table 2, and Bangkok subsoil properties are presented in Table 3. Water is assumed to be withdrawn from the mid-depth of each aquifer. The numerical results of the Laplace transform of the land surface subsidence and their approximations are illustrated in Fig. 2. The real time functions of such subsidence are compared in Fig. 3 and shown that the numerical surface settlement agrees closely with that predicted by Premchitt (1978), by means of a geological model. The vertical displacement profile along the depth (z-direction) is as shown in Fig. 4, and this shows that the largest settlement occurs at the surface and decreases with soil depth.

EFFECTS OF SLIP BETWEEN A PILE AND SURROUNDING SOIL

Table 1 Rates of Pumping in (m³/day)

Bangkok	Phra Padaeng	Nakhon Luang	Nonthaburi
120,000	227,500	310,000	142,500

Table 2 Aquifer Thickness and Depth

Aquifers	Approximate Depth to Mid Layers (m)	Approximate Thickness (m)
Bangkok	35	10
Phra Padaeng	67.5	35
Nakhon Luang	132.5	35
Nonthaburi	182.5	35

Table 3 Properties of Bangkok Subsoil

Layer No.	Soil Types	Thickness (m)	Permeability k, (mm/day)	Young's modulus E (MN/m ²)	Poisson's ratio 'ν'
1	Clay	30	0.864	15	0.4
2	Sand	10	864.0	40	0.25
3	Clay	10	0.432	20	0.35
4	Sand	35	691.2	50	0.25
5	Clay	30	0.173	20	0.35
6	Sand	35	432.0	60	0.25
7	Clay	15	0.173	30	0.30
8	Sand	35	432.0	60	0.25
9	Clay	∞	0.043	35	0.35

Stress on Pile

The circular cylindrical piles adopted in this study are 0.5 m in radius, 50 m pile length and Young's modulus $E(P) = 30 \times 10^6$ MN/m² is considered. For the case of perfect bonding between the pile and the surrounding soil, the total vertical stress in the pile and skin friction stresses on pile are shown in Fig. 5. The total vertical stress is very high at the center part and quite low at the ends of the pile and increase with time. The skin friction stress is very high at the ends of the pile, negative at the top and positive

EFFECTS OF SLIP BETWEEN A PILE AND SURROUNDING SOIL

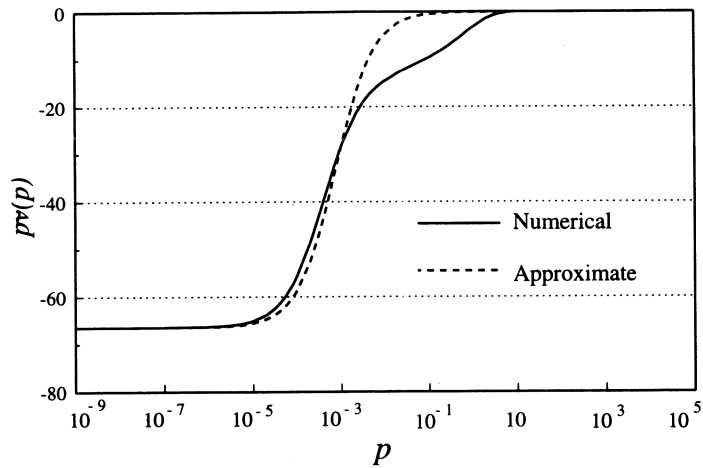


Fig. 2 Land Surface Subsidence.

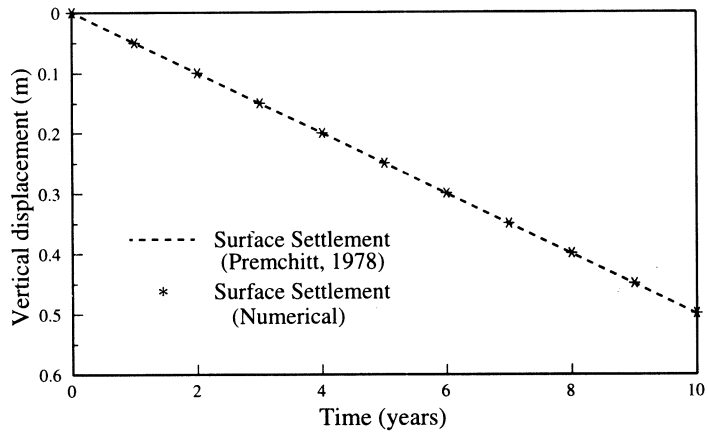


Fig. 3 Settlement in Central Bangkok Due to Water Withdrawal.

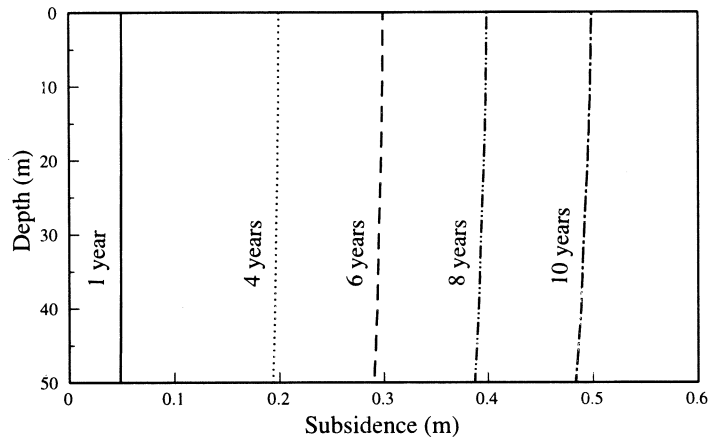


Fig. 4 Vertical Displacement in Central Bangkok Due to Water Withdrawal.

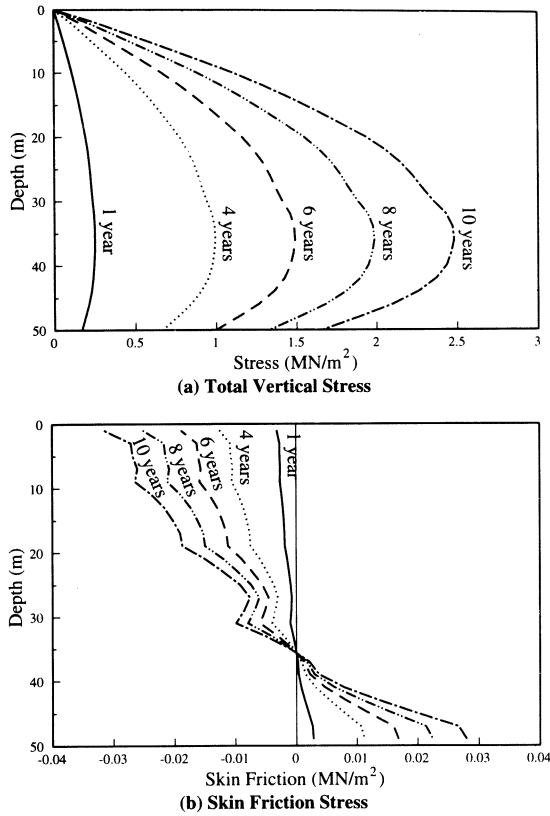


Fig. 5 Stress on Pile for No Slip (Perfect Bond) Between Pile and Soil.

at the bottom, and the neutral point is located at a depth of about 35 m. The neutral point corresponds to the location of the maximum vertical stress.

Results of the analysis which include the effects of pile-soil interface yielding or non-linear analysis are illustrated in Fig. 6. The allowable yielding interface shear stress from Phamvan (1989) varies from 0.005 MN/m² at the top surface to 0.15 MN/m² at a depth of 50 m. The total vertical stress profiles along the pile length are shown in Fig. 6a. This figure shows that at the points that have already yielded, i.e., the upper part of the pile, the stress does not increase with increasing time because these points can no longer take the load. The graphs of skin friction stress on pile versus soil depth are shown in Fig. 6b for various time durations. The neutral points are located at about 35 m. The values of the skin friction stress at elements where slip has taken place are equal to the allowable yielding interface shear stress at those elements. The neutral points of skin friction stress of all cases are located in the range 0.60L - 0.70L, in which L is the pile length. Yielding always occurs on the upper part of the pile.

EFFECTS OF SLIP BETWEEN A PILE AND SURROUNDING SOIL

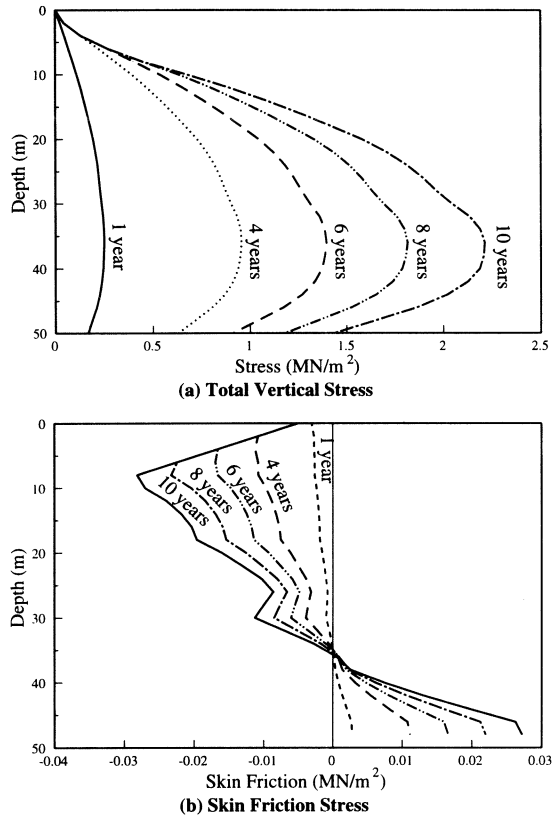


Fig. 6 Load on Pile for Non-linear Solution.

The assumed slip values versus time is depicted in Fig. 7. The slip value is used to decrease the embedded pile length in the analysis which incorporates the interface yielding effect. Comparisons of the pile stress results between different analyses are illustrated in Fig. 8. This figure shows that the pile-soil slip has little effect on pile stresses.

CONCLUSIONS

In this study finite elements and efficient infinite elements are used for solving problems in multilayered porous elastic half spaces incorporating Biot's theory (1941). The numerical results in terms of the Laplace transform at each Laplace parameter p , are determined first. Then, the approximate time solutions for taking the inverse Laplace transform are assumed. This approximation gives very accurate initial and final results, and is fairly accurate at other times t . The accuracy of the solution depends on the suitability of the approximate curve that is assumed. Subsidence by the proposed

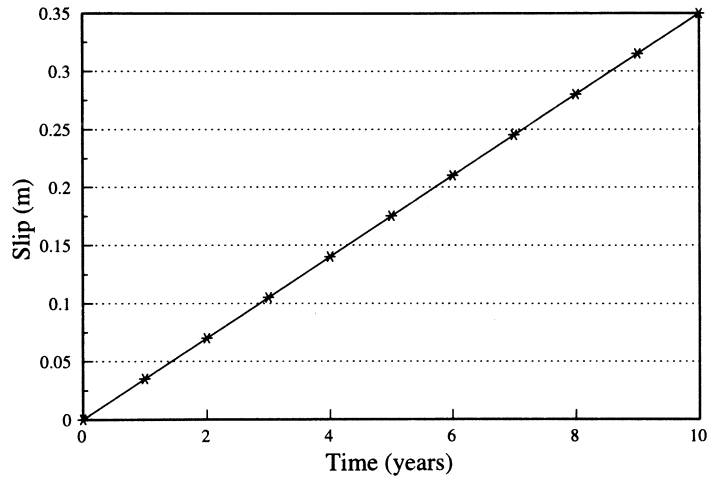
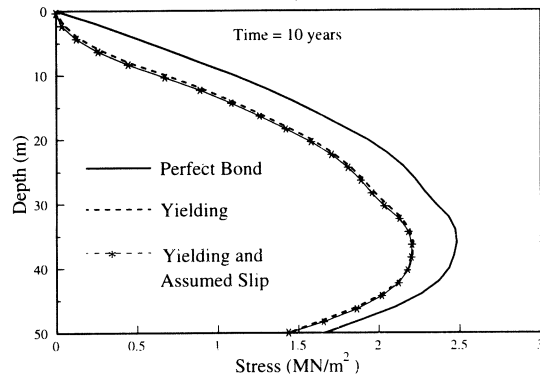
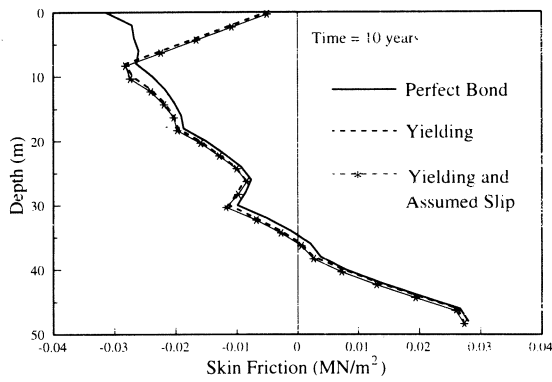


Fig. 7 Assumed Slip Values Versus Time.



(a) Total Vertical Stress



(b) Skin Friction Stress

Fig. 8 Comparison of Load on Pile Between Different Analyses.

EFFECTS OF SLIP BETWEEN A PILE AND SURROUNDING SOIL

method for the first ten years varies almost linearly, agreeing very closely with the results of Premchitt (1978).

The negative skin friction stress was found to be dependent on the relative movement between the pile and the soil. The maximum vertical stress and the neutral point of skin friction stress of all cases are located at a depth in the range 0.60L-0.70L. The load on pile varies with time because of the increasing subsidence.

In cases where pile-soil slip is dominant, non-linear interaction at the pile-soil interface can easily be accommodated using the 'initial stress' method. The allowable yielding interface shear stress can be evaluated using the Coulomb expression and varies from 0.005 MN/m² at the top surface to 0.15 MN/m² at 50 m depth. Incorporating pile-soil interface yielding results in a more realistic behavior than an elastic analysis. The elastic solutions of the maximum vertical stress and negative skin friction stress are greater than the interface yielding solutions. Slip between a pile and the surrounding soils that occurs after interface yielding has little effect on vertical stress and negative skin friction stress.

REFERENCES

- BIÔT, M.A. (1941). General theory of three dimensional consolidation. *Journal of Applied Physics*. Vol. 12, pp. 155-164.
- KARASUDHI, P. (1992). A rational infinite element scheme for quasi-statics of saturated elastic half space. *2nd Tri-Lateral (Kyoto University - Korea Advanced Institute of Science and Technology - National Taiwan University) Joint Seminar on Civil Engineering, Taipei*, November 16-18, pp. 109-112.
- KARASUDHI, P. (1993). An efficient scheme for land subsidence and negative skin friction. *Impact of Computational Mechanics on Engineering Problems*, edited by V.A. Pulmano and V. Murti, Balkema, Rotterdam, pp. 55-62.
- KARASUDHI, P. AND POONSAWAT, P. (1994). Land subsidence and negative skin friction. *Geotechnical Engineering*, Vol. 25, No. 2, pp. 21-35.
- LEE, S.L., CHIN, J.T. AND CHOW, Y.K. (1990). Negative skin friction on pile groups. *International Journal of Numerical and Analytical Methods in Geomechanics*, Vol. 14, pp. 75-91.
- LIM, C.H., CHOW, Y.K. and KARUNARATNE, G.P. (1993). Negative skin friction on single piles in a layered half-space. *International Journal for Numerical Analytical Methods in Geomechanics*, Vol. 17, pp. 625-645.
- MUKI, R. AND STERNBERG, E. (1970). Elastostatic load-transfer to a half space from a partially embedded axially loaded rod. *International Journal of Solids and Structures*, Vol. 6, pp. 69-90.
- NG, H.K., KARASUDHI, P. and LEE, S.L. (1976). Prediction of negative skin friction and settlement in piles due to fill surcharge. *Geotechnical Engineering*, Vol. 7, pp. 25-45.
- PREMCHITT, J. (1978). Analysis and simulation of land subsidence with special

reference to Bangkok. *D. Eng Dissertation, Asian Institute of Technology, Thailand.*

PHAMVAN, P. (1989). Negative skin friction of driven piles in Bangkok subsoils, *D. Eng. Dissertation, Asian Institute of Technology, Thailand.*

RAJAPAKSE, R.K.N.D. AND KARASUDHI, P. (1985). Elastostatic infinite elements for layered half spaces. *Journal of Engineering Mechanics, ASCE, Vol. 111, No. 9, pp. 1144-1158.*

SANDHU, R.S. and WILSON, E.L. (1969). Finite element analysis of seepage in elastic media. *Journal of Engineering Mechanics, ASCE, Vol. 95, pp. 641-652.*

SMITH, I.M. and GRIFFITHS, D.V. (1988). Programming the finite element method. *John Wiley and Sons Ltd., 2nd Edition, Vol. 1.*

APPENDIX

Matrices in formulating element stiffness

Constitutive matrix **D** is

$$\mathbf{D} = \begin{bmatrix} \lambda + 2\mu & \lambda & \lambda & 0 \\ \lambda & \lambda + 2\mu & \lambda & 0 \\ \lambda & \lambda & \lambda + 2\mu & 0 \\ 0 & 0 & 0 & \mu \end{bmatrix} \quad (18)$$

where λ and μ are Lamé's constants.

Matrix of strain-displacement relationship **B** is

$$\mathbf{B} = \begin{bmatrix} \frac{\partial N^u_r}{\partial r} & 0 \\ \frac{N^u_r}{r} & 0 \\ 0 & \frac{\partial N^u_z}{\partial z} \\ \frac{\partial N^u_r}{\partial z} & \frac{\partial N^u_z}{\partial z} \end{bmatrix} \quad (19)$$

Vector of displacement gradient **A** and pore pressure gradient **A^P** are

$$\mathbf{A} = \left\{ \begin{array}{c} \frac{N^u_r}{r} + \frac{\partial N^u_r}{\partial r} \\ \frac{\partial N^u_z}{\partial z} \end{array} \right\} \quad \mathbf{A}^P = \left\{ \begin{array}{c} \frac{\partial N^p_f}{\partial r} \\ \frac{\partial N^p_f}{\partial z} \end{array} \right\} \quad (20-21)$$

It should be noted here that the matrices presented above are applicable only for axisymmetric problems and the coordinate system referred is the cylindrical coordinate system.

BOOK REVIEW

Book Title: Soft Ground Improvement in Lowland and Other Environments by *D.T. Bergado, L.R. Anderson, N. Miura, and A.S. Balasubramaniam.*

Book Description: This book first outlines the problems encountered during infrastructure constructions on soft ground conditions in Lowland and Other Environments. Then, the various soft ground improvement techniques are reviewed. The authors also discuss how to determine and select the most appropriate improvement technique for various soils. They also discuss key factors considered when building on soft ground, including applied loading, site conditions, existing problems and construction time. Topics include surface compaction, deep compaction, prefabricated vertical drains, granular piles, lime/cement stabilization, and mechanically stabilized earth. This book is published by the *American Society of Civil Engineers (ASCE)* Publication No. 40151 with List Price of US\$48 for non-ASCE member and US\$36 for ASCE Member.

ERRATA ON

Paper on "Cation Exchange Studies on a Lime-Treated Marine Clays" by *G. Rajasekaran and S. Narasimha Rao*, Geotechnical Engineering Journal, Vol. 26, No. 2, December, 1995.

Re: Printing Errors

Pages	Existing Statements	Correction
Page 29	Symbol 186/f"Symbol"	≡
Page 32 Line 19	Symbol 187/f"Symbol"	∩
Page 33 Lines 1,2,3,6-10,12	Symbol 187/f"Symbol"	∩

NOTES FOR THE GUIDANCE OF AUTHORS

General: Manuscripts of original papers, technical notes and discussions should be submitted to: The Editor, School of Civil Engineering, Asian Institute of Technology, P.O. Box 2754, Bangkok, Thailand. Papers will be accepted for review on the understanding that they have **not been submitted or published elsewhere** and that they become the copyright of the South East Asian Geotechnical Society.

Papers on major geotechnical topics of wide interest to the South East Asian region are welcomed, where as those of a specialist interest that are more suitable for other specialist journals are less likely to be accepted. Normally, **papers should not exceed 16 pages, including references, figures and tables**: there are about 450 words on a printed page. Short topical papers of 8 pages or less will be reviewed more quickly.

The format which must be followed for the preparation of manuscripts is in general that adopted in this issue of the Journal. **Manuscripts which do not conform to this format will be returned to the author(s) without review.**

Three complete copies of the manuscript, in English, should be submitted to the Editor (two copies for technical notes and discussions) together with the original drawings and photographs. In addition, a copy of the text should be submitted on 5 1/4" or 3 1/2" floppy disc formatted using DOS 3.0 (or later version) and the file should be in ASCII or Wordperfect 5.0 (or later version) format. Typescripts must be accurate and in their final format as outlined below. Owing to the high cost of corrections at proof stage, the Editor reserves the right to charge authors the full cost of corrections resulting from changes made at the proof stage.

Layout: Typescripts **must be double spaced**, including references, on one side only of **A4 paper**, with a **25 mm margin on each side**. All pages should bear the authors name and be numbered serially. Papers should be succinct and arranged as follows:

1. **Title:** brief and specific in **bold and uppercase, centred** at the top of the first page
2. The **author(s) full name(s) should appear centred below the title in bold**. The author(s) position and affiliation should be indicated as a footnote at the bottom of the first page. A **synopsis (with main heading) of not more than 200 words** should appear immediately below the authors name(s). The synopsis must be intelligible **without** reference to the paper and should highlight the essential new information and interpretations in the paper; it should not be a mere recital of the subjects covered. A synopsis is not required for technical notes.
3. **Figures** should be drawn boldly in black ink on one side of good quality tracing paper or smooth white board, with a **line weight and lettering suitable for reduction to fit the journal page width**. A separate caption list should be included. All maps should include a metric scale and north point. **Photographs** should be sharp and of **good contrast** (black and white preferred). The authors name should be given on each sheet and the **"top" indicated**.
4. **Formulae** should be expressed as simply as possible, and lengthy proofs avoided. **SI units** should be used throughout.
5. **Symbols** should be defined when they first appear.
6. **References** should appear in the text as the author(s) name(s) followed by the year of publication in brackets. A **list of references** should be given at the end of the text in alphabetical order of author(s) name(s) with the author(s) name(s) in capitals and bold. Some examples of the format to be used in the reference list are given below:

PREMCHITT, J. & SHAW, R. (1991). Marine geotechnical engineering for development projects in Hong Kong. *Proceedings of the International Workshop on Technology for Hong Kong's Infrastructure Development*, Hong Kong, pp 721-738.

PUN, W.K. (1990). Seismicity of Hong Kong. M.Sc. Thesis of the University of London (unpublished)

PUN, W.K. & AMBRASEYS, N.N. (1992). Earthquake data review and seismic hazard analysis for the Hong Kong region. *Earthquake Engineering and Structural Dynamics*, vol. 21, pp 433-443.

HOEK, E. & BROWN, E.T. (1982). *Underground Excavations in Rock (2nd Edition)*. The Institution of Mining & Metallurgy, London, 527 p.

GEOTECHNICAL ENGINEERING

CONTENTS

Photographic Feature:

Modernization of Laboratory Testing Equipments to Measure Strength and Deformation of Geomaterials

by *S. Shibuya*

Main Papers:

Compressibility and Flow Parameters from PVD Improved Soft Bangkok Clay
by *D.T. Bergado, P.V. Long and A.S. Balasubramaniam* 1

Interactive Behavior of Cylindrical Anchors in Dense Sand
by *H.J. Liao, J.K. Chen and S.C. Shu* 21

Analysis and Design of a Tied Back-To-Back Geosynthetic Reinforced Soil Wall
by *S.C.R. Lo, S.Q. Li, M. Gopalan and Z. Gao* 37

Case Studies of Rock-Socketed Piles
by *C.F. Leung* 51

Effects of Slip Between a Pile and Surrounding Soil on Negative Skin Friction
by *P. Karasudhi, A.C. Wijeyewickrema and S. Katawaethwarag* 69

Book Review:

Soft Ground Improvement in Lowlands and Other Environment
by *D.T. Bergado, L.R. Anderson, N. Miura, and A.S. Balasubramaniam* 83

Errata:

Cation Exchange Studies on a Lime Treated Marine Clay
by *G. Rajasekaran and S. Narasimha Rao*, *Geotechnical Engineering*,
Vol. 26, No. 2, December 1995 85

Abstracted and/or Indexed in *Geotechnical Abstracts*